SCHOOL OF SCIENCE
Department of Industrial Chemistry “Toso Montanari”

Second cycle degree in

Low Carbon Technologies and Sustainable Chemistry

Classe LM-71 - Scienze e Tecnologie della Chimica Industriale

Acid catalysts for glucose isomerization and 5-hydroxymethylfurfural etherification

Experimental degree thesis

CANDIDATE

Carolina Zampieri

SUPERVISOR

Prof. Nikolaos Dimitratos

CO-SUPERVISOR

Prof. Pedro Jesus Maireles Torres

Academic Year 2022-2023

Abstract

One of modern society's fundamental problems concerns the extensive use of fossil resources that are dangerous both to environment and people. Several solutions are being studied in order to reduce the environment threatening and, among those, the use of biomass is a viable option because of the low environmental impact and the low cost. Starting from biomasses is possible to obtain glucose that is considered one of the most important building blocks from renewable resources. The isomerization of glucose to fructose is extremely important since it is an equilibrium reaction and it is thermodynamically prohibited to obtain fructose yields higher than the imposed one. Because of this, fructose is an expensive compound but is still largely used in the chemical industry considered that from it is possible to obtain 5-hydroxymethylfurfural (HMF), an important platform molecule, with an easy and fast dehydration process. HMF is, as said before, an important platform molecule used as starting material in different chemical processes due to the different functional groups that it possess. HMF etherification is one of these because it gives the opportunity to obtain precursors of biofuel. The type of precursor obtained highly depends on the type of sites present on the catalyst.

In this work both the reaction conditions of glucose isomerization to fructose and HMF etherification were studied. For the isomerization reaction a commercial zeolite was used to catalyze the reaction while for the HMF etherification two different types of materials were synthesized: mixed metal oxides and zeolites. The optimization of these two materials was also studied, especially for what concerns the zeolites that were modified first with a dealumination and then with the intercalation of Zr in the empty Al sites.

At the end of the work it was possible to observe that with the best reaction conditions a 30% fructose was obtained. Mixed metal oxides and Zr doped zeolites were active on HMF etherification but for two different types of etherified products, respectively one-etherified and bis-etherified. Furthermore, the use of Zr doped zeolites led to a almost 100% HMF conversion and carbon balance with the best reaction conditions.

INDEX

1. Introduction

1.1. Biomass

In the last years of the last century, the raising of the global temperatures together with the increasing of extreme climate events, such as floodings or hurricanes, has moved the attention towards finding new solutions, sustainable and environmentally friendly, to produce energy, fuels and chemicals[1]. Consistent with that, the government of several countries have tried to implement legislations and agreements to reduce climate change. An example of that is the Paris Climate Agreement signed in 2015 by 187 countries, that has the long-term goal to limit the increase in the global temperature below 2 °C. Environmental legislations play a pivotal role in addressing the pressing global issue of climate change. These laws establish a framework for the action, set emission reduction targets and encourage the adoption of sustainable energy practices. In Europe, the European Green Deal is a landmark initiative aimed at making the European Union climate neutral by 2050. The plan encompasses various measures such as the EU Emissions Trading System (EU ETS), that encourages industries to reduce their carbon footprint by putting a price on it, and the Renewable Energy Directive, that establishes binding targets for EU member states to increase the share of renewable energy sources in their energy mix. On an international level, the Kyoto Protocol was a pioneering climate law that set emission reduction targets for industrialized countries and has now been supplanted by the already mentioned Paris Agreement.

Renewable energy has emerged as a critical component of global efforts to combat climate change and reduce the dependence on fossil fuels. With the help of laws and legislation, energy landscape and sustainable practices have been shaped to be more appealing also from an economical point of view.

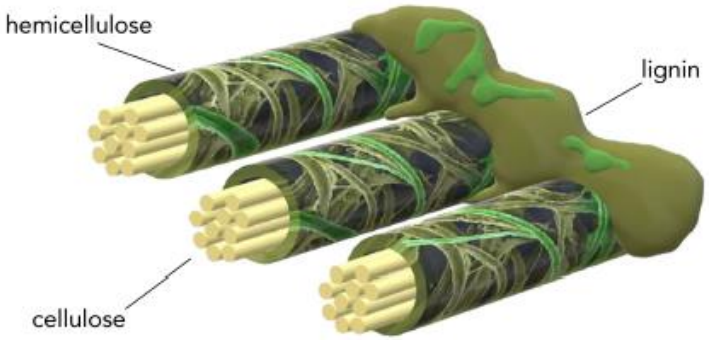

Figure 1. Structure of biomass (adapted)[1].

Among the various alternatives that have been taken into account to diminish the use of fossil resources, renewable biomass is considered as one of the best solutions to obtain biofuels and platform chemicals[2]. Biomass, mainly lignocellulose, is every organic substance that derives directly or indirectly from the photosynthesis process[3], the reaction between carbon dioxide (CO_2), water and sunlight to produce carbohydrates. Lignocellulosic biomass is heterogeneous and is a combination of naturally derived materials, as well as all the materials composed of organic matrix, except for the ones deriving from fossil materials[4]. Depending on the source, that might be weeds and wild-growths[5], woody species, aquatic crops or wastes[1], their composition changes and so the way they should be treated. Lignocellulosic biomass is mainly composed of cellulose, hemicellulose and lignin (Figure 1), but their amounts differ from source to source[1]; for example, woody species have a much higher lignin content compared to the other types of biomass[4]. It is important to mention that, even if the technologies might differ, the total amount of energy that could potentially be recovered from a biomass is the same, what changes between technologies is the actual amount of energy recovered and the form[4]. The treatment of lignin is the most challenging step[6] and it can be done in several ways: chemical, biological, thermochemical or by using catalysts, the choice will depend on the type of lignin used and on the target product[7]. The principal products that are obtained from lignin are part of three macro-groups: biofuels, macromolecules and aromatics.

Cellulose (Figure 2) is the most abundant organic polymer that can be found in nature, possessing a structural function in plant cell walls[1]. It is a complex polysaccharide made of monomeric units of D-glucose linked by β-1,4-glucosid bonds, where each glucose is rotated of 180° compared to the previous, in this way the basic repeating unit is cellobiose[8]. The intermolecular hydrogen bond between the hydroxyl group with C-3 carbon and the oxygen of the glycosidic ring influences both reactivity and morphology of cellulose chains[9] and can be the cause of the formation of crystalline zones due to the stabilization and the enhancement of the rigidity of macromolecules[8]. This fact may influence the accessibility to its functional groups and reduce the reactivity. On the other hand, amorphous regions of cellulose are the most reactive of this macromolecule, being also the most exposed part. The hydrolyzation of cellulose starts from here and it is possible to obtain glucose, cellobiose and small polysaccharides[1].

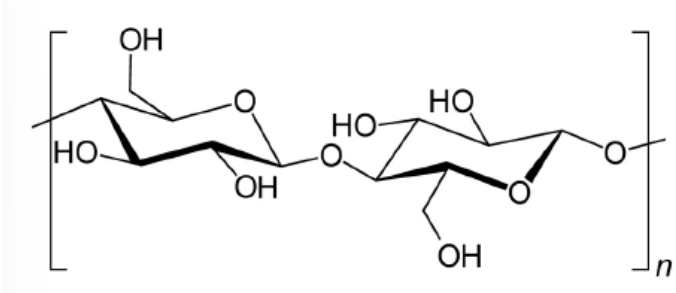

Figure 2. Structure of cellulose (adapted)[1].

Hemicellulose (Figure 3) is the second major constituent of the plant cell walls and consist of heterogeneous branched polysaccharides. Depending on the type of plant, the content and structure of hemicellulose may vary by changing the way sugar units are arranged with the substituents and their proportions[10]. It entirely consist of pentose and hexose sugars, like xylose, glucose, mannose and similar[4], and on contrary of cellulose is amorphous and has adhesive properties[11].

Lignin (Figure 4) is made of amorphous aromatic polymers with a three-dimensional network[1]. The monomeric units are held together by different ways: through oxygen bridges between different compounds, through carbon-carbon bonds[12]. In its structure, there are many polar groups and hydroxyl groups allowing the establishment of strong intramolecular and intermolecular hydrogen bonds. As said before and like hemicellulose, lignin composition varies depending on the plant species and can be between 25-30% up to 50% for very hard woods[13].

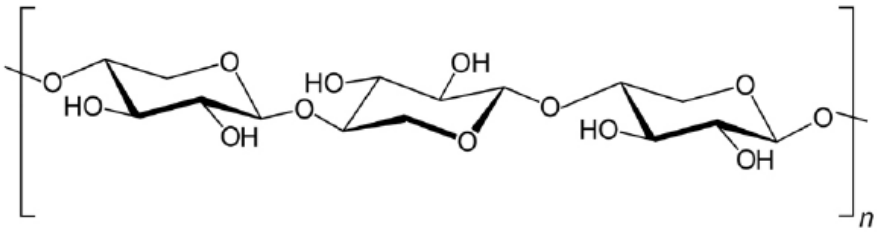

Figure 3. Structure of hemicellulose[1].

Biomass is considered carbon neutral material, meaning that the amount of CO_2 that they release is equal to the one that the plant absorbs during its lifetime, giving a total balance of zero carbon emissions[1]. The benefits of using biomass as energy source are several: starting from decreasing greenhouse gas emissions; moving to replacing the imported fossil fuels with local biomass reducing the dependence between countries; decrease in the waste disposal issues; as last, the possibility of developing economic opportunities in rural areas[14].

The main sources from which biomass is obtained are food crops, hydrocarbon-rich plants, wastes, weeds and wild growths, fast-growing grasses and woody species[5], algae and aquatic crops[1]. Among all these sources, food crops are a discussed and avoidable source, since they are in competition with the food market[5].

Herbaceous biomass comes from plants that have a non-woody stem and which die at the end of the growing season. They are divided into two main groups: agricultural residues and energy crops. Agricultural residues are by-products of food, fibers or food-industries and their availability differs depending on the region. However, energy crops are specifically cultivated for the bioenergy sector[1]. There are some particular type of plants that have a high potential to become source of fuel, these are hydrocarbon rich plants[15]. In these plants, the organics are generally concentrated in stem and bark, while the leaves contain a lower amount[5].

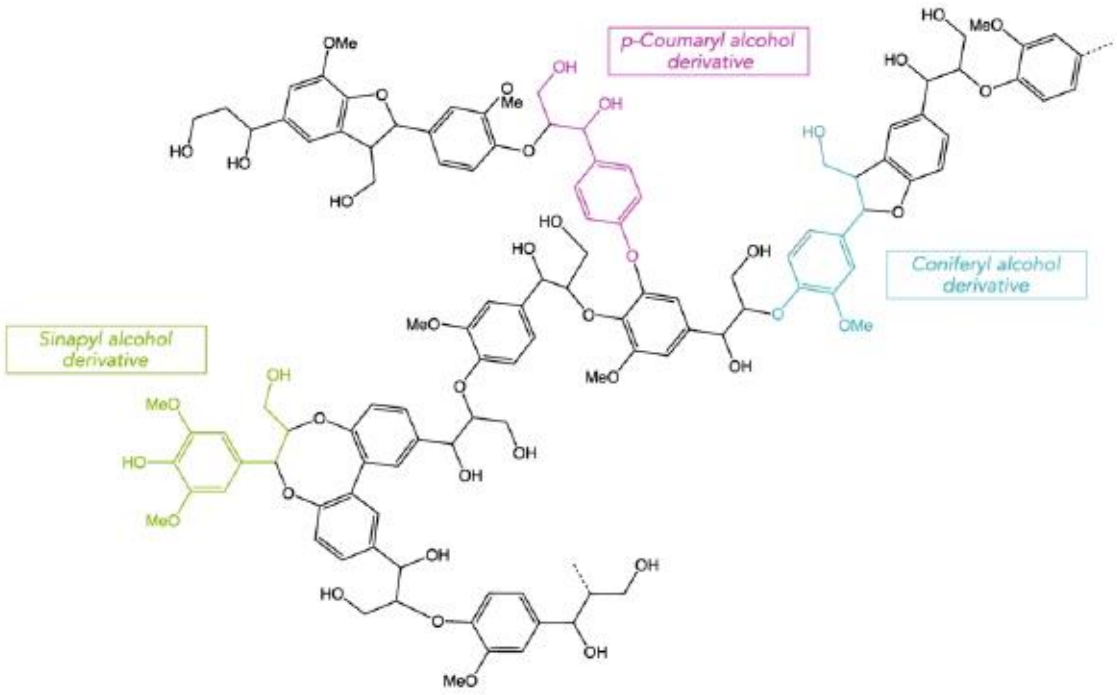

Figure 4. Structure of lignin[1].

The term waste is referred to agricultural residues, forestry, food, and others. Theoretically, they should be able to meet a high amount of energy needs, but actually the possibility of obtaining a great amount of energy from these plants is lower than expected because of technical challenges[5]. In the past, these wastes were recovered and sold as fertilizers, but the regulations have become more stringent overtime leading to the necessity of a proper waste management[16].

The upgrading and valorization of the compounds obtained from biomass is a significant issue. Usually, the effective transformation to valuable chemical products is carried out by using catalysts in different catalytic transformations, and it can be obtained different chemicals among which it can be found some important chemical building block[17].

1.2. Acid catalysts

The new resources and the new reaction conditions that are nowadays being improved every year imply always more frequently reactions in liquid phase, especially in water[18]. This requires a continuous adaptation of existing catalysts to these new experimental conditions, or the development of new approaches that fit better the new requirements[19]. Among catalysts, zeolites and supported metal oxides are taking in good consideration for biomass conversion[20] because they are able to provide good performance at an industrial level, even in the last developed conditions (Figure 5). This particular type of catalysts is called acid catalysts and are used in several and different applications from biorefineries to fine-chemical synthesis to biomass conversion[21]. Isomerization, etherification, hydrogenation are just some of the processes in which acid catalysts are used, even if they are mostly known for their application in petrochemical industry[22]. Zeolites and mixed metal oxides are the most used catalysts on industrial level because of their adaptable properties.

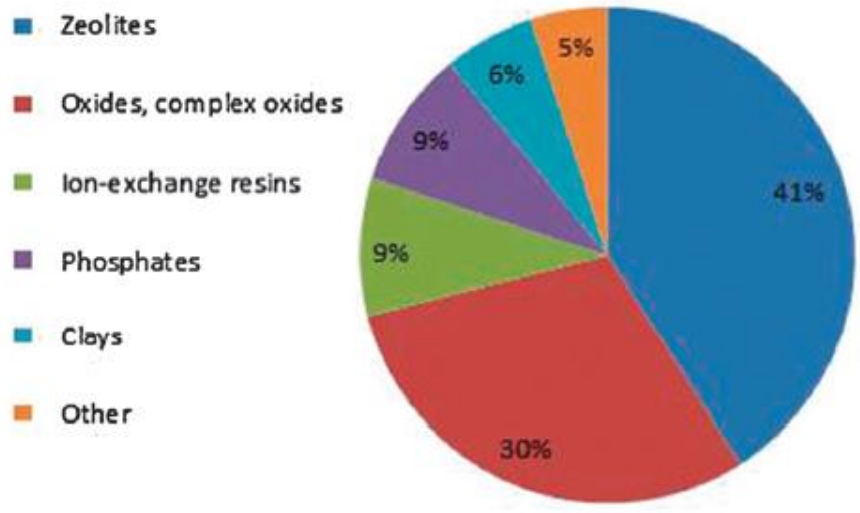

Figure 5. Heterogeneous catalysts with industrial relevance (adapted)[78].

1.3. Zeolites

Zeolites are widely used as catalysts both in glucose isomerization and HMF valorization. They present both Lewis and Brønsted acidic sites[23]. They are crystalline, hydrated aluminosilicates, whose general formula could be written as follows:

$$M_{x/n}[(AlO_2)_x(SiO_2)_y] \cdot wH_2O$$

In this general formula, M is the positive counter ion which balances the charge due to the (AlO_2^-) groups. The y/x ratio represents the Si/Al molar ratio and is a parameter important to describe the zeolite's properties[24]. The microscopic structure of each zeolite is based on the tetrahedral formed between a Si^{4+} or Al^{3+} cation and four oxygen atoms as shown in Figure 6.

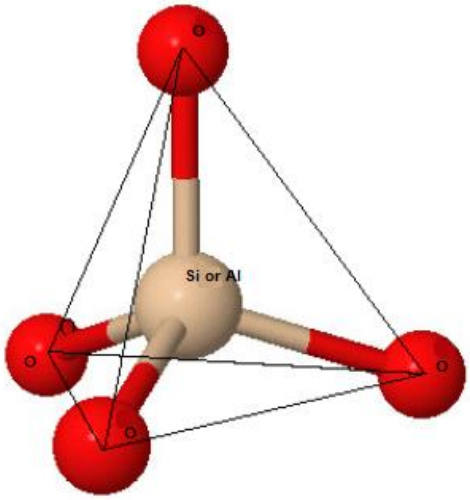

Figure 6. Zeolite tetrahedral structure.

Thanks to the micro/mesoporous crystalline structure and molecular sized pores, they have been widely employed as molecular sieves as well as catalysts that take advantage of shape selectivity[25]. The huge potential of zeolites lies in the possibility of controlling the size of these channels through synthesis, making them extremely specific. The diameter of a channel is determined by the type of structure and the number of oxygen atoms that are on the edge of the aperture ring. An example of this is the Y zeolite (Figure 7) that is characterized by spherical, large internal cavities linked tetrahedrally by pore openings of 0.8 nm[26].

Another important property that governs the zeolite's reactivity is the Si/Al molar ratio, because it influences both the water affinity and the quantity of positive counter-ions needed to balance the negative AlO_4^- charge. The quantity of positive counter-ions is strongly related to the amount of Al ions because, as said before, the negative charge needs to be balanced, so the

higher the amount of Al the higher will be the number of counter-ions present[24]. Regarding the water affinity, a higher Si/Al molar ratio corresponds to a high hydrophobicity and vice-versa. These properties are important to consider when performing a reaction to avoid the deactivation of the zeolite due to a massive water adsorption.

Concerning the counter-ion, its nature is also an important factor to take into account when synthesizing zeolites. Usually, the counter-ions that can be found are alkali metal ions, such as Li^+, Na^+ or K^+, or alkaline-earth metal ones, together with ammonium cation and they define the acidity of the catalyst, that is maxima when the cation is hydrogen, H^+ [27].

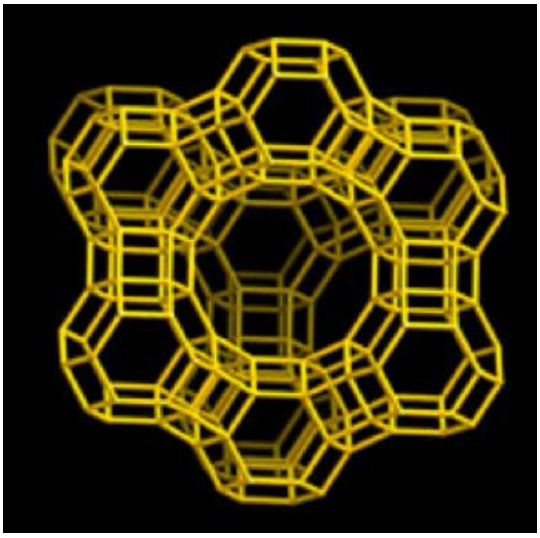

Figure 7. Structure of Y zeolite (adapted)[34].

Dealumination

The dealumination process is a top-down approach able to remove Al atoms to create mesoporosity and has been used in industry for years. The aim of this process is to hydrolyze Si-O-Al bonds to eliminate the Al and decrease the zeolite stability. This process can be adopted for different purposes but reducing the coke formation on the catalyst is one of the main objectives. Depending on the adopted dealumination process, the zeolites acidic properties (number and ratio of Brønsted and Lewis acid sites) might change due to the crystallinity changes and consequently the catalytic activity. There are mainly two ways to dealuminate a zeolite: using high temperatures or using low pH acid solutions[28].

The effect of high temperature calcination and steaming (400- 600 °C) on the acidity of the β-zeolites were studied by Otomo et al.[29]. It was discovered that at the same treatment temperature the steaming process produced lower Brønsted acid sites and a higher quantity of Lewis acid

sites. It was also seen that depending on the treatment temperature the Brønsted-Lewis sites ratio could be adjusted, revealing that increasing the temperature decreases the mentioned ratio.

The modification of zeolites with acid solutions can be done using phosphoric acids, nitric acids, oxalic acids or others. Zhang et al.[30] carried out a study with phosphoric acid. Compared with thermal treatment, in this case the loss of acidic sites is reduced. The main change that was discovered was related to the average pore diameter of the zeolite that increased after the treatment. The surface area seemed to be affected too but without a significant increase.

Zr-doped zeolites

Zirconium has been increasingly used in catalytic reactions because of its acidic properties and oxidizing capabilities. Especially in combination with zeolites it has proved to be a good catalyst for catalytic transfer hydrogenation reactions. The incorporation of Zr in the zeolite can occur in presence of Al atoms or after dealumination (Figure 8). There are several procedures to incorporate Zr atom in zeolites, the most important are wet impregnation[31,32], solid-state ion exchange[33], hydrothermal method[34].

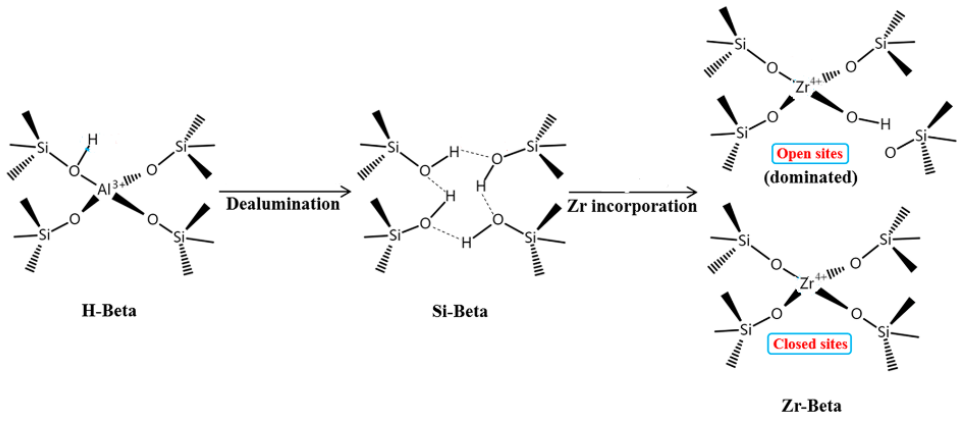

Figure 8. Zeolite dealumination followed by Zr incorporation (adapted)[33].

Among these methods, the most used procedure is wet impregnation. The method consists in pouring on the zeolite a solution containing the Zr precursor in the desired amount and then on drying the material. The working mechanism of this technique is the filling of the vacancies all over the material[32]. The main disadvantage of this method is the loss of material that can occur because of the excess of solution that is used.

The solid-state ion exchange involves the exchange of cations from one solid to another mediated by the presence of small quantities of water. This technique is extremely useful if the cations are hardly soluble or if they possess large hydration spheres that interfere with their

diffusion into zeolites cavities. It usually involves a thermal treatment of the zeolite and cation precursor mixture to facilitate the exchange[33].

The hydrothermal method uses water at high temperature and pressure and exploits its ability to hydrolyze and dehydrate metal salts. The particle size and morphology can be adjusted by changing concentration, temperature and reaction time. The Zr precursor is dissolved in an aqueous solution and then zeolite seeds in a acid solution are added to the previous one until an homogeneous mixture is obtained. Then, the crystallization is carried out in an autoclave at the required temperature[34,35]. The advantage of this technique is that it does not need excess of material because of the high working pressure.

In this study is explored the possibility of using a different technique that involves the grafting of the Zr precursor to the material before the temperature treatment.

1.4. Mixed metal oxides

Mixed metal oxides represent one of the most important and widely employed categories of solid catalysts[36], since they constitute the largest family of catalysts in heterogeneous catalysis and are utilized for their acid-base and redox properties[37]. Single metal oxides can crystallize with different morphologies at room temperature, even if many phases may remain amorphous at modest calcination temperatures[36].

Among the metal oxide catalysts, transition metals occupy the first place due to their low cost of production, easy regeneration and selective action. Their catalytic activity may be attributed to the presence of partially filled d-shells of the metal ion and to the influence of the oxide ligand field on this partially filled d-shell[36].

Metal oxides containing at least two different metal cations are known as mixed metal oxides. They are generally obtained in the form of powder, or single crystals, and have a wide spectrum of industrial applications[38]. They can be classified on whether they are crystalline or amorphous. The arrangement of cations of a given element differs by the co-ordination and the nature of the neighboring cations and this governs the type of bonding between the cations[36]. Even though this type of catalyst is usually a multiphase system, it is important to know that some phases are more active on some reactions than others, so their presence is essential to achieve good yields.

It has been demonstrated that some mixed metal oxide exhibits a better catalytic activity than single metal oxide in various reactions. These results can be attributable to an increase in both active acidic or basic sites and specific surface area[39].

Among the several mixed metal oxides that can be synthesized, multilayer polyoxometalates seem to be a good alternative of other solid acid catalysts to convert 5-hydroxymethylfurfural (HMF) into high value-added chemicals, through etherification reactions[40]. The use of these materials permits to obtain over 80% HMF conversion into ethoxymethylfurfural (EMF) with a selectivity of over 90%. Compared to supported transition metal oxides, these materials possess sites of good acidity and high stability in liquids[41].

A specificity of these layered materials is the possibility to intercalate molecules in their interlayers[42]. Layered $HNbMoO_6$, and its tungsten counter-part $HNbWO_6$, seemed to have a remarkable easy intercalation of reactants between the interlayer, thus an easy access to the acidic sites that are located in the interlayer region[43]. That is due to the particular structure of the material that is constituted of layers of randomly located MO_6, where M stands for both Mo and W, and NbO_6 octahedral with the cations in the interlayer region[44] as seen in Figure 9.

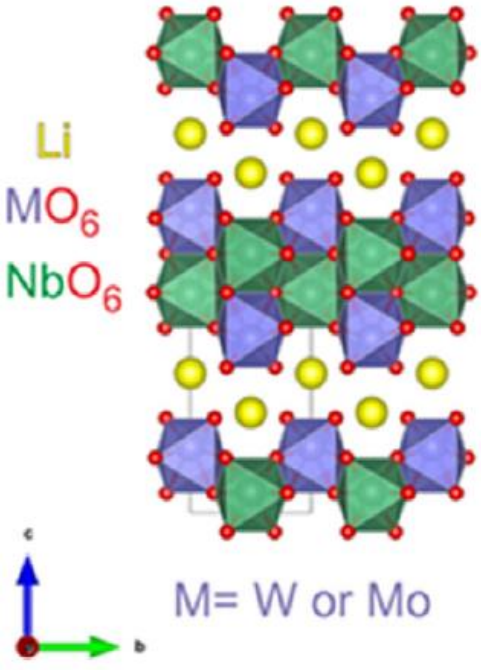

Figure 9. Crystal structure of $LiNbMoO_6$, where M=Mo, W (adapted)[88].

Wet and dry methods

There are two ways to obtain mixed metal oxides wet synthesis and dry synthesis. Wet synthesis is a method that involves liquid-phase precursors. Wet chemical techniques include chemical precipitation, chemical bath deposition, electrochemical deposition, microemulsion (Figure 10), hydrothermal and sol-gel[45]. The use of these techniques permits to obtain materials with a broad particle size distribution and a complicated morphology through a series of chemical reactions. The advantages of the wet chemical method are the flexibility of the process, adaptable to different needs, the high yields of product and the use of mild reaction conditions[46].

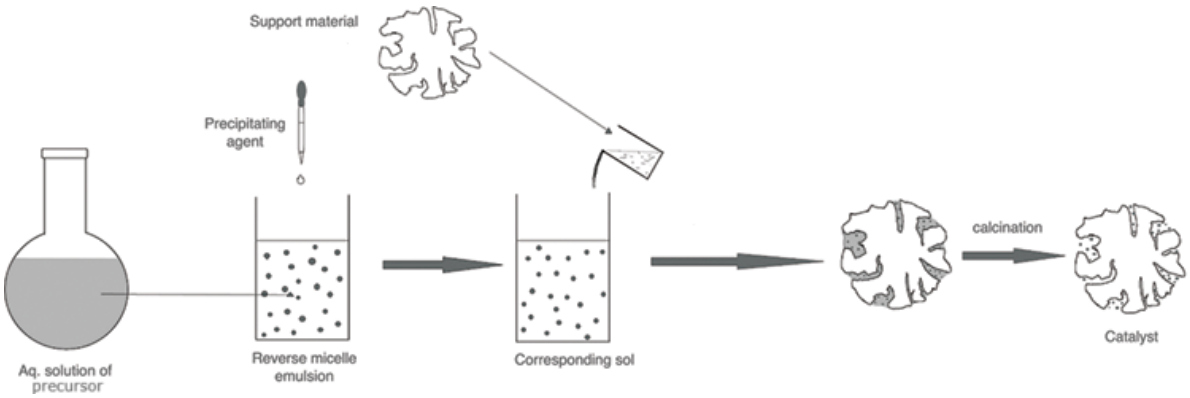

Figure 10. Example of wet chemical method: microemulsion.

Dry chemical method (Figure 11), also known as solid state synthesis, consists in placing the precursors of the material at really high temperatures and letting the reaction occurs in just one step. The overall reactions consist of melting, diffusion, nucleation, growth. This method has the advantage of being extremely simple because done in one step but the unfavorable kinetics and thermodynamics affect the yield of the technique[45].

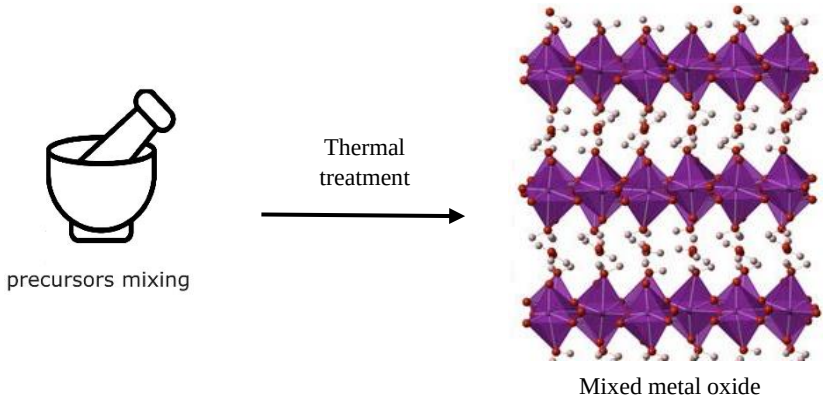

Figure 11. Dry chemical method scheme.

1.5. Isomerization of biomass-derived sugars

As described in Chapter 1.1., biomass represents one of the most promising carbon sources for chemicals. From biomass is possible to obtain carbohydrates, from which is possible to produce mono-saccharides. After the recovering of these monomers, the upgrading is necessary to synthesize commodity and fine chemicals.

The main monosaccharides that are obtained from biopolymers are D-glucose, D-fructose, D-xylose, L-arabinose, D-ribose, D-mannose and D-galactose[47]. Even if the most abundant building block is D-glucose, is possible to isomerize more available monosaccharides to obtain less common ones. As an example, D-xylose can be converted into D-xylulose or D-galactose into D-tagatose, a promising ketose in pharmaceutical and cosmetic applications.

1.5.1. Glucose isomerization

Glucose is the most abundant and the cheaper hexose present in nature[48] and it represents a promising alternative to petroleum derived raw materials for the synthesis of platform chemicals, fuel components or other base materials on the market[49]. Glucose isomerization into fructose is an important example of isomerization processes on an industrial scale[50]. Despite the lower natural accessibility of fructose, it is the most used hexose on the market[51] since it has the highest relative sweetness compared with all the naturally occurring sugars and, simultaneously, has the lowest glycemic index[48]. Fructose has also gained a lot of attention during the last years because it is used as starting material to obtain 5-hydroxymethylfurfural (HMF), levulinic acid and other building blocks[20] that can be further converted into fuels and monomers for biopolymers. It goes without saying that finding cheap and fast solutions to isomerize glucose to fructose is really important to proceed in the direction of renewable resources. Even if the glucose isomerization to fructose is favored under acidic conditions, there are some side reactions that can occur together with it. Glucose epimerization and etherification are two of these reactions and are favored by the use of both basic and Lewis acid catalysts even if Lewis' ones are more selective on isomerization[47] (Figure 12).

The most used industrial process for fructose production through glucose isomerization employs glucose isomerase as catalyst. Considering that it is an enzyme, it is important to keep some specific reaction conditions to avoid its denaturation, making it harder to improve the process[52] and to lower the costs. The fact that the glucose isomerization to fructose is limited

by the thermodynamic equilibrium does not simplify the process, because there is a limit that is not possible to overcome[53].

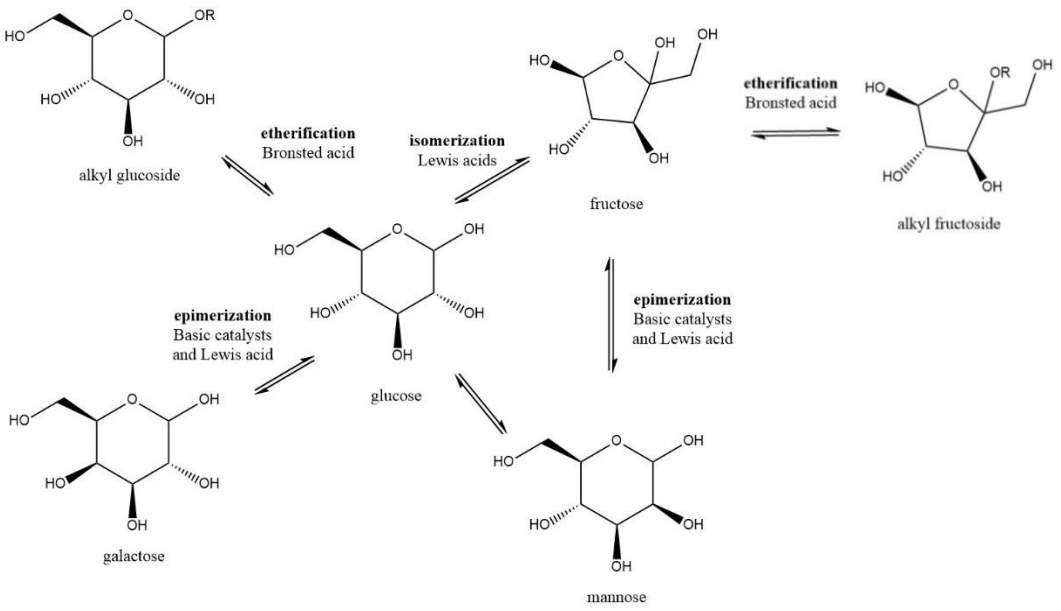

Figure 12. Reaction scheme of glucose isomerization and side reactions.

The reaction can be carried out under both acidic and basic conditions. Basic conditions were the first to be studied since 1885 and the reaction can also be called the Lobry de Bruyn-Alberda van Ekenstein transformation in honor of the discoverers[47]. Using a base, the reaction products are an epimeric aldose and a ketose that occur simultaneously[54] (Figure 13), even if usually the isomeric ketose is formed in higher amounts. The first catalysts used were sodium hydroxide or calcium hydroxide at high pH values and at room temperature[55] but, under these conditions the reaction rate was very low together with the selectivity[56]. The selectivity seemed to improve with the use of organic bases, such as amines, while the yield improved with the addition of borates or aluminates due to fructose complexation with an anion[57]. Indeed, anions such as borates are more prone to create stable complexes with ketoses than with aldoses[58] causing a shift in glucose-fructose equilibrium towards fructose. Nowadays investigation is focusing on heterogenous solid base catalysts such as hydrotalcites, zeolites in alkaline-exchange form and anion exchange resins. The reactions are usually conducted in a water-alcohol mixture[59] and with temperatures not higher than 120 °C to preserve saccharides stability. Even if these are newly studied zeolites, the kinetic is strongly controlled by thermodynamic so that fructose yield is theoretically around 50%[53], in practice it usually does not exceed 35%[60].

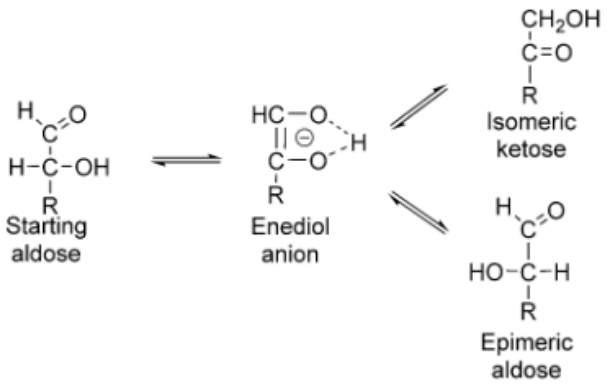

Figure 13. Isomerization of aldoses using base catalysts.

Acid catalyzed isomerization was studied much later than basic one considered that classic Lewis acids are deactivated in water[61]. Among the others, Sn silicalite with β-zeolite topology (Sn-β-zeolite[53]), mesoporous-Sn-MFI [62] are the ones that have produced the most promising results permitting to obtain respectively 55% and 35% glucose conversion and 32% and 25% fructose yield. The progressive interest in the Sn-β-zeolite have led to the proposal of a mechanism mainly divided in 3 steps: coordination of glucose to an active site; intramolecular hydride shift from glucose C2 to C1; fructose desorption[56]. More recent researches have focused on Ti-β-zeolite, discovering a new mechanism that involves an hydride shift from C1 to C5[63] and led to obtain 26% conversion and 14% fructose yield (Table 1).

Catalyst	Temperature (°C)	Conversion (%)	Fructose yield (%)	Mannose yield (%)
Sn-β-zeolite	110	55	32	9
mesoporous-Sn-MFI	80	35	25	1
Ti-β-zeolite	110	26	14	5
$AlCl_3$	120	32	26	-
$SnCl_4$	120	18	5	-

Table 1. Catalytic tests with different catalysts and relative results on glucose isomerization.

An interesting new approach on glucose isomerization was proposed by Saravanamurugan et al.[51] and consists in carrying out the reaction in two steps using an alcohol as solvent in the first step and water in the second. In the first step (Figure 14), glucose is isomerized to fructose, but it is immediately converted into an alkyl-fructoside, because it reacts with the alcohol in the alcoholic media. In the second step (Figure 14), water is added to the same reactor, without removing the alcohol, and hydrolyzes the alkyl-fructosides to obtain fructose[51]. This same procedure was seen to be effective also on xylose isomerization to xylulose[64].

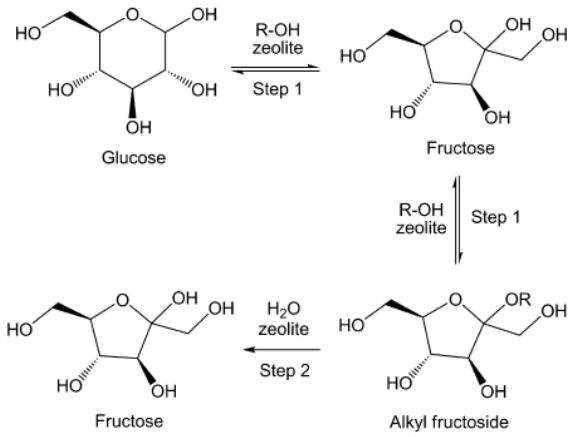

Figure 14. Reaction mechanism of the two-step glucose isomerization (adapted).[39].

1.6. 5-hydroxymethylfurfural (HMF)

1.6.1. Production

The interest to furanic derivatives from biomass sources has been grown significantly in the last decades[20]. These five-membered ring compounds are attractive because of their multifunctionality, as they can possess a furan ring, hydroxyl, carbonyl and carboxylic groups and because they come from renewable sources, which are abundant, diverse and cheap. HMF is the main candidate in replacing the oil-derived platform molecules in polymers' production, chemicals and fuels. The production of HMF (Figure 15) is a field that has been studied since the 19th century, even if with low research activities until the middle of the century when the first review article was published[65]. The first research interest was towards producing HMF from carbohydrates in an aqueous-based catalyzed system[66]. The temperature used varied from 100 to 300 °C and the reaction time from seconds to hours[67]. The main problem was the low yield, below 50% from fructose[20]. The continuous improvement of catalysts together with the screening of various solvents has led to an improvement of the HMF final yield and of the experimental conditions[67].

HMF is a heterocyclic furanic molecule substituted in 2,5-positions with hydroxide and aldehyde functionalities[68]. It is a multifunctional molecule because it contains an aromatic alcohol, an aromatic aldehyde and a furan ring system[69], so it can both be oxidized to a dicarboxylic acid or reduced to a diol[68]. Recently, many catalytic pathways for production of HMF via acid-catalyzed dehydration of different C6 carbohydrates, such as fructose and glucose, have been described[70–72]. The use of glucose results in lower yields due to the higher stability of glucopyranoside ring structure compared to fructose[73,74].

The production of HMF starting from a C6 fraction is quite complex because several reactions occur together[2]. The ideal process should be in three steps:

1- Hydrolysis of glucan to glucose
2- Isomerization of glucose to fructose
3- Dehydration of fructose to HMF

Carbohydrates dehydration can be conducted in different systems. Single phase systems are the most economic ones and are divided into: simple aqueous phase systems, polar aprotic organic solvent systems, green solvent systems.

Simple aqueous phase systems study focused on the study of reaction conditions testing different catalysts groups: organic acids, metal halides, metal oxides and phosphates in fructose dehydration. The investigation led to low HMF yield and selectivity due to the poor stability and the high solubility of HMF in water, reaching a maximum of 60% HMF yield using FeVOP[75].

With polar aprotic organic solvent systems we refer to all the tests that use DMSO, dimethyl acetamide or N-methyl pyrrolidinone as solvents. Among these three solvents, the most used in carbohydrate dehydration is DMSO that was tested with both homogeneous and heterogeneous catalysts and HMF yields over 80% were obtained using many different systems[76]. As an example, using $LaCl_3$ 95% yield was obtained, while with $Sc(OTf)_3$ an 83% yield was obtained[77]. A consequent study showed that using high boiling point aprotic solvents leads to higher HMF yields. The main problem of this systems is the isolation of the products that is either energy intensive or consumes a large amount of solvent, making it not adaptable to bigger scales[67].

Green solvent systems utilize environmentally friendly, readily available and cost-efficient solvents with a low boiling point such as 1,4-dioxane, tetrahydrofuran (THF) or valerolactone (GVL). Alcohols can be part of this system too since they are environmentally friendly and possess a variety of boiling points. Several solid acid catalysts were tested using this type of systems leading to obtain 87% HMF yield with Amberlyst 15 in iso-propanol[78].

Biphasic systems are carbohydrate dehydration reactions that are performed in a combination of two solvents such as aqueous-organic. They have the main advantage of extracting the HMF in situ, reducing the costs and avoiding HMF decomposition in water[79]. Several studies were done by testing different catalysts and reaction conditions but the most important progress was

done in 2000 when a reaction system for the direct conversion of fructose to furandicarboxylic acid (FDCA) were done. The reaction was done in a combined process that used a reactor equipped with a membrane that allows only HMF passage avoiding the interference between the acidic dehydration and the oxidation[80]. Nevertheless, the efficiency of the process was too low to be industrially relevant but it gave an important boost to the development of other systems.

The last type of system studied for carbohydrate dehydration is based on ionic liquid, that can also be used in a biphasic ionic liquid-solvent system. Within these systems it was possible to obtain quite good results but their high costs and low stability at high temperatures makes them extremely difficult to be used on large scale[67].

Carbohydrate dehydration is the main pathway followed to obtain HMF, but a less impactful alternative might be to start directly from the raw lignocellulosic biomass. In this way, the treatments needed to transform the biomass into a purified bio-based feedstock are avoided and both the energy consumption and the CO_2 emissions are reduced[2].

The mechanism of HMF synthesis depends on the fructose configuration, cyclic or linear (Figure 15). In the cyclic configuration, D-fructofuranose is dehydrated to form a carbenium ion, which undergoes three subsequent dehydration steps to obtain HMF. In the meantime, linear D-fructose is isomerized into a 1,2-enediolglucose, which can suffer from three dehydration steps through 3-deoxy-hexosulose and 5,6-dihydroxy-2-oxohex-3-enal formation, resulting in HMF[81,82].

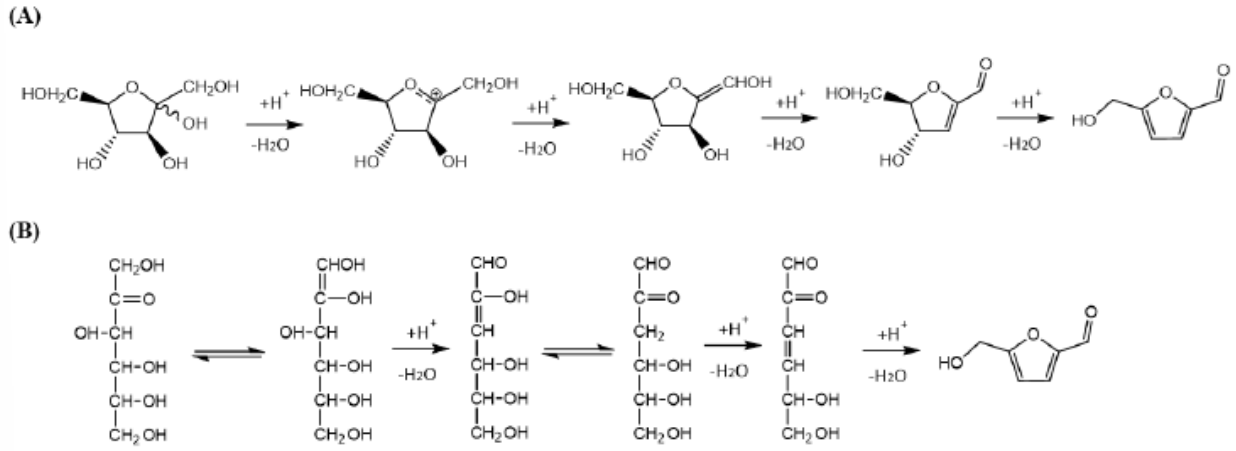

Figure 15. Mechanism of cyclic D-fructofuranose (A) and linear D-fructose (B) dehydration to HMF[32,33].

1.6.2. Upgrading

HMF is considered a 'sleeping giant' because of its enormous market potential, but the difficulties in storing it for long periods of time due to its low stability[83]. Starting from HMF is possible to obtain several products depending on both the catalysts and the experimental conditions (Figure 16).

Oxidation of HMF can be used to obtain FDCA and 2,5-diformylfuran (DFF), a precursor of pharmaceutical agents, biopolymers and furan-urea resins[84]. It's a reaction catalyzed by both homogeneous and heterogeneous systems. The catalysts that resulted in the best product yields were noble metal (Au, Pt, Pd) supported on an oxide in an aqueous media under high pH conditions. It is the need of high pH conditions and therefore the necessity of large amounts of base represents one of the main disadvantages of this oxidation reaction.

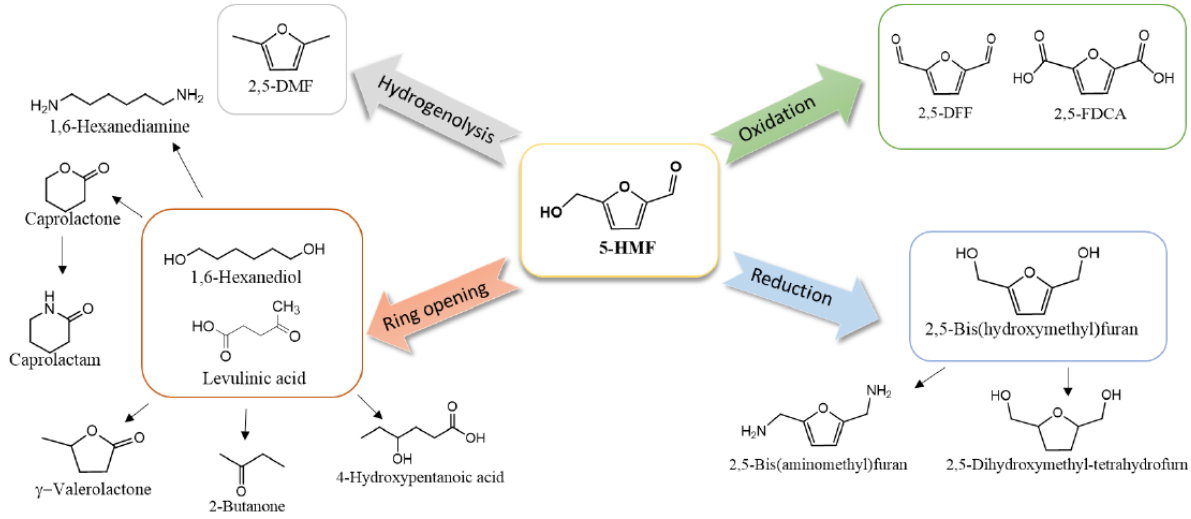

Figure 16. Different routes that 5-HMF can follow to obtain building blocks (adapted)[2].

HMF reduction has also gained incredible attention because is possible to obtain 2,5-bis(hydroxymethyl)furan (BHMF), DMF, linear polyols and diketones that be used as fuel additives, in polymers and pharmaceutical industry. This particular type of reaction involves the aldehyde and hydroxy group and the furan ring meaning that multiple reaction networks may occur during the conversion[85]. It was seen that the development of active sites able to be selective on the different HMF functional groups was extremely important. For example, it is reported that single-atom Pd and Pd nanoparticles supported on TiO_2 worked for the hydrogenation of ketones and aldehydes.

Rehydration of HMF with consequent ring opening is one of the side reactions that can occur during the carbohydrate dehydration for HMF synthesis. The main products of this reaction are levulinic and formic acids, two important building blocks in the polymer industry[86]. Because of the presence of Bronsted acids in the depolymerization of biomass, it is more cost-effective to produce levulinic acid and formic acid directly from the biomass treatment instead of first obtaining HMF and then converting it.

1.6.3. HMF etherification

HMF etherification is another upgrading solution to obtain interesting chemicals. Among the various approaches used for the production of biofuels, etherification of HMF seems a very promising route[87]. Indeed, these ethers have been recognized as intermediate in the pharmaceutical industry, non-ionic surfactants and oxygenated fuel additives[88]. The attention of researchers has been attracted by the etherification of furan compounds to furanic ethers, since furfuryl ether was first patented by Shell in 2009[89].

There are two ways to obtain furanic ethers and both of them require an acid catalyst (Figure 17). The first route exploits Brønsted acid sites and is also called direct etherification. The second route involves Lewis acid sites and is called reductive etherification[90].

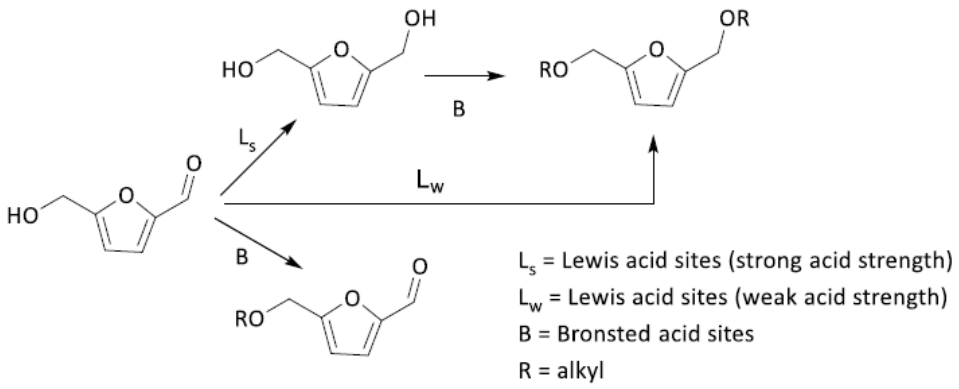

Figure 17. Route of the conversion of HMF to etherified products (adapted).

Reductive etherification can be divided in two steps. In the first one, there is formation of an intermediate through the use of an alcohol as the hydrogen source, through a CTH reaction, and it requires, as explained before, a bifunctional acid-base catalyst, or a Lewis acid catalyst[91]. The appropriate acidity and basicity is necessary to achieve high selectivity toward (hydroxymethyl)furfuryl alcohol[92]. Metal isopropoxide cations are produced in alcohol solutions with metal chlorides, through an alcoholysis reaction and then they act as a catalyst

for the reduction of 5-hydroxymethylfurfural. Metal isopropoxides are easily hydrolysable due to their hygroscopicity, causing the formation of various metal species that may have different catalytic activities[93].

Regarding the catalyst acidity needed for the etherification of HMF, several studies have been conducted[87,94]. It was found that Al_2O_3, ZrO_2, TiO_2 that possess purely Lewis acid properties, were extremely active for the etherification of 5-hydroxymethylfurfural. On the other side, it was demonstrated that Sn-beta zeolites were active on both etherification and catalytic transfer hydrogenation reaction of HMF, due to the presence of both strong and weak acid sites[87,94]. When instead Al_2O_3 was supported on a SBA-15 silica, acid properties changed and Brønsted acid sites were present. The modification of acidity caused a change in the selectivity of the reaction resulting in an inhibition of the CTH process[87]. A different result was obtained when ZrO_2/SBA-15 was used. In this case, the Lewis acid sites were not inhibited by the presence of weak Brønsted acid sites, leading to the same product as the unsupported catalyst[87] (Table 2).

Catalyst	Temperature (°C)	Conversion (%)	Product	Yield (%)
Al_2O_3	180	11.1	Isopropoxyfurfuryl alcohol	7
ZrO_2	180	7.1	2,5-bis-hydroxymethylfuran	6.5
TiO_2	180	3.7	2,5-bis-hydroxymethylfuran	3
Al_2O_3/SBA-15	180	60	isopropoxymethylfurfural	95
ZrO_2/SBA-15	180	75	2,5-bis-ispropoxymethylfurfural	70

Table 2. Catalysts tested on literature on HMF etherification and their activity.

The use of mixed catalysts to etherify HMF in ethanol was also studied, discovering that several supported metal catalysts were extremely effective in the studied reaction under mild conditions[95]. It was seen that, together with the etherified compounds, the production of intermediate hemiacetal and acetal compounds was detected[74]. In addition, reaction temperatures higher than 120°C caused further ethanolysis of 5-ethoxymethylfurfural (EMF) to produce alkyl levulinate, especially occurring with catalysts having strong Brønsted acid sites[96].

In the direct etherification, the etherification of 5-HMF is separated from hydroxyfurfuryl formation. In this case, the concentration and type of acid and base sites influence the

conversion of hydroxyfurfuryl alcohol to furanic ethers. The presence of moderately strong acid sites seemed to favor a high selectivity to furanic ethers[97]. To accelerate the etherification reaction, the presence of Lewis acid sites was seem to be very important[98], but it is the combination of them with the Brønsted ones that gives the best results. Indeed, Brønsted acid sites seem to be responsible for the high catalytic performance[98].

1.7. Catalytic Transfer Hydrogenation (CTH)

Catalytic transfer hydrogenation (CTH), known also as Meerwein-Pondorf-Verley (MPV) process, is an hydrogenation reaction where there is no need to use pressurized hydrogen and it can avoid the use of high pressure conditions. Instead, it utilizes an hydrogen donor to carry out the substrate hydrogenation[99]. The hydrogen donor is usually highly available, inexpensive, easy-to-handle and a renewable chemical, such as alcohol, formic acid, formate and hydrosilane[100,101]. The use of this particular process has the advantage to produce smaller amounts of side products and to be active with the use of inexpensive and non-sensitive catalysts[102].

The general principle of this process is the transfer of a hydride and a proton from the hydrogen donor AH_2, for example an alcohol, to an acceptor B, like a ketone or an aldehyde, which is then reduced[99]. The process can be carried out following two main pathways: direct hydrogenation transfer and metal hydride route[101].

$$AH_2 + B \underset{\leftarrow}{\rightarrow} A + BH_2$$

Direct hydrogen transfer route

Through direct hydrogen transfer route, the hydrogen is transferred directly from the donor (alcohol) to the acceptor (carbonyl group) through the formation of a cyclic six-membered transition state[103]. This mechanism occurs especially when a catalyst with an electron deficient Lewis acid site and a neighboring base site is used [99]. Even though there are still some concerns about the roles of acidic and basic sites, when strong basic sites start the reaction (Figure 18a), they absorb a proton from the alcohol and facilitate the formation of a six-membered intermediate between alcohol, aldehyde and acid sites. Then α-H is transferred to the carbonyl group of the aldehyde[104]. If instead the lead of the reaction is of acidic sites (Figure 18b), they bond with electron-rich oxygen from hydroxyl and carbonyl groups to form six-membered intermediates and promote the hydrogen transfer from alcohol to aldehyde. In the meantime, basic sites attract the hydrogen from the hydroxyl group to weaken the O-H group[105].

The most investigated catalysts that are shown to follow this route are metal-organic hybrids, metal-based carbon materials, zeolites. Indeed, these materials possess both acidic and basic sites with suitable strength and, in addition, show excellent thermal and chemical stability. Metal-organic hybrids based on Zr and Hf with the inclusion of phosphate or carboxylate groups, that create the right basicity, shown a great catalytic performance, with high conversion rates and etherified product yields even at mild temperatures between 80 and 150 °C, showing a HMF conversion above 90% and over 80% 2,5-bis-hydroxymethylfuran (BHMF) yield. Moving to metal-based carbon materials, they showed improved activity when modified with the introduction of different groups such as -SO_3H that create Bronsted acid sites or N-containing that simply increase the basicity of the catalyst. Last catalyst group is zeolites that possess both acidic and basic sites and have adjustable acidity, basicity and pore structure[101]. The incorporation of Zr in the catalyst was seen to be essential to increase the activity on CTH of the catalyst both if located in the framework (Zr-doped materials) or on the surface (Zr-loaded materials).

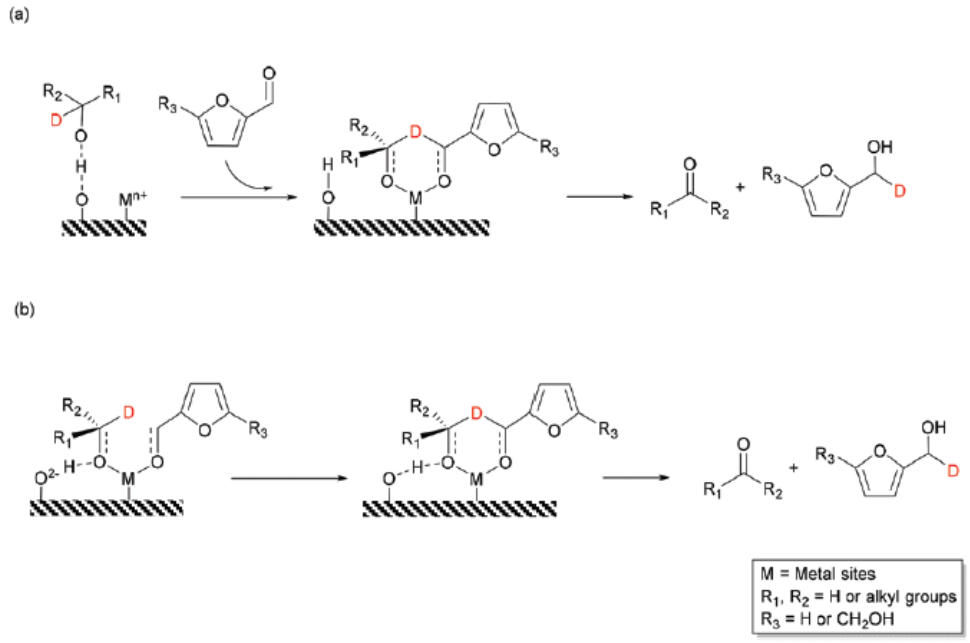

Figure 18. Two different mechanism of direct hydrogenation transfer route:
(a) basic site is the lead, (b) acid site is the lead[94].

Metal hydride route

The hydride metal route takes place in the presence of a transition metal and requires the formation of a metal hydride. The metal catalyst is supposed to remove the hydrogen from the donor through β-hydride elimination. The hydrogen is then transferred from the metal to the carbonyl of the acceptor[99]. In this route, there are two possible pathways (Figure 19) that depend

on the number of metal sites involved. The involvement of multiple metal sites provides active centers for both the abstraction of hydrogen from the alcohol and the adsorption of CO from the substrate. Meanwhile, single metal sites can't activate the substrate together with the alcohol[101].

Metal hydride route is promoted by the use of metal oxides and Cu, Co, Ru, Pd and Ni based catalysts that facilitate the hydrogen adsorption from the hydrogen donor due to their strong dehydrogenation properties[106]. Furthermore, these catalysts possess Lewis acidic sites that promote the O adsorption of the substrate carbonyl group. Even if all the metals before mentioned shown great CTH efficiency, the combination of two or more of them on the same support increased the selectivity. For example, the introduction of Cu into Ni improves the selectivity of the main product suppressing the opening of the furan ring. Another example is the combination of Cu with Pd that reduce the selectivity towards the hydrogenation of the double bonds[67]. Therefore, the use of muti-metallic catalysts improves the selectivity of the CTH reaction if compared to the single-metal catalysts.

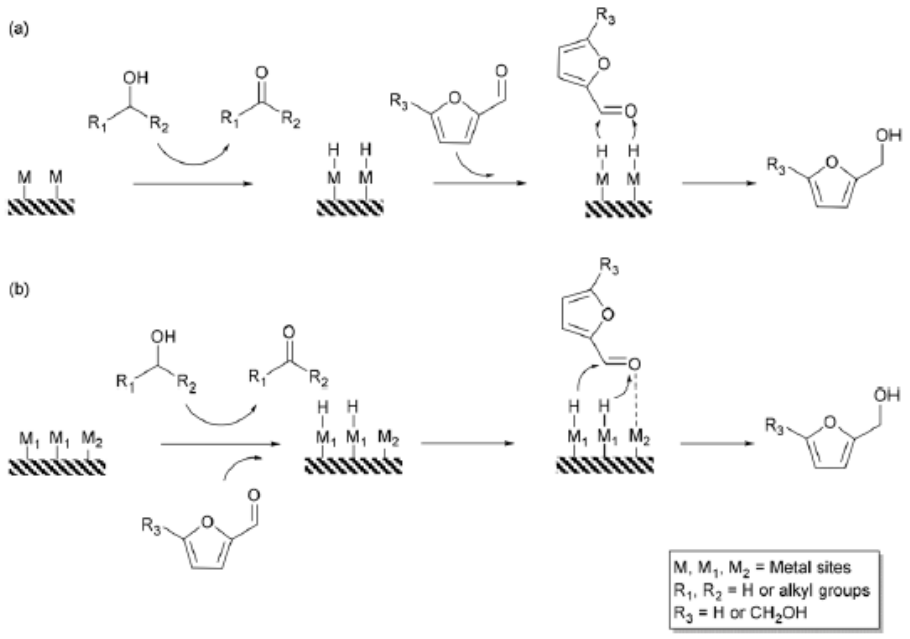

Figure 19. Scheme of the two possible pathways of metal hydride route: (a) one metal site, (b) multiple metal sites[94].

Hydrogen sources

As said above, the advantage of CTH is that it uses a renewable and liquid-phase as hydrogen source instead of pressurized H_2. There are main hydrogen sources that are used: alcohols, formic acid and hydrosilane.

Alcohols are extremely suitable hydrogen sources due to their low costs, sustainable production, easy preparation and to the fact that they can be used as solvents in the reaction[107]. Among the various alcohols available methanol, ethanol and 2-propanol are the most studied. Methanol is the most convenient H_2 donor from an atom economy point of view but, compared to the other two alcohols, is more threatening to the environment. In addition to that, the reaction conditions necessary to obtain the CTH using methanol are harsher than the one necessary using the other alcohols. Further research is necessary to optimize this reaction with methanol as H_2 source. Ethanol and 2-propanol, due to the milder reaction conditions, are able to enhance the selectivity of the products making them the most attractive H_2 donors among alcohols[108]. Ethanol is a primary alcohol while 2-propanol is a secondary one and this difference influences the reaction in different ways. The use of primary alcohols was seen to lead to preferential acetalization. On the other hand, the use of secondary alcohols enhanced the selectivity and the conversion of the substrate. Tertiary alcohols were tested as well but they strongly decreased the conversion because they did not possess a β-H[107].

Formic acid is a sustainable alternative as well, since it is a compound that can be obtained from biomass oxidation, is convenient and is safe. It is already largely utilized in hydrogenation reactions together with various catalysts[109]. If compared to alcohols, the main disadvantage that occurs when formic acid is used at high concentration is the corrosion that requires the use of corrosion resistance equipment that raises the costs. Because of that, the possibility of using polymer-loaded formats seems to bring several advantages: corrosion is reduced, reactivity is improved together with the product purity[110].

Hydrosilane compounds, such as polymethylhydrogensiloxane (PMHS), are low price and non-toxic materials that can be exploited as hydrogen sources due to the difference in electronegativity between Si and H atoms. This difference can be activated by a catalyst to produce H^+ and then applied as hydrogen donor[111]. Hydrosilation is an interesting reaction that has been extensively developed in the last years because of its high selectivity, mild reaction conditions and high sustainability.

2. Aim of the work

The aim of the presented study is to synthesize catalysts possessing both Lewis and Brønsted acidic sites where the ratio of the acid sites could be tuned and that can be selectively active in the reaction of HMF etherification to BIMF. The chosen catalysts to be studied are mixed metal oxides and Zr doped zeolites and they are characterized to evaluate the main reasons that led to different results in terms of catalytic performance. The HMF etherification reaction is optimized based on the reaction temperature, its reaction time, the amount of catalyst and the amount of Zr doping.

Another part of the study is focused on the optimization of glucose isomerization to fructose using commercial zeolite. In this case the study is focused on the improvement of the conditions of a two steps in one pot reaction based on the amount of the two solvents, the type of alcohol used and the possibility of adding an additional step to eliminate the first solvent.

3. Experimental part

This chapter is divided in 4 sections:

I. All the chemicals used in the study are listed.
II. Description of the catalysts' synthesis.
III. Description of the characterization technique used.
IV. Description of the catalytic tests and the products identification and quantification methods.

3.1. Chemicals

All the chemicals used are listed in Table 3

Formula	Name	Brand	Purity	Molecular weight (g/mol)
Li_2CO_3	Lithium carbonate	Sigma-Aldrich	99%	73.89
Nb_2O_5	Niobium oxide	Alfa Aesar	99.5%	265.81
MoO_3	Molybdenum oxide	Sigma-Aldrich	99.5%	143.94
WO_3	Tungsten oxide	Alfa Aesar	99.8%	231.84
HNO_3	Nitric acid	VWR	65%	63.01
$Zr(O(CH_2)_2CH_3)_4$	Zr n-propoxyde	Sigma-Aldrich	70%	327.57
$C_6H_6O_3$	5-hydroxymethylfurfural	Sigma-Aldrich	99%	126.11
$C_6H_{12}O_6$	D-Glucose	Sigma-Aldrich	99.5%	180.16
CH_3OH	Methanol	Sigma-Aldrich	99.9%	32.04
CH_3CH_2OH	Ethanol	Sigma-Aldrich	99%	46.07
$(CH_3)_2CHOH$	2-propanol	Sigma-Aldrich	99%	60.10
$C_6H_4(CH_3)_2$	o-xylene	Sigma-Aldrich	97%	106.16

Table 3. List of the chemicals used.

3.2. Synthesis of catalysts

3.2.1. Commercial zeolites

The three zeolites used in the glucose isomerization tests are commercially available and produced by Zeolyst International: CP814E (β-zeolite), USY-CBV500, ZMS5-CBV2314.

3.2.2. Synthesis of mixed metal oxides

The synthesis of the multilayered mixed metal oxide $HNbMoO_6$ and $HNbWO_6$ is performed by mixing stoichiometric amounts of the precursors: Li_2CO_3, Nb_2O_5, MoO_3 or WO_3, using ball milling for 1 hour. The obtained powders are calcined at 580 °C for 24 hours for the Mo-based oxide (a yellow powder is obtained), while the material containing tungsten is calcined at 760 °C for 72 hours (greyish powder). Both $LiNbMoO_6$ and $LiNbWO_6$ underwent an acid treatment to exchange the Li cations with the protons to obtain the H-form derivatives. This treatment is carried out by adding HNO_3 2 M to the powder and by keeping it under stirring at room temperature for 3 days with an intermediate exchange of the acid. When the acid was changed the catalyst was grinded in a mortar. The final powder is filtered using a small pore filter and washed several times with distilled water before being air dried. The whole process is shown simplified in Figure 20.

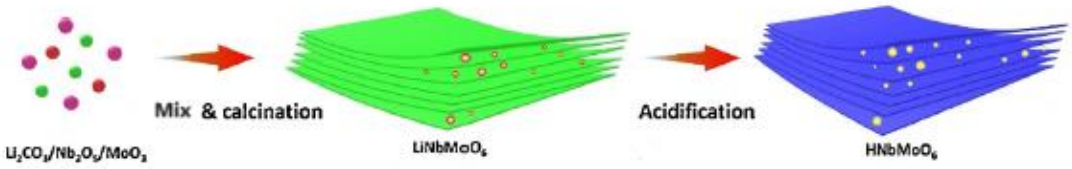

Figure 20. Scheme of the main steps of the preparation of the catalysts (adapted)[27].

3.2.3. Synthesis of Zr doped zeolites

The synthesis of Zr-doped zeolites started with the dealumination of zeolite (Zeolyst International, 100%). The dealumination was carried out in a HNO_3 aqueous solution (a mixture of 18.4 mL of water and 21.6 mL of HNO_3 per 2 g of zeolite) at 80 °C for 24 h. The mixture was then cooled and centrifugated to recover the zeolite, which was washed with deionized water to remove nitric acid. The so-obtained dealuminated zeolite was dried in a furnace at 200 °C overnight. 2.0g of the previously synthesized zeolite was immersed into dehydrated toluene (50 mL) together with $Zr(O(CH_2)_2CH_3)_4$, the Zr precursor, in the desired amount at room temperature to stabilize them with the silanol groups. The mixture was then refluxed at 125 °C

under N_2 atmosphere for 3 h. The obtained powder was filtrated and washed with hexane. Then it was dried at 100 °C, calcined at 500 °C for 5 h. The obtained samples were called as β-10_Zr, β-16_Zr, β-96_Zr depending on the Si/Zr molar ratio.

3.3. Physico-chemical characterization of catalysts

3.3.1. X-ray Diffraction (XRD)

The identification of the crystalline structure of the catalysts and to evaluate their stability after different treatments, XRD analysis was performed. Powder X-ray diffraction patterns were obtained using an X-Pert Pro-automated diffractometer (Figure 21), with a Ge (111) primary monochromator with Cu Kα1 radiation and a X'Celerator detector with a step size of 0.017◦.

Figure 21. X-Pert Pro-automated diffractometer.

This technique uses the interference of diffracted X-rays from crystallographic planes. The adopted model to interpret the phenomenon is the Bragg law:

$$2d \cdot \sin\theta = n \cdot \lambda$$

Where d is the distance between planes; Θ is the angle between the plane and the X-ray; λ is the wavelength of the X-ray; n > 0.

The crystallographic plane can be seen as a semi-transparent mirror, meaning that part of the incident light will be reflected and part will pass through to the next plane. The reflection is to

be intended as back-scattering of X-rays by the atoms belonging to the crystallographic plane of a photon with the same wavelength that the absorbed one but at a specular angle (Figure 22).

What is obtained is a diffractogram where the x axis is the Θ angle, usually expressed as 2Θ for instrumental reasons, and the y axis is the peak intensity.

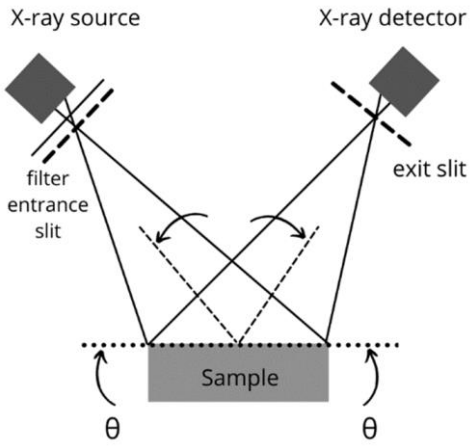

Figure 22. XRD scheme.

From the diffractogram is possible to obtain further structural information on the material like the crystallite size. Using the Scherrer equation is possible to link the full width at half maximum to the crystallite size:

$$FWHM(2\theta) = {K \cdot \lambda}/{L \cdot \cos\theta}$$

Where FWHM is the full width half maximum; λ is the wavelength; L is the crystallite size; K is the Scherrer constant.

3.3.2. X-ray Photoelectron Spectroscopy (XPS)

The surface composition of different solids was analyzed by X-ray photoelectron spectroscopy (XPS), using a Physical Electronics PHI 5700 spectrometer with non-monochromatic Mg Kα _radiation (300 W, 15 kV, 1253.6 eV) with a multichannel detector. Spectra were recorded using the constant pass energy mode at 29.35 eV with a 720 μm diameter analysis area. The C1s peak at a binding energy of 284.8 eV, assigned to adventitious carbon, was used as the reference for the peak correction. In addition, a PHI ACCESS ESCA-V6.0 F software package was used for acquisition and data analysis. The peaks were deconvoluted by using the least squares method, Gaussian–Lorentzian (90% G and 10% L) curves to more accurately determine

the binding energy (BE) values of the different element core levels, and a Shirley-type background line.

This quantitative technique is based on the photoelectric effect using photons of a specific energy to excite the electronic state of atoms below the surface. A detector records the electrons emitted by the surface and a spectra is obtained (Figure 23). This spectra represents the electronic structure for atoms at the solid surface created by the electrons ejected from layers not deeper than 10 nm. The spectra has the binding energy E_B on the x axis and the intensity I on the y axis.

The binding energy E_B is calculated:

$$E_{binding} = E_{Xray} - (E_K + \Phi)$$

Where E_{xray} is the energy of the x-ray photons; E_K is an electron's detected kinetic energy; Φ is the work function depending on the spectrometer and on the material.

The intensity I is calculated:

$$I = N \cdot \sigma \cdot \lambda \cdot K$$

Where N is the average atomic concentration of element in the surface under analysis; σ is the photoelectron cross-section for the element; λ is the inelastic mean free path of a photoelectron from element; K represents al other factors related to quantitative detection of a signal.

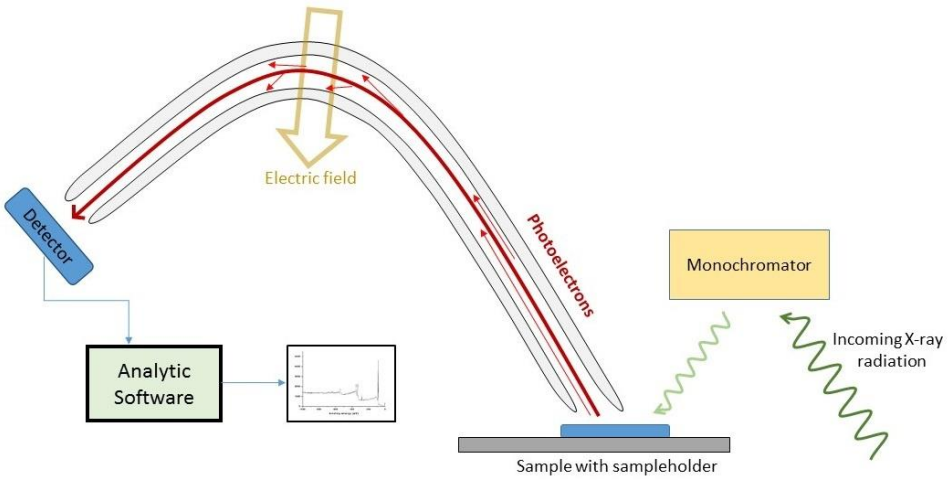

Figure 23. XPS scheme.

3.3.3. N_2 adsorption-desorption at -196 °C

The superficial area and porosimetry analysis were determined using a Micromeritics ASAP 2420 (Accelerated Surface Area and Porosimetry System) (Figure 24). Using this instrument, it is possible to obtain adsorption-desorption isotherms of N_2 at -196 ºC, that are build up varying the gas relative pressure at constant temperature and registering the gas volume adsorbed on the solid surface. The unit used for the measure is m^2/g.

This technique uses the Langmuir adsorption model to evaluate the surface area. This model assumes that the adsorbent is an ideal solid surface and the adsorbate behaves like an ideal gas at isothermal conditions adsorbed as a monolayer. The interaction between the adsorbate molecule and the adsorbent is treated as a equilibrium chemical reaction:

$$A_g + S \underset{\leftarrow}{\rightarrow} A_{ad}$$

Where A_g is the adsorbate molecule; S is an empty sorption site; A_{ad} are the adsorbed species.

The Langmuir adsorption equation can be derived from the kinetics or the thermodynamics and is the one that follows:

$$\Theta_A = \frac{V}{V_m} = \frac{p_A K_{eq}^A}{1 + p_A K_{eq}^A}$$

Where Θ_A is the fractional occupancy of the adsorption sites; V is the volume of adsorbed gas on the solid; V_m is the volume of the gas monolayer; p_A is the adsorbate partial pressure; K_{eq}^A is the equilibrium constant associated to the chemical reaction.

A modification of the Langmuir model that takes into account multilayer adsorption is the BET theory to measure the amount of gas adsorbed on the material. The analysis of the specific surface area (S_{BET}) happens after the cooling of the sample with liquid nitrogen. The model to calculate S_{BET} is:

$$\frac{\frac{p}{p_0}}{n(1 - \frac{p}{p_0})} = \frac{1}{n_m C} + \frac{(C-1)p}{n_m C p_0}$$

Where p is pressure, p_0 is saturation pressure, n is the number of moles adsorbed, n_m is the number of moles adsorbed in the monolayer, C is the BET constant relative to the heat adsorption.

A linear relationship is obtained by plotting $\frac{\frac{p}{p_0}}{n(1-\frac{p}{p_0})}$ versus $\frac{p}{p_0}$ from which the values of C and n_m can be calculated. The specific area of the material is determined from the value of n_m using the following equation:

$$S = n_m \cdot a_m \cdot N_a \cdot 10^{-21}$$

Where S is the apparent surface area (m^2/g), a_m is the area occupied by one adsorbed molecule (m^2/molecule), N_a is the Avogadro's number (molecules/mol).

Before the N_2 adsorption the sample needs to be outgassed under vacuum at 150 °C.

Figure 24. Micromeritics ASAP 2420 instrument.

3.3.4. Scanning Electron Microscopy (SEM)

The field emission scanning electron microscopy (FESEM) and energy dispersive X-ray (EDS) analyses for morphological and elemental mapping investigations were performed on FEI's Quanta FEG 650 microscope equipped with an Oxford XMax 50 Silicon Drift EDS detector (Figure 25).

Figure 25. FEI's Quanta FEG 650 microscope.

SEM is a non-invasive analysis that uses a focused beam of high-energy electrons to generate a variety of signals at the surface of solid specimens. The obtained signals allow to obtain information about the external morphology, chemical composition and crystalline structure and orientation of materials making up the sample. Different types of signals arise from electron-sample interactions such as secondary electrons, the one that produce SEM images; backscattered electrons; diffracted backscattered electrons, used to determine crystal structures and orientations of minerals; photons, used for elemental analysis and continuum X-rays, visible light; heat. X-ray generation is produced by collision of the incident electrons with electrons in discrete orbitals of atoms in the sample (Figure 26). SEM is also able to perform analyses of selected point locations on the sample. This approach is useful especially in quantitatively or semi-quantitatively determining chemical compositions using EDX.

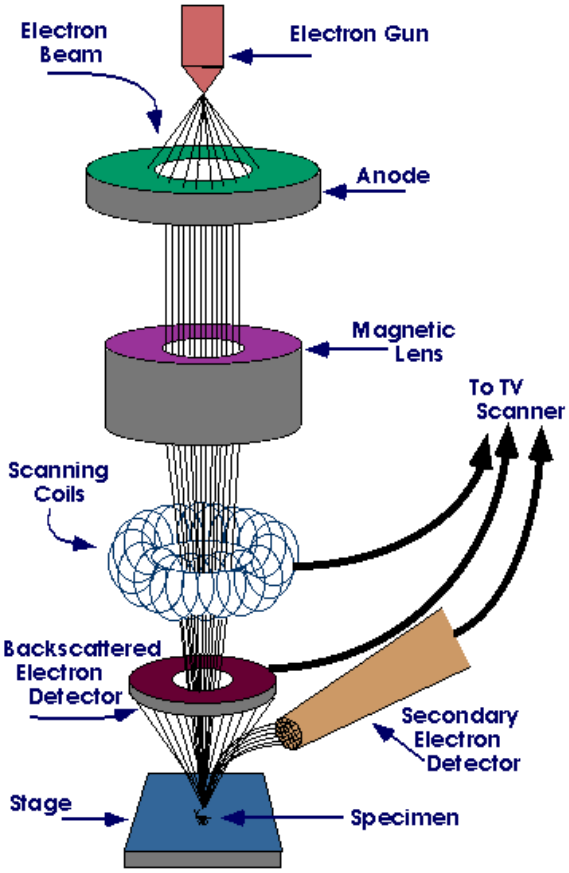

Figure 26. Scheme of how SEM works.

3.3.5. Elemental analysis: CHN

Elemental chemical analysis of carbon, hydrogen and nitrogen was performed using a Perkin Elmer 2400 CHN with a LECO VTF900 pyrolysis furnace (Figure 27).

Figure 27. Perkin Elmer 2400 CHN.

This analytical method is used to determine the elemental composition for C, H, N of a sample through combustion at high temperature in a pure oxygen environment of the material to convert the previously said elements in the corresponding gases CO_2, H_2O, N_2. Usually, a carrier gas is added, typically He. After the combustion the gas mixture is purified passing through an absorbent that traps impurities. Purified gases can be detected in two ways. They can be separated using a chromatographic column that then detects the individual gases with a thermal conductivity detector or they can be detected passing through a series of separate infrared and thermal conductivity cells (Figure 28). To obtain the content of each element the results are compared to theoretical values and then expressed as mass percentages.

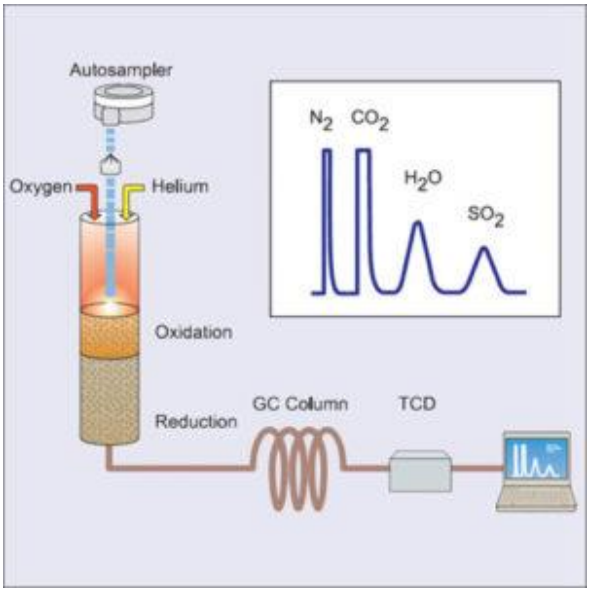

Figure 28. Elemental analysis scheme.

3.4. Catalytic tests

The reaction tests for both glucose isomerization and HMF etherification were done in glass tubular reactors closed with a screwable plug. The plug was equipped with a gasket to avoid the release of reaction gases and the entrance of air (Figure 29). The reactors were put inside a metal plate over a heating plate to keep the temperature with controlled magnetic stirrer at 450 rpm. At the end of the reaction, the reactor was immersed in cold water to quench the reaction. During all the reactions, the system was kept under continuous stirring.

For all the reactions tests that were done before closing the reactor was fluxed with nitrogen for 30 seconds to eliminate the oxygen dissolved in air and avoid any oxidation processes.

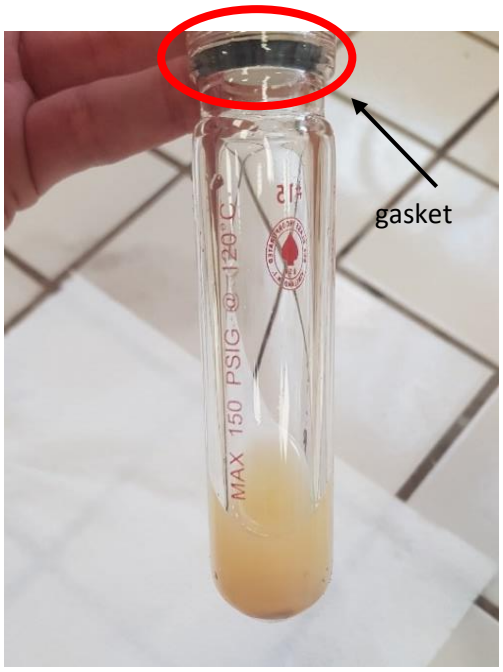

Figure 29. Reactor used, in the red circle is highlighted the gasket.

3.4.1. Catalysts recovery

The catalysts were recovered from the reaction mixture following three steps. First of all, the reaction mixture was centrifugated at 5000 rpm for 10 minutes to separate the catalyst from the liquid. The liquid was recovered in a beaker to be later analyzed, while the catalyst was dried at 100 °C overnight to let the solvent evaporate. The recovered catalyst was then sent to elemental CHN analysis.

3.5. Products analysis

3.5.1. Gas Chromatography (GC)

The liquid products obtained with the HMF etherification have been analyzed using a Shimadzu GC-14B chromatograph equipped with a flame ionization detector and a TRB-14 capillary column (Figure 30). For the analysis, the temperature was maintained first at 40 °C for 5 minutes before heating 10 °C/min until 280°C. It was followed by a plateau at the temperature of 280 °C.

Figure 30. Shimadzu GC-14B.

This technique is based on a chromatographic column, enclosed in a controlled temperature oven, where a gas mobile phase transports the sample mixture and a stationary phase that interacts with the mobile one retaining the compounds for different amounts of time.

The sample is vaporized when injected in the mobile phase stream and passes through the column where the different compounds of the sample mixture are separated because of the different strength of interaction with the stationary phase. When the stream exits the column it passes through a detector that can be based on flame ionization (FID) or on thermal conductivity (TCD). FID is able to detect a compound because of the generation of a current between two electrodes due to the pyrolysis of the compounds that pass through the flame; they are more sensitive than TCDs but can't detect water and CO_2. TCD relies on the difference between the

thermal conductivity of the pure stream and the stream containing the sample; it is less sensitive but has a low detection limit (Figure 31).

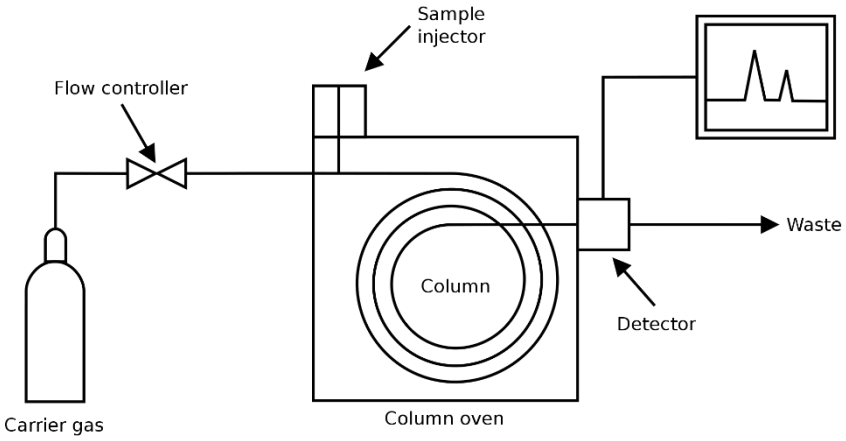

Figure 31. GC scheme.

To quantify the analytes a calibration curve for each compound was made using solutions with different concentrations. To each sample 50 μL of an internal standard (o-xylene) at the same concentration was added. The internal standard was chosen to have a retention time well separated from the other compounds but still close; it does not interact with the solution; it is introduced at a similar analytes' concentration. It is used to compensate for changes of detector response or other instrument variations.

To obtain the product concentration is necessary to take into consideration both the area of the analyte and the area of the standard (std) using the following equation:

$$C_i = \frac{Area_i}{Area_{std}} \cdot \frac{1}{m_i}$$

Where C_i is the analyte concentration; $area_i$ is the analyte area; $area_{std}$ is the standard area; m_i is the slope obtained from the calibration curve.

Conversion (X) is the amount of reactant that has converted overtime and is calculated as:

$$Conversion_Y = ((mol_{InitialFeedstock} - mol_{finalFeedstock}))/mol_{initialFeedstock}) \cdot 100$$

The yield (Y) is the amount of a specific product that has formed over the initial amount of reactant and is calculated as:

$$Yield_X = (mol_{product\ X}/mol_{InitialFeedstock}) \cdot 100$$

The carbon balance is the amount of carbon products that are found at the end of the reaction respect to the ones present at the start of the reaction and is calculated as:

$$Carbon\ Balance = (mol_{Product1} + mol_{Product2} \dots)/mol_{Feedstock}$$

3.5.2. High Performance Liquid Chromatography (HPLC)

The liquid products obtained from the glucose isomerization were analyzed using a JASCO HPLC (Figure 32). The different compounds were detected and quantified using both a multiwavelength detector (MD-2015) and a refractive index detector (RI-2031-PLUS). The different components in the matrix were previously separated through a Phenomenex REZEX Ca^{2+} -monosaccharide (300 mm x 7.8 mm) heated at 70 °C by a column oven (CO2065). The employed flow conditions were 0,4 mL/min of deionized and microfiltered water, provided by a quaternary gradient pump (PU2089).

Figure 32. JASCO HPLC.

This analytical method is based on a chromatographic column where a mobile phase, a solvent in which the analyte (sample) is transported, interacts with a stationary phase contained in the column separating different compounds depending on the affinity. Retention time is the identification factor and is necessary to calibrate the column with standard to obtain quantitative results.

The machine works by injecting a small volume of sample in the mobile phase stream and then is pumped through the stationary phase where all the sample components will be separated. The column is usually placed in an oven to keep the temperature constant throughout the analysis. At the end of the column is placed a detector that can be based on UV spectroscopy, if the compounds are able to absorb light in the UV range, or on refraction if the compounds do not absorb light; in this case the detection of the compound is based on the difference of refractive index between the eluent containing the sample and a reference pure eluent.

To identify and quantify the different compounds a calibration curve is needed. It was done by analyzing solutions containing different concentrations of the main reaction reagents and products. From the calibration curve equation obtained is possible to extrapolate the slope (m_i) of the curve.

The moles of the reaction products were obtained in this way:

$$n_i = \frac{Area_i}{m_i} \cdot \frac{V}{1000}$$

Conversion, yield and carbon balance were calculated as defined in Chapter 3.5.1.

4. Results and discussion

4.1. Mixed metal oxides

The synthesis of mixed metal oxides based on Li, Nb, Mo or W, was carried out following the procedure described in Chapter 3.1.1. The materials obtained were analyzed before and after the exchange of protons with Li cations to evaluate if there were any changes after the acid treatment. In addition, two different mixing times of the catalyst precursors were used to evaluate its influence on the resulting material.

4.1.1. XRD analysis

Powder XRD analysis were performed to determine the crystalline structure of mixed metal oxides (Figure 33). Since in the reference paper[40] used for the synthesis of these mixed metal oxides, there is no indication over the mixing time of the precursors before calcination, it was decided to mix during 1 and 2 hours to evaluate if there were differences in the results. It can be inferred from the corresponding XRD patterns that the two different mixing times do not lead to different results, meaning that it was enough 1 hour of mixing. The diffractograms were similar to that shown in the reference paper[112] (Figure 33), where it was possible to distinguish the characteristic diffraction peaks at 2Θ(º): 9.27; 26.88; 34.86 and 52.34 related to pristine crystal unit.

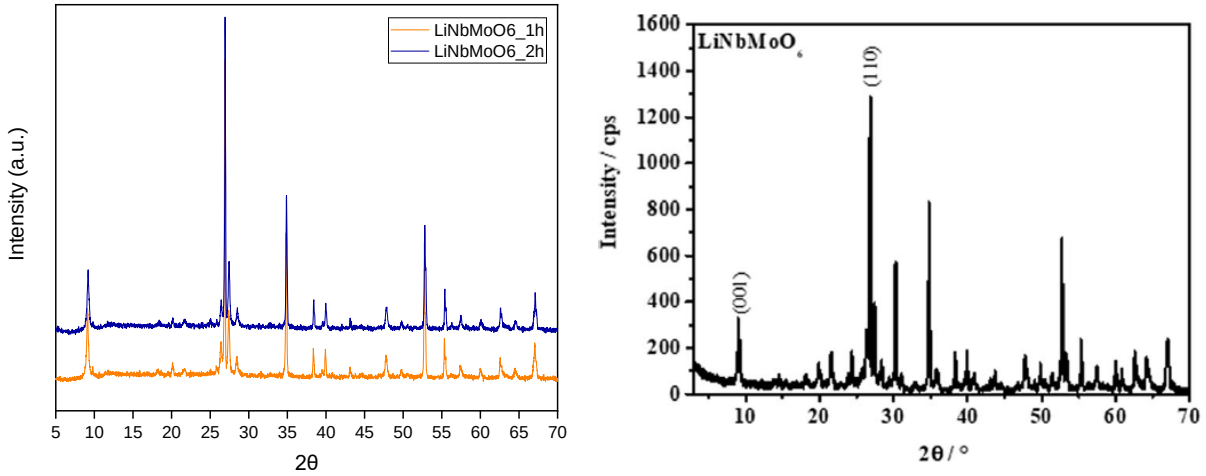

Figure 33. On the left: XRD diffractogram of mixed metal oxides with two different mixing times: 1h (in orange), 2h (in blue). On the right: XRD pattern of the reference paper[64].

The XRD patterns obtained post treatment with HNO_3 are shown in Figure 34. They were compared with the diffractograms of $LiNbMoO_6$ to evaluate if the acid treatment has influenced and changed the crystalline structure. It is clear that the crystalline structure was not influenced by the acid treatment since the diffraction peaks at 2Θ (º): 9.27; 26.88; 34.86; 52.34 of the untreated catalyst correspond to the treated one. In addition, it was compared to a reference[112], and, in this case, some differences were found. Supposedly, the diffraction peaks should have shifted a little after the acid treatment with peaks at 2Θ (º): 8.25; 27.3, and should have reduced intensity with the disappear of the peaks at 2Θ (º): 34.86; 52.34. Instead they remained the same as before. This could be a signal that the exchange of protons with Li^+ ions has not been effective.

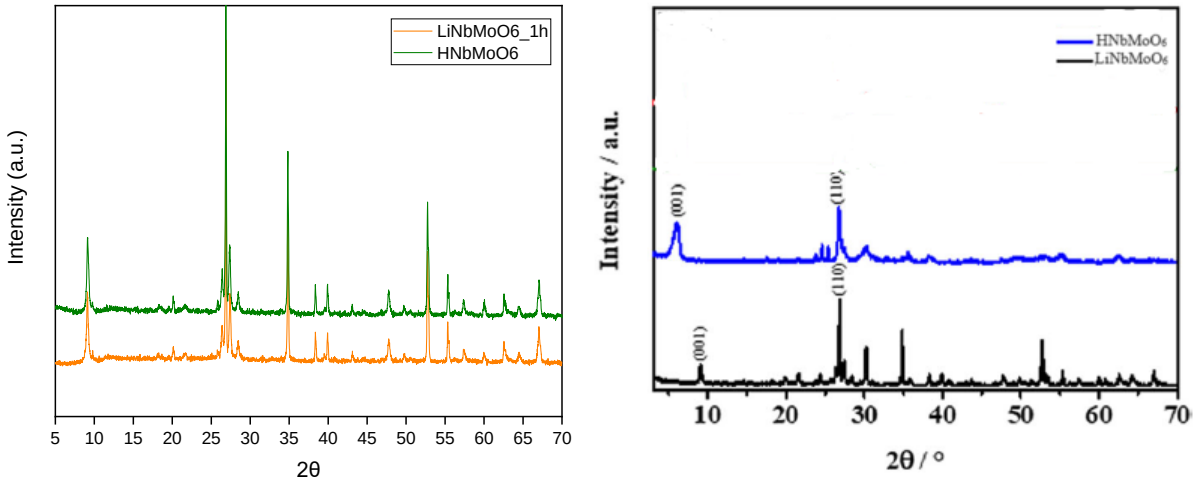

Figure 34. On the left: the diffractograms of $HNbMoO_6$ and $LiNbMoO_6$ obtained in this work. On the right: the diffractograms of the same catalysts obtained in one of the reference papers (adapted)[83].

Regarding the mixed metal oxide with W, the precursors were mixed only for 1 hour, because the results obtained in the synthesis performed with Mo were taken into consideration. In Figure 35, the diffractograms of the material, before and after acid treatment, are shown. In this case, it is possible to see that there is modification of the crystalline structure with the HNO_3 treatment. The characteristic peaks of $LiNbWO_6$ at 2Θ (°) = 9.85; 22.3; 27.9; 35.0; 53.4 are not visible in the $HNbMoO_6$ diffractogram. It is clear that the diffraction peaks are almost all shifted at low diffraction angles and their intensities have changed.

Mixed metal oxides were tested on HMF etherification reaction under different experimental conditions, but none of them brought interesting results so they are not shown in this work.

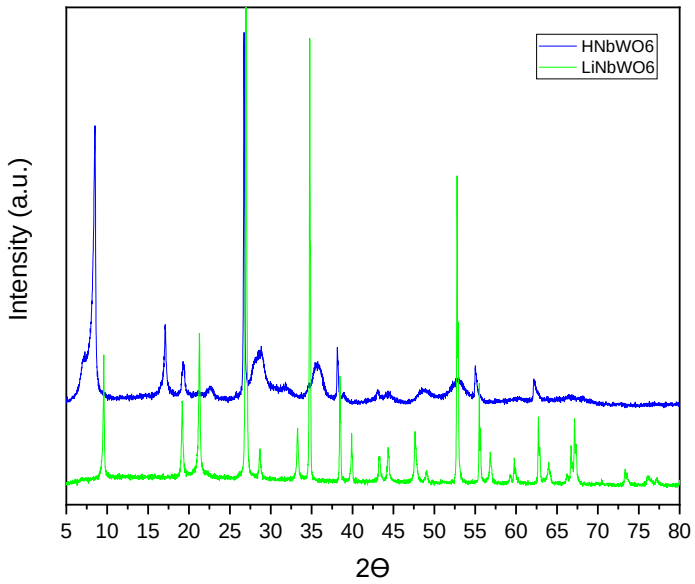

Figure 35. Diffractograms of $LiNbWO_6$ and $HNbWO_6$.

4.2. Zeolites

The synthesis of zeolites was performed following the synthesis described in Chapter 3.1.2. The zeolites were dealuminated using an aqueous solution of nitric acid. The dealumination was done in order to facilitate the incorporation of zirconium atoms into the crystalline structure. In this way, the concentration of Zr atoms on the catalyst should increase and consequently it is expected to affect the catalytic activity.

4.2.1. N_2 adsorption/desorption

The Zr-doped zeolites, as well as the raw zeolites, were analyzed by using different characterization techniques in order to explain their catalytic performance.

The specific surface area of the catalysts, together with the pore size and volume were determined from N_2 sorption. The results are shown in Table 4.

The textural data clearly demonstrate that the insertion of the zirconium into voids reduces the specific surface area (Langmuir) due to the bigger size of Zr compared to Al, together with its high atomic weight, although the external surface area is not greatly changed, unlike to that observed for the micropore area. Among the Zr-doped zeolites, β-10_Zr has the bigger pore size and volume, while the other two samples, β-16_Zr and β-96_Zr, have similar values. It is very important to determine the textural properties to assess if bulky molecules will suffer steric hindrance to access the active sites, mainly using β-16_Zr and β-96_Zr as catalysts.

Comparing the pore volume and the pore size of the samples before and after zirconium deposition, it is evident how they both diminish after the metal deposition. This behavior is due to two factors: Zr atom size and particle aggregation. As noted before, zirconium atoms are bigger than aluminum ones and this means that they occupy more space, leading to a reduction in the pore dimension. As will be seen in the following section in SEM images (Figure 39), after Zr deposition, some particles aggregates were present, which might reduce the pore dimensions.

Catalyst	Langmuir surface area (m^2/g)	External surface area (m^2/g)	Micropore area (m^2/g)	Pore volume (cm^3/g)	Average pore size (Å)
β-10_Zr	644	173	470	0.517	88.4
β-16_Zr	650	104	546	0.284	39.9
β-96_Zr	649	101	548	0.285	40.2
B-10	727	196	531	0.611	91.1
β-16	734	88	646	0.284	43.1
β-96	667	76	589	0.289	40.5

Table 4. Textural properties of Zr-doped and undoped zeolites by nitrogen adsorption-desorption isotherm.

In Figure 36, the adsorption-desorption isotherms of the three catalysts are shown. It is possible to see how the isotherms of β-16_Zr and β-96_Zr look very alike, while that of β-10_Zr is different. All the three samples present micropores, even if β-16_Zr and β-96_Zr are more microporous. This can be deduced from the increase of the quantity of N_2 adsorbed at low relative pressures. They all present hysteresis loops, due to the different adsorption and desorption values; this difference is due to the fact that desorption is delayed because of different reasons, such as cavitation or pore blocking[113].

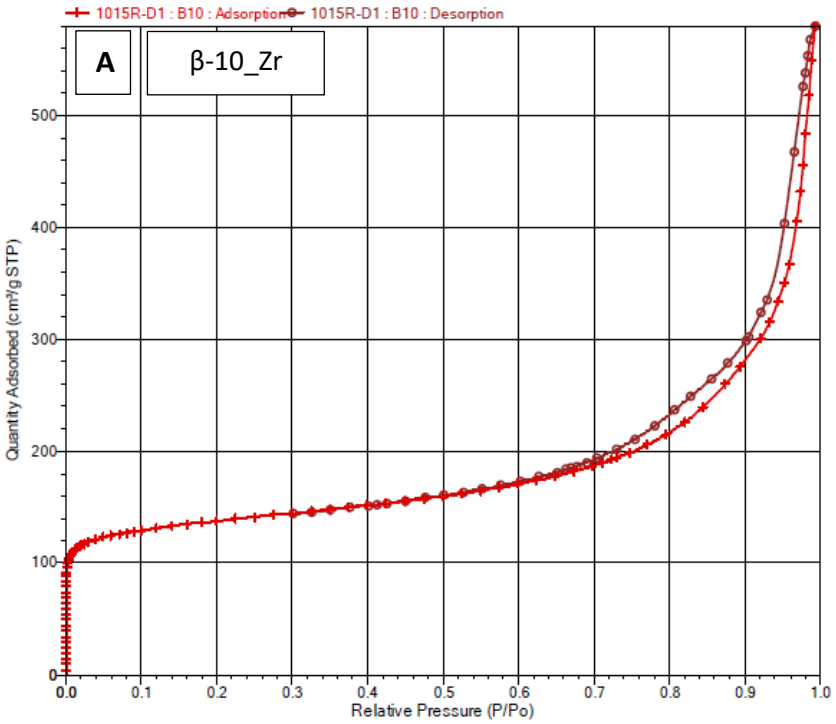
1015R-D1 : B10 : Adsorption
1015R-D1 : B10 : Desorption
A
β-10_Zr
Quantity Adsorbed (cm³/g STP)
Relative Pressure (P/Po)

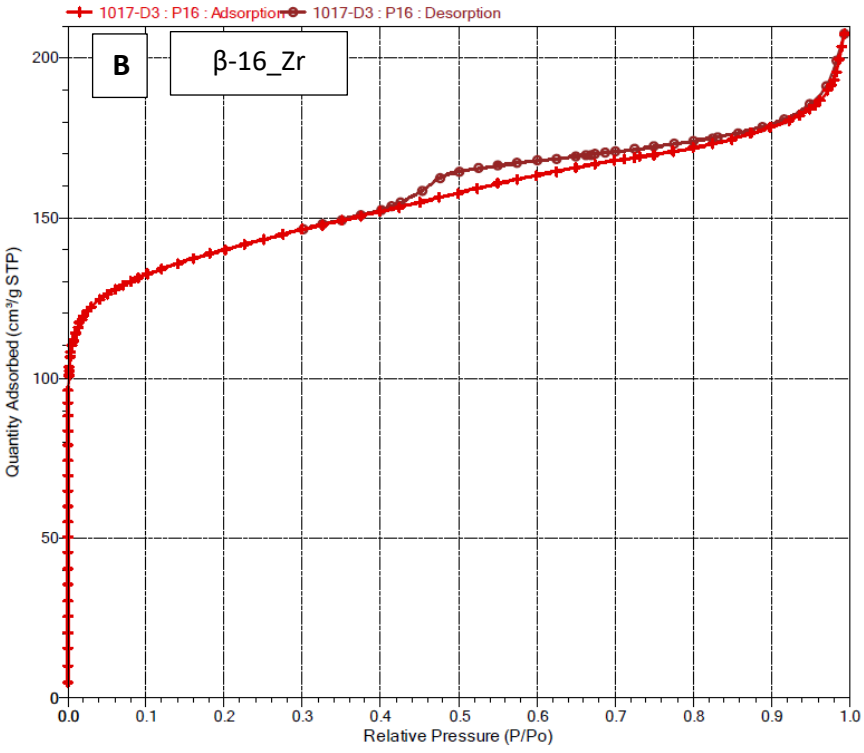
1017-D3 : P16 : Adsorption
1017-D3 : P16 : Desorption
B
β-16_Zr
Quantity Adsorbed (cm³/g STP)
Relative Pressure (P/Po)

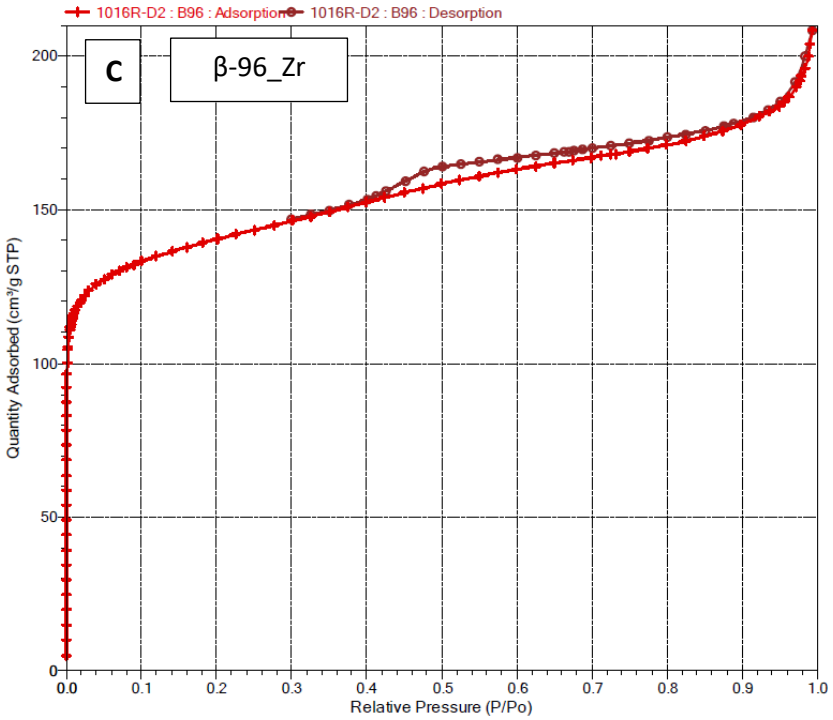

Figure 36. Adsorption-desorption isotherms of β-10_Zr (A), β-16_Zr (B) and β-96_Zr (C).

4.2.2. XRD analysis

To confirm the stability of the crystalline structure after Zr insertion, X-ray diffraction (XRD) analysis was performed (Figure 37). The XRD patterns obtained were compared to reference diffractograms[34] of a β-zeolite that did not undergo dealumination process, or Zr substitution, to detect structural changes caused by these treatments. The XRD patterns of the three samples synthesized exhibit the same characteristic diffraction peaks at 2Θ (°) = 8.2; 14.9; 22.73 [33] with a similar intensity, denoting that the crystalline structure of these zeolites is preserved during both dealumination and Zr substitution. In all cases, the same diffraction peaks are observed, including the broad peak at 2Θ (°) = 7.8; 14.9; 22.7, which means that the crystals contain a random intergrowth of the same polytypes[34].

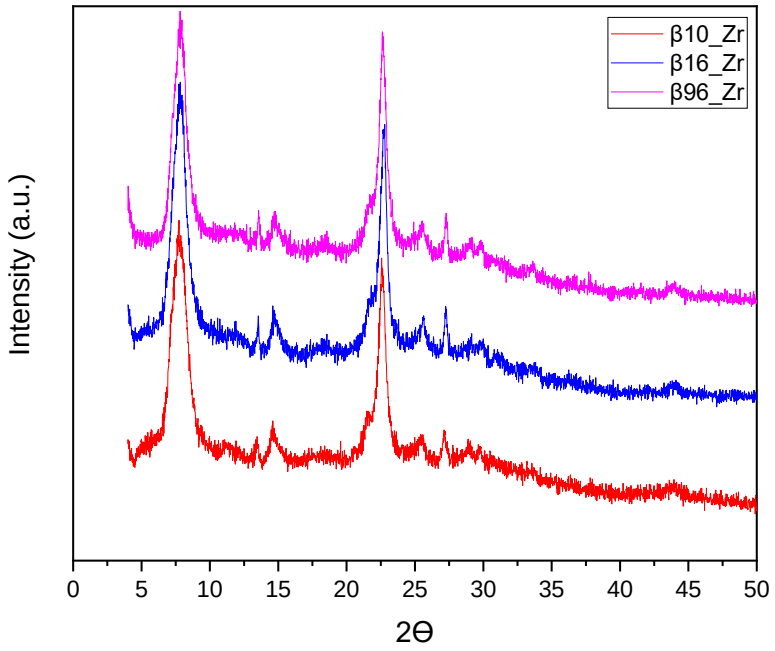

Figure 37. XRD patterns of the three zeolite with different amounts of Zr.

4.2.3. XPS analysis

The XPS analysis were used to evaluate the effect of the dealumination process and the quantity of Zr that has been deposited, but relative to the external surface of the zeolite. The results are shown in three tables. Table 5 show the atomic percentages of different elements on the surface, whereas Tables 6 and 7 provide the atomic concentration of Zr and Si, respectively, as well as their binding energies.

Catalyst	%Si	%Zr	%O	%C
β-10	26.4	-	63.1	10.6
β-16	26.1	-	62.2	11.4
β-96	26.4	-	62.2	11.3
β-10_Zr	24.5	3.4	57.1	14.7
β-16_Zr	20.7	7.5	56.5	15.3
β-96_Zr	20.5	7.2	56.5	15.7

Table 5. Composition of the synthesized zeolites obtained from XPS analysis.

It can be inferred from data displayed in Table 2 that the dealumination process has occurred successfully, because there is no trace of Al in the samples. Moreover, there is an important

decrease in Si and O signal after Zr deposition. Another important point to underline is the similarity between the results of the samples β-16_Zr and β-96_Zr, although β-96_Zr should contain a higher percentage of Zr. Despite this, the percentages of the different atoms present in the samples are almost the same. Although the reasons behind this behavior are still unknown, ongoing research is now focused on this topic.

Catalyst	Binding Energy (eV)	% Zr
β-10_Zr	183.1,185.5	3.4
β-16_Zr	182.7,185.3	7.5
β-96_Zr	182.6,185.3	7.2

Table 6. Binding energies and percentage of Zr present in the zeolites.

Catalyst	Binding Energy (eV)	% Si
β-10_Zr	103.7	24.5
β-16_Zr	103.5	20.7
β-96_Zr	103.5	20.5

Table 7. Binding energies and Si percentage in the zeolites.

On Table 6 and Figure 38 (left), the binding energies of the doublet of the Zr 3d core level spectra electrons, corresponding to the Zr $3d_{5/2}$ and Zr $3d_{3/2}$ signals, which are shifted to higher BE values (~182.7-183.1 and ~185.4 eV, respectively) compared with that of bulk ZrO_2 (182.0 and 184.5 eV)[34]. This shift is due to a more electron-deficient Zr present in Zr-O-Si bonds and it is consistent with the formation of intra-framework Zr species in Zr-β-zeolite[34].

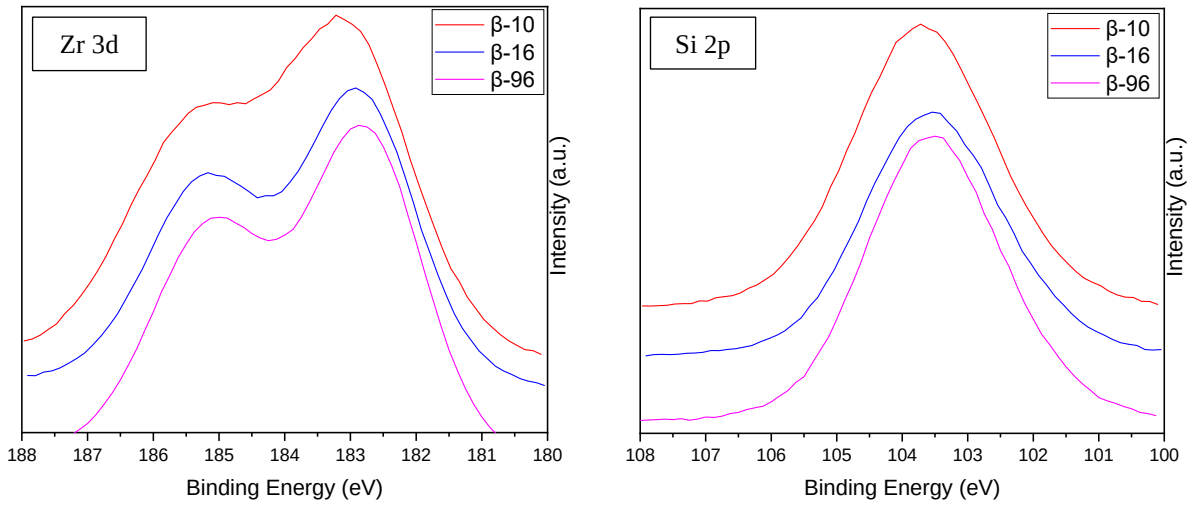

Figure 38. XPS results: (right) Si 2p and (left) Zr 3d core level spectra.

4.2.4. SEM and EDX

The SEM analysis allows to determine the morphology of catalysts, while EDX data provides the composition and dispersion of different chemical elements in samples using the different areas from the sample (Figure 39). From the images, it is clear that the nanoparticles of β-10_Zr are bigger (10 μm) than those of β-16_Zr and β-96_Zr (around 2 μm or smaller). It can also

been deduced from SEM analysis of Zr-doped zeolites (Figure 39 (B, D and F)) the existence of particle agglomeration, while the samples that were only dealuminated (Figure 39 (A, C and E)) have more distinct particles. Even if having agglomerations, might reduce the surface area and the catalytic activity, the incorporation of Zr should avoid this to happen.

Concerning EDX analysis (Figure 40) of Zr-doped and undoped zeolites, it can be observed the homogeneous distribution of Zr species on the three samples (Figure 40A-B-C). The two samples β-16_Zr and β-96_Zr present some Zr clusters, maybe due to the aggregations that were observed in SEM analysis. Si and O species, as expected, in all the samples, they are uniformly distributed.

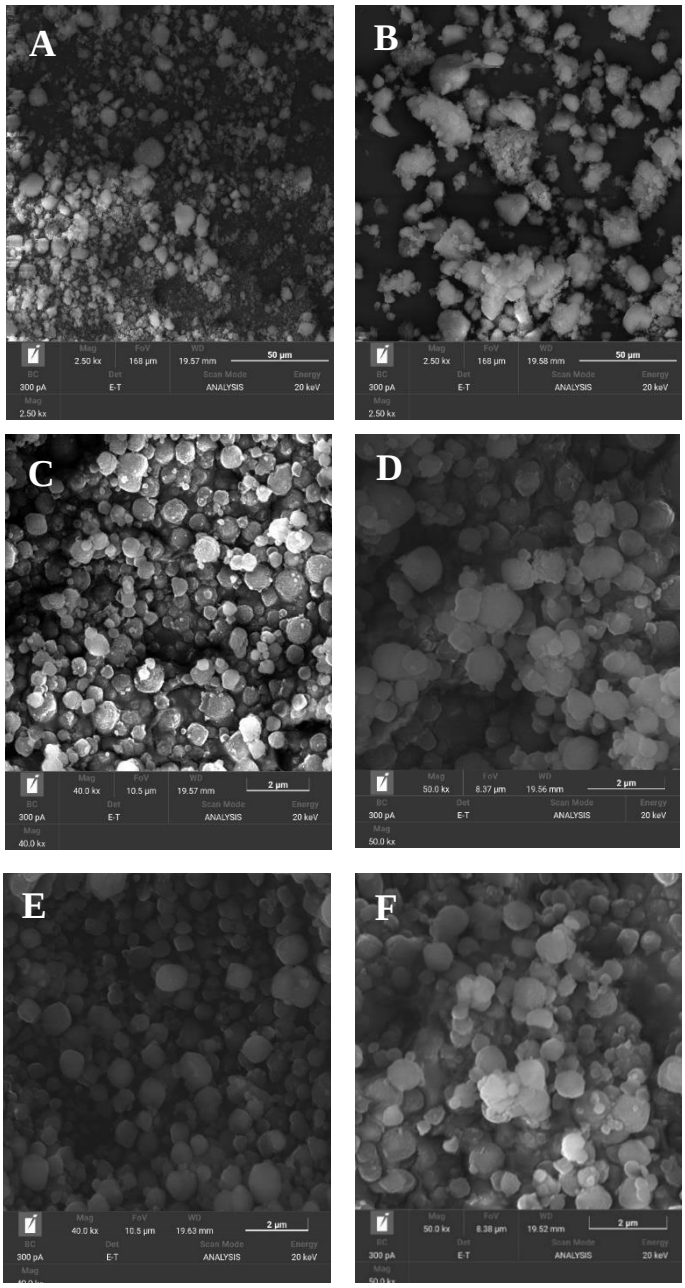

Figure 39. SEM analysis. (A) β-10; (B) β-10_Zr; (C) β-16; (D) β-16_Zr; (E) β-96; (F) β-96_Zr.

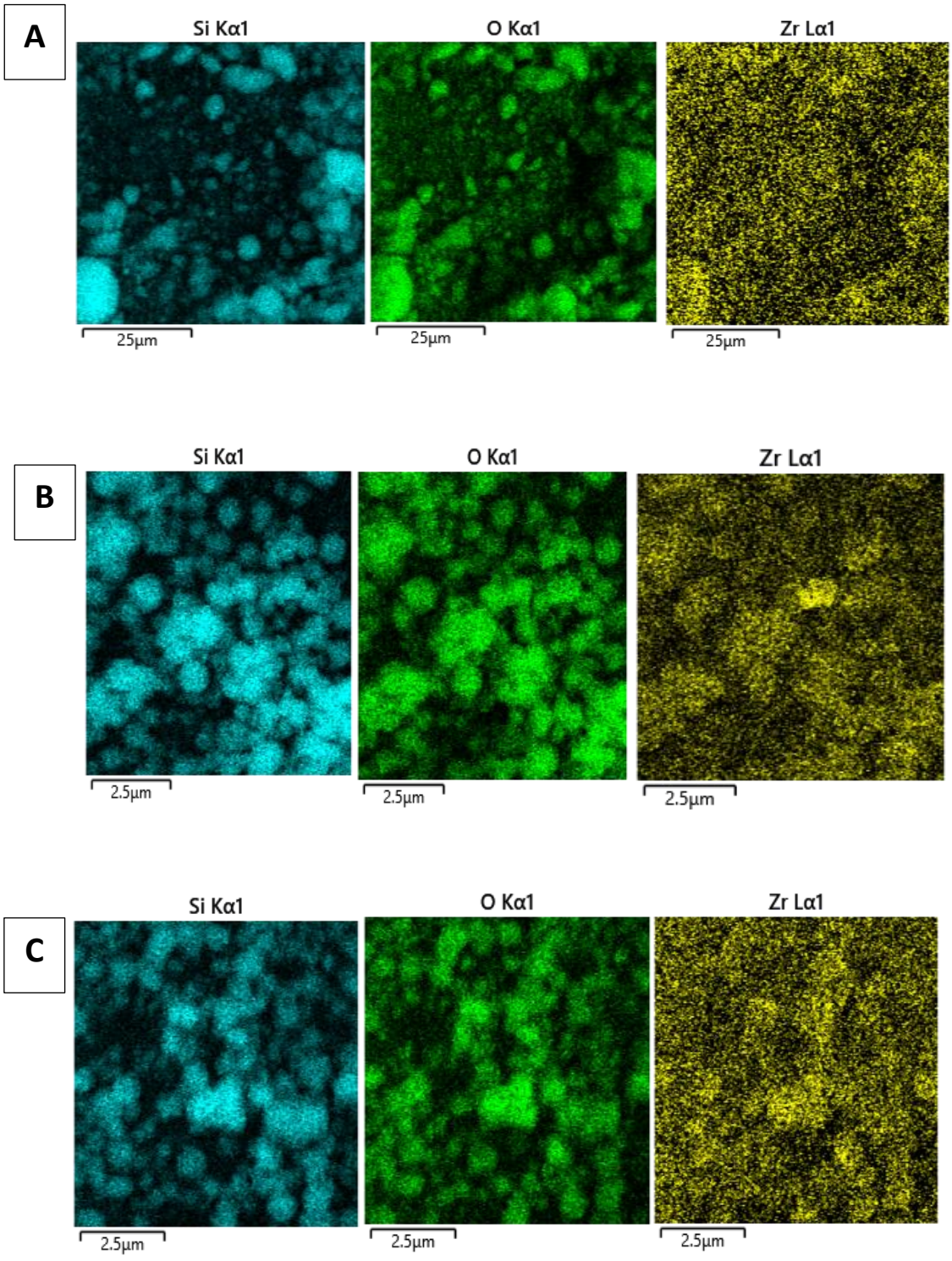

Figure 40. EDX results mapping analysis: A) β-10_Zr; B) β-16_Zr; C) β-96_Zr.

4.3. Glucose isomerization

Glucose isomerization to fructose is a crucial step for current and future applications in industries and reaction processes[48] considered its importance in the synthesis of bio-based chemicals and also in the food industry[20]. The conversion of glucose is limited by the thermodynamic equilibrium between the two sugars at each specific reaction temperature[53].

In the current study, three different types of zeolites were tested and, after having chosen the one with the better performance, different experimental conditions were varied to achieve the highest fructose yield.

The glucose isomerization reaction was performed in a glass reactor, under stirring, in a one-pot reaction divided in two steps. In the first step, an alcohol was used as a solvent. In the second one, water was added to the reaction mixture.

Zeolite	Langmuir surface area (m^2/g)	t-Plot micropore area (m^2/g)	Si/Al molar ratio (XPS)
β-zeolite CP814E	726.8	530.9	14.1
ZSM5 CBV2314	493.6	463.2	10.9
USY CBV500	907.0	854.7	1.2

Table 8. Textural properties of the three commercial zeolites.

Based on the literature[114], the highest activity in this catalytic process with zeolites is attained with those having a Si/Al molar ratio around 10. Accordingly, three different types of zeolites with a similar ratio were chosen: β-zeolite with a Si/Al = 10; USY zeolite with Si/Al = 5.2; ZSM5 with a Si/Al = 9. These are commercial zeolites, so available on the market and in big quantities. These three zeolites differ from each other by their surface area and the size of the pores and acidity. Table 8 contains the data regarding Langmuir surface area, micropore area and Si/Al molar ratio. It is possible to see that the higher surface area is 907.0 m^2/g and is attributable to USY CBV500 zeolite, this material also possess the highest micropore area. On the other side the lowest surface and micropore area is of the ZMS5 material of 493.6 m^2/g and 463.2 m^2/g. This should mean that the ZMS5 material is the least active among the three because of the lack of active sites. This hypothesis is confirmed by the dimension of the pores that, in the case of this zeolite are 6.3 Å that is way smaller than the kinetic diameter of glucose (~8 Å)[115]. On the other side USY zeolite has a pore diameter of 7.4 Å [116] and the β-zeolite of around 8 Å meaning that they are more prone to be active on the glucose considered its kinetic diameter[115].

The catalytic tests were carried out at 120 °C for 1 h per step, so two hours of total time. The alcohol used in the reaction was methanol (MeOH), adding 2.5 mL; the same quantity was used for water[114].

4.3.1. Catalytic performance of commercial zeolites

The catalytic performance was evaluated starting from commercial zeolites. The main products that can be obtained with this reaction are fructose, mannose and alkyglucosydes depending on if the glucose follows the isomerization route or epimerization. Together with these products there is the possibility of obtaining galactose, even if it was not found in any of the tests performed (Figure 41). ZSM5 only produced mannose. Meanwhile, the β and USY zeolite gave a similar amount of fructose (yield of ca. 28%), being the percentage of mannose very similar for the three zeolites (yield ca: 25%). The differences between the activity of the ZSM5 zeolite and the other two are due to the difference in active sites present on the surface of the zeolite.

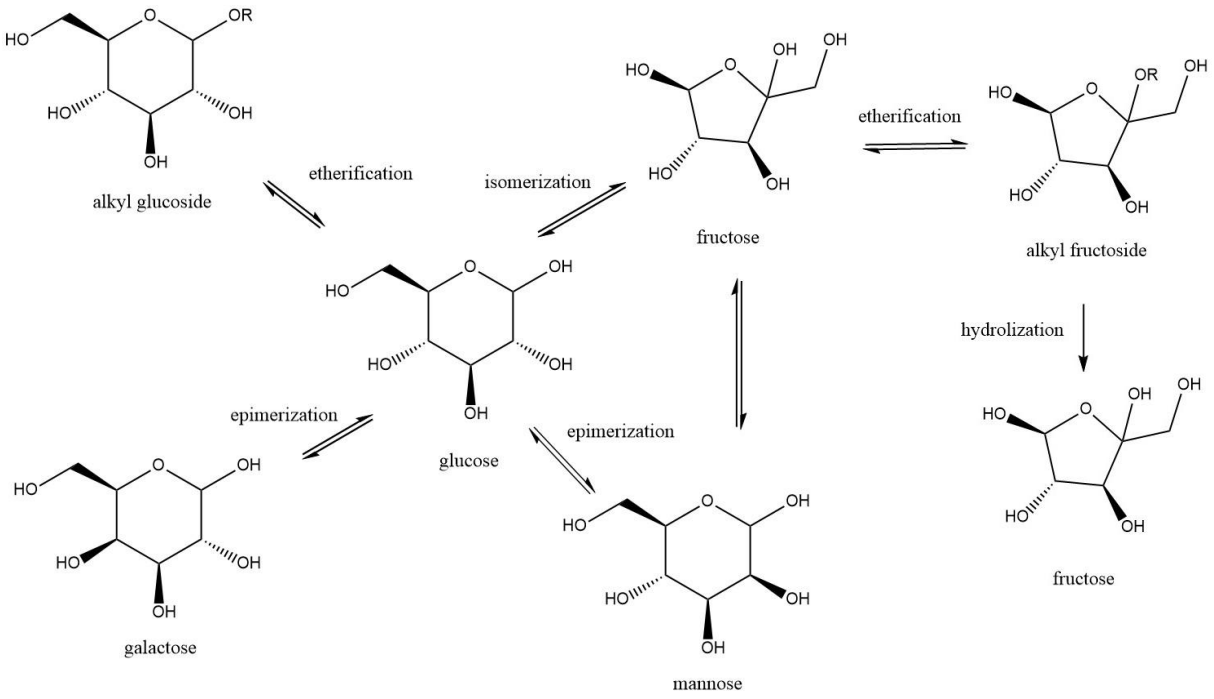

Figure 41. Reaction scheme of glucose isomerization and side-reactions.

An important data that can be extracted from Figure 42 is the carbon balance of the reaction. As can be seen from the sum of the products found in the final solution, it is over 90% for all three reactions. This result means that there are no products adsorbed on the catalyst and that there is almost no loss of substance.

Considering the results obtained in the previous tests, the study of the reaction conditions was performed by using the β-zeolite CP814E, considered that it has a slightly lower production of mannose.

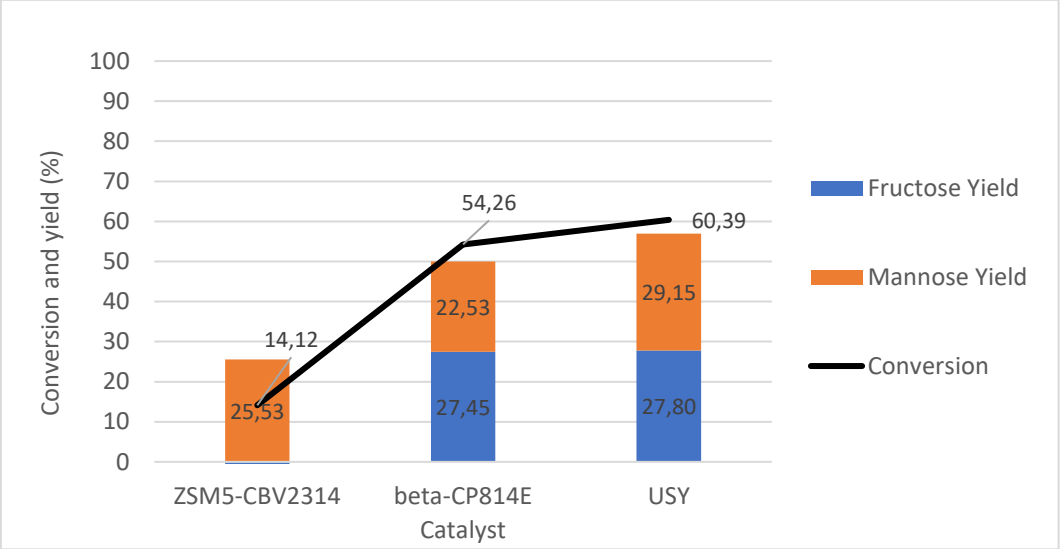

Figure 42. Unconverted glucose (glucose yield), product yields and carbon balance of the tests done with different zeolite with similar Si/Al ratio.

Firstly, the influence of the reaction temperature was studied. The tests were carried out at three different temperatures: 80, 100 and 120 °C. The results of these tests showed that only at 120 °C isomerization of glucose to fructose is achieved. At temperatures below 120 °C, only methylglucosides and glucose were detected, revealing that the isomerization reaction happens at temperatures above 100 °C. The temperature was not risen above 120 °C because other reactions, such as glucose dehydration, would have been favored leading to the production of HMF, furfural and alcoxymethylfurfural. Therefore, an optimum reaction temperature of 120 °C was chosen for the next studies.

4.3.2. Effect of water quantity

Another crucial point was the quantity of water to be added in the second step. It is important to mention that adding water in a successive step and not together with alcohol was seen to be essential to succeed in the reaction. Water is used to hydrolize the alkyl fructoside obtained in the first step to fructose. The use of solvent mixtures containing alcohol in water was studied by Saravanamurugan et al.[51] and it was seen that it led to low glucose isomerization, reaching 8% fructose yield. This happens because a large excess of alcohol is needed to obtain alkyl fructosides and the presence of water inhibits their formation[117]. The tests were done by adding in a second step 2.5, 3.5 and 4.5 mL of water. The tests were done, like the ones done before,

by using 2.5 mL of methanol in the first step and by keeping the reaction at 120 °C, under stirring, for 1 hour per step. The results are shown in Figure 43 and highlight how the amount of water doesn't really affect the activity of the isomerization reaction keeping the fructose yield between 25% and 30%. Indeed, regardless of the amount of water, the production of both fructose and mannose is very similar. These results can be explained by the fact that water is already present in excess in the reaction mixture, so changing its amount doesn't affect the final results. A data worth underlining is the carbon balance. Carbon balance is close to 100 % by adding 2.5 and 4.5 mL of water, while with 3.5 mL of water the carbon balance is reduced to around 85 %.

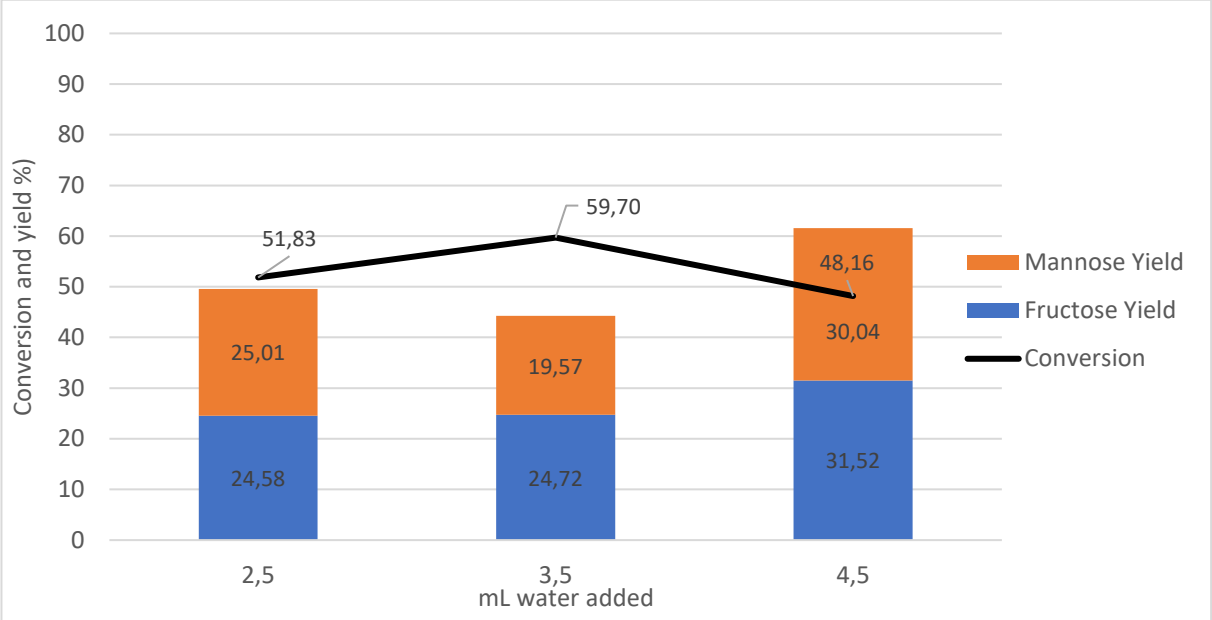

Figure 43. Results of the tests done by changing the amount of water used in the second step of the reaction.

4.3.3. Effect of 1st step reaction time

Finally, the effect of reaction time was evaluated, including the first and second step. The tests were carried out for 0.5, 1, 2 and 3 hours. Figure 44 exhibits the results of the tests of the 1st step reaction time. It is possible to see that, after 3 hours reaction time, the fructose yield is equal to zero, maybe due to the degradation of the sugars to formic acid[118], acetic acid, formaldehyde, diacetyl[119], phenolics[118] after long reaction time, and will also explain the reduction of the final carbon balance. It is also possible that the reduction of the carbon balance is related to the adsorption of substrate and products on the surface of the catalyst that trapped the substances. Going back to the description of the results in Figure 44, it is clear that with a 1st step reaction time below 2 hours the carbon balance is optimal, being around 100%. The

fructose yield seems to be more or less constant, even if after 2 hours it increases reaching 28% together with mannose yield that reaches 30%. It could be affirmed that the reaction has almost the same activity in between 30 minutes and 2 hours long for the 1st step reaction time. The here obtained results, if compared to some results from the literature[120] where they use alkaline-treated Y-zeolites, show an increase of almost 10% in fructose yield and of more than 20% in glucose conversion working at the same reaction conditions.

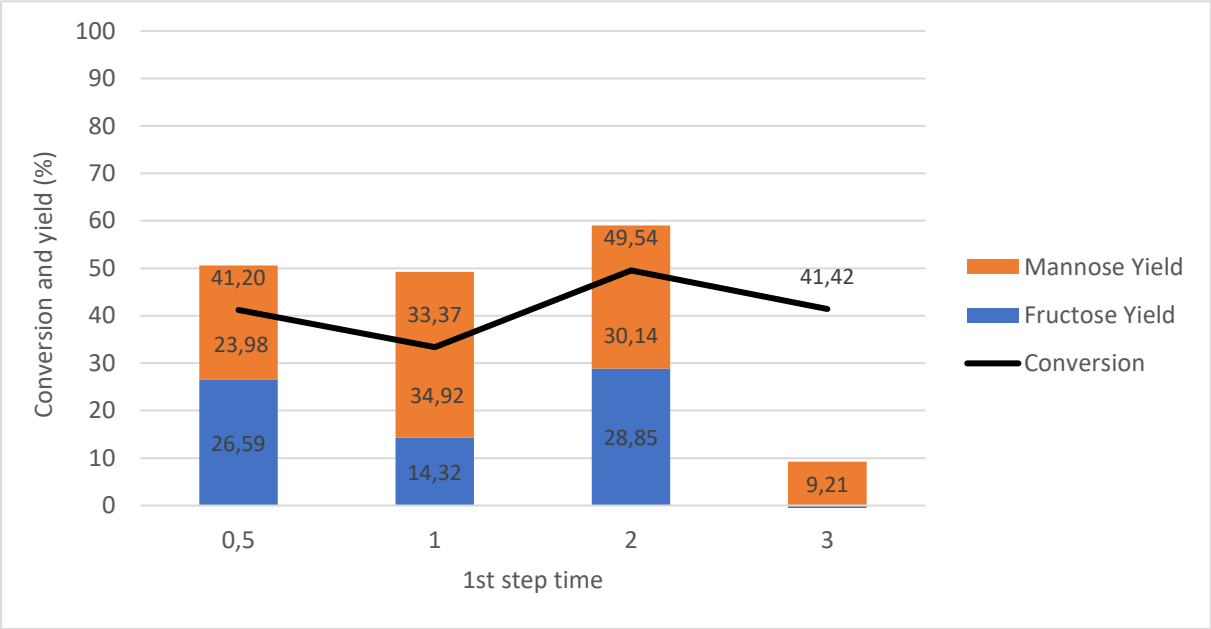

Figure 44. Results of the tests done by changing the 1st step reaction time.

4.3.4. Comparison of solvents: methanol versus ethanol

After having studied the different reaction conditions, it was possible to test how using a different alcohol from methanol would have influenced the results. Ethanol was used instead of methanol, at 120 °C, under mixing for 1 hour per step and by using 2.5 mL of alcohol and 2.5 mL of water. Ethanol was chosen because it is a greener option compared to methanol, considered that it is highly produced from renewable sources, especially from sugarcane, therefore it is consider a green solvent. The comparison between the reaction done with methanol and the one with ethanol is shown in Figure 45. The first thing to be highlighted is the higher production of mannose (ca. 22%) from the reaction where methanol is used. That results are related to the production of alkylglucosides, since methylglucosides are more stable compared to ethylglucosides, that, instead, are easier to be then transformed into fructose when water is added. To confirm this hypothesis, NMR analysis was performed on both the reaction mixture in between the first and second step and at the end of the reaction. From these analyses,

it was possible to confirm the presence of alkylglucosides in both the reaction with methanol and ethanol, but the decrease in these compounds at the end of the second step was more evident for the reaction performed with ethanol. The carbon balance is above 90% for both tests, meaning that changing alcohol does not influence the adsorption on the catalyst surface, or the degradation of the sugars. Regarding fructose yield, it was around 27% using methanol and 21% using ethanol.

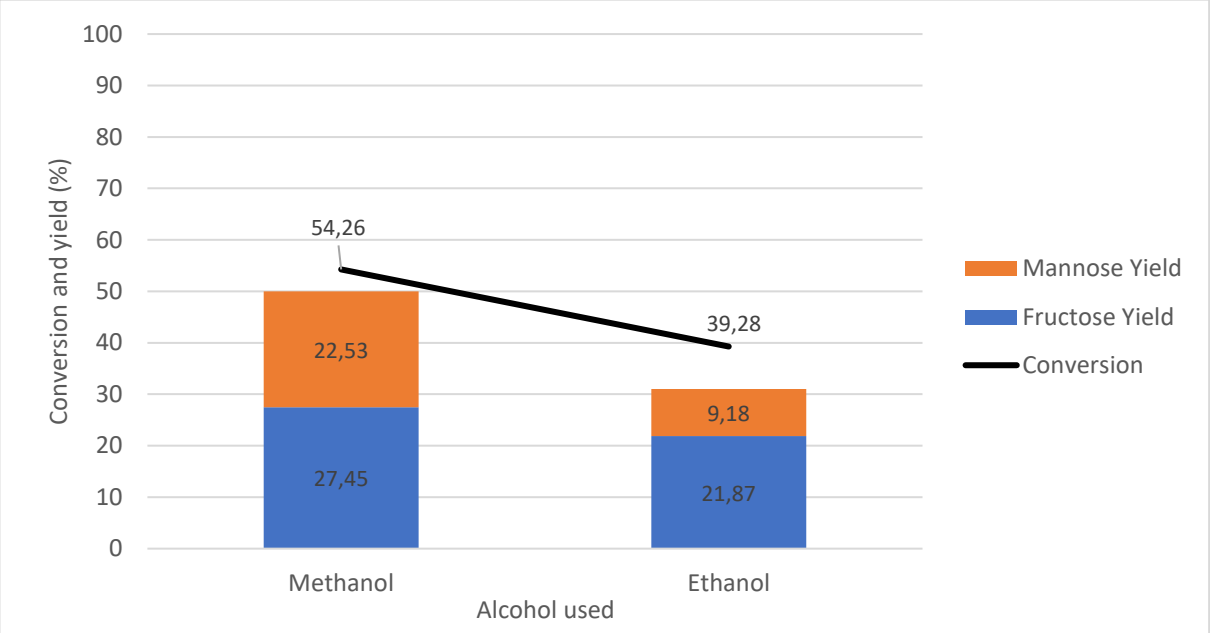

Figure 45. Results of the tests done by changing alcohol.

4.3.5. Effect of alcohol evaporation

To evaluate if it is possible to reduce the mannose formation, the evaporation of the alcohol before the addition of water (second step) was tried. The evaporation was carried out by using a rotavapor. The reason behind this choice is to try to reduce the amount of alkylfructosides that will be formed in the reaction mixture, which are responsible for the production of mannose instead of fructose. The results are shown in Figure 46, where, on the left, it is possible to see the products without the evaporation of the alcohol, while on the right there are the results after evaporation. Evidently, the presence of alcohol during the second step of the reaction significantly affects the final mannose yield going from 22% to 8%. The fructose yield increases when the alcohol is removed having a 27% yield without eliminating the alcohol and 30% with the alcohol elimination. On the other hand, the mannose yield experiences a substantial reduction in the experiment where alcohol is eliminated after the initial step. The overall carbon

balance exceeds 90% in both experiments, confirming that the compounds do not remain trapped within the catalyst and can be readily recovered.

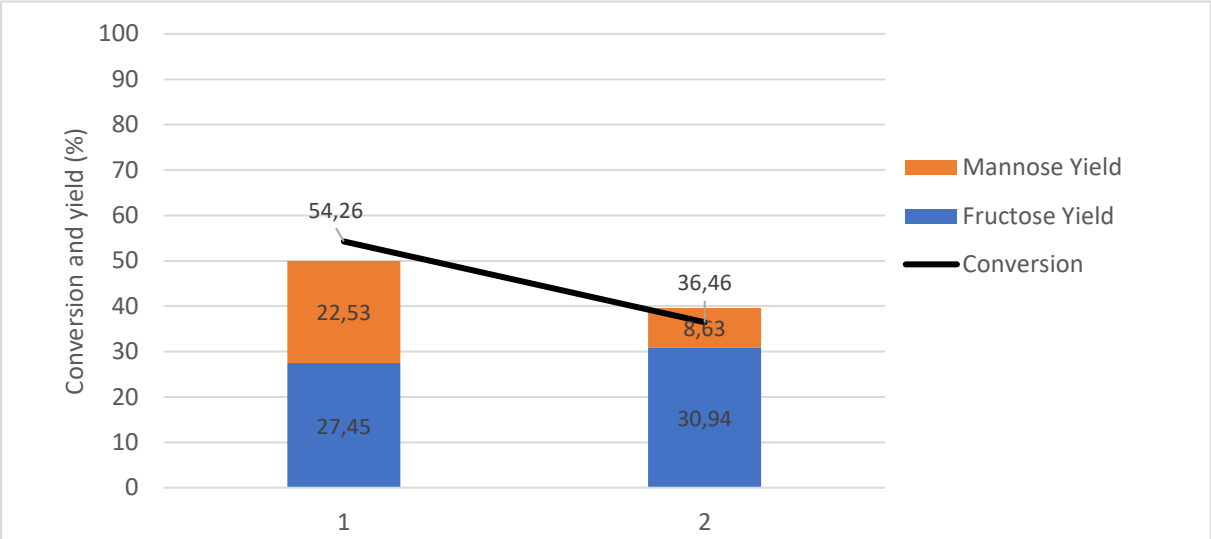

Figure 46. Results of the tests without (left, 1) and with (right, 2) evaporation step before the addition of water.

4.3.6. Conclusions on glucose isomerization study

The study on glucose isomerization to fructose divided in three steps permitted to obtain a maximum of 30% fructose yield. The study of the three commercial zeolite activity resulted in no activity on fructose production for ZSM5 zeolite, while the other two zeolites, β and USY, were seen to be active on the reaction. The optimization of the reaction was performed using β-zeolite and the best results were obtained at 120°C, for 2 h for each reaction step, using 2.5 mL of ethanol and 2.5 mL of water and resulted in 28% fructose yield. The possibility of eliminate the alcohol in between the first and the second step through evaporation was studied to evaluate if it reduced the mannose production. The results showed a reduction of mannose yield going from 22% to 9% and an increase from 27% to 30% of fructose yield. Beside the results obtained, the fructose yield still needs to be increased considered that the thermodynamic equilibrium is 45% fructose and 55% glucose.

4.4. HMF etherification

As indicated in the introduction, HMF is an important building block that can be obtained from fructose or, in general, from hexose dehydration. The treatment of HMF with different catalysts and conditions can lead to the production of several chemicals with important applications. Among them, the etherification reaction can be used to produce etherified compounds like 2,5-bis(isopropoxymethyl)furan (BIMF), a precursor of biofuels.

The objective of this study presented here was to find a catalyst that was able to selectively produce BIMF from HMF, through etherification (Figure 47). Several catalysts were studied to find the catalysts with optimal physico-chemical properties to carry out the process. The tested catalysts were mixed metal oxide ($HNbMoO_6$), two different types of zirconium phosphate and zeolites. It was possible to understand that mixed metal oxide and both the types of zirconium phosphate were active on HMF etherification but to obtain isopropoxymethoxyfurfural. On the other side, zeolites were seen to be active on the production of the target product (BIMF) through HMF etherification.

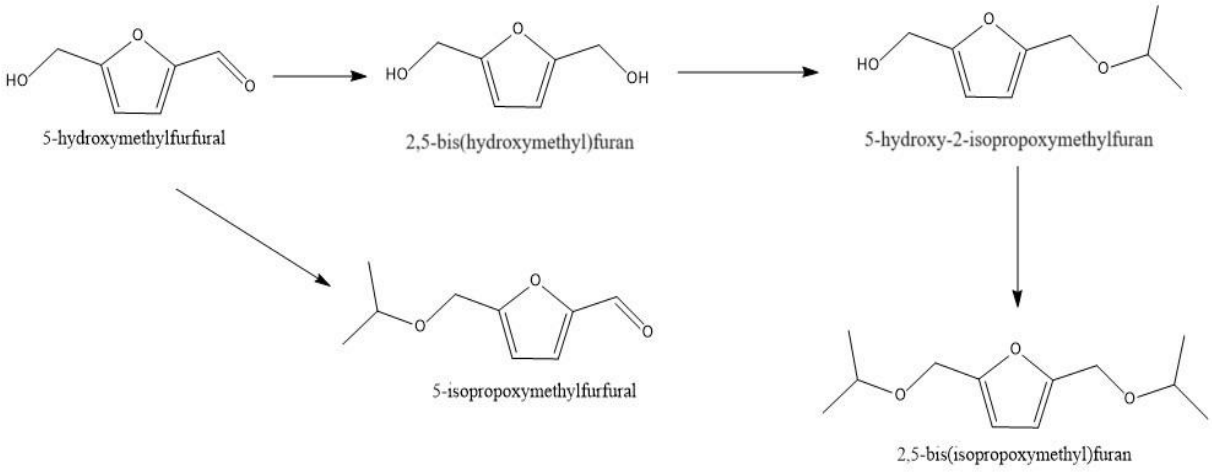

Figure 47. Reaction scheme of HMF etherification.

After the synthesis of the catalyst was completed, the investigation proceeded with the study of the optimization of both the catalyst and the experimental reaction conditions. The studies were done with β-10_Zr, β-16_Zr and β-96_Zr to evaluate also how the different amount of Zr on the zeolite influences on the catalytic activity. Together with these catalysts, zeolites without Zr were tested under the best experimental conditions to confirm if the presence of Zr is necessary.

All the reactions were carried out at 150 °C, using 50 mg of catalyst, 150 mg of substrate and 5 mL of isopropanol, under stirring. The effect of reaction time in the products distribution was studied. The time tested were 0.5, 1, 2, 3, 4, 5 hours.

4.4.1. Effect of reaction time at 150 °C

The results in Figure 48, Figure 49 and Figure 50 show a trend in which a maximum of BIMF could be obtained after 5 h of reaction. A 91% BIMF yield (figure) could be obtained with the use of β-10_Zr, compared with a 71% yield obtained with β-96_Zr. In the case of the catalyst β-16_Zr, the maximum yield achieved was 46% after 3 h. On the other hand, overtime, a constant increase in the yield of 5-hydroxy-2-isopropoxymethylfuran has been observed. The results concerning this compound are interesting, considered that it seems to increase with the reaction time until 4 h, and then, after 5 h, its yield decreases. The reason behind this strange behavior might be related to the longer time of the reaction that has helped to increase the amount of the converted intermediate compound.

Another interesting result, deducible from Figure 48, is that β-10_Zr is more active on the reaction than the other two catalysts. Indeed, the results after 5 hours are around 90% of BIMF yield produced using β-10_Zr and below 70% for the other two catalysts. The reason has to be searched on the dimension of the pores of the catalysts. As it is visible in Table 1 in Chapter 4.2, the pore volume of β-10_Zr catalyst is 0.517 cm^3/g and the pore size is 88.4 Å, dimensions that are quite bigger than the ones of β-16_Zr and β-96_Zr that have a pore volume of 0.284 cm^3/g and a pore size around 40 Å. This difference in dimension makes it easier for BIMF to be released from β-10_Zr pores instead of the other two catalysts that will keep that compound inside and might be converted again to the intermediate.

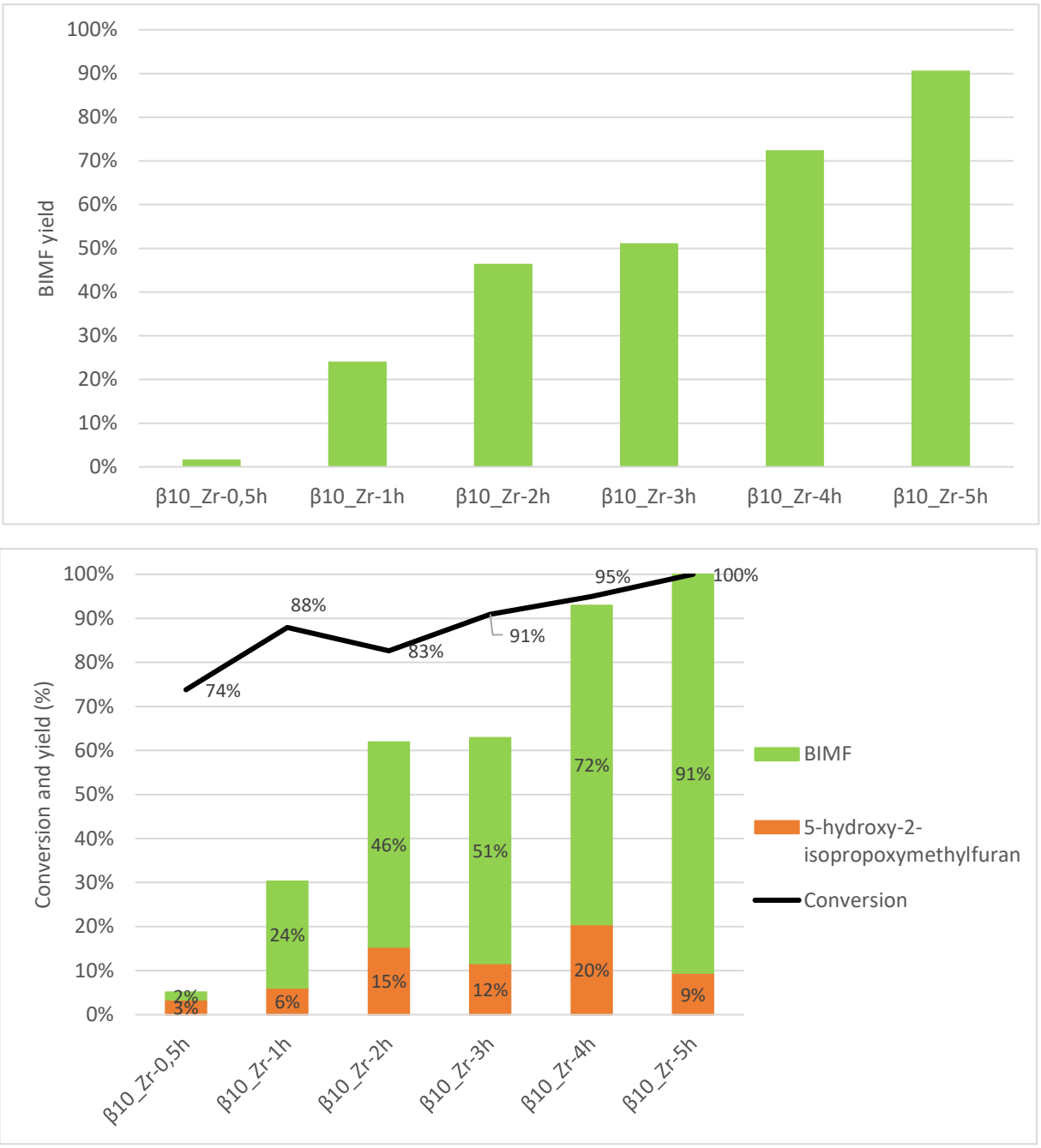

Figure 48. Results of HMF etherification with the use of β-10_Zr at different reaction time. Above are shown only BIMF yield. Below HMF conversion, 5-hydroxy-2-isopropoxymethylfuran and BIMF yield.

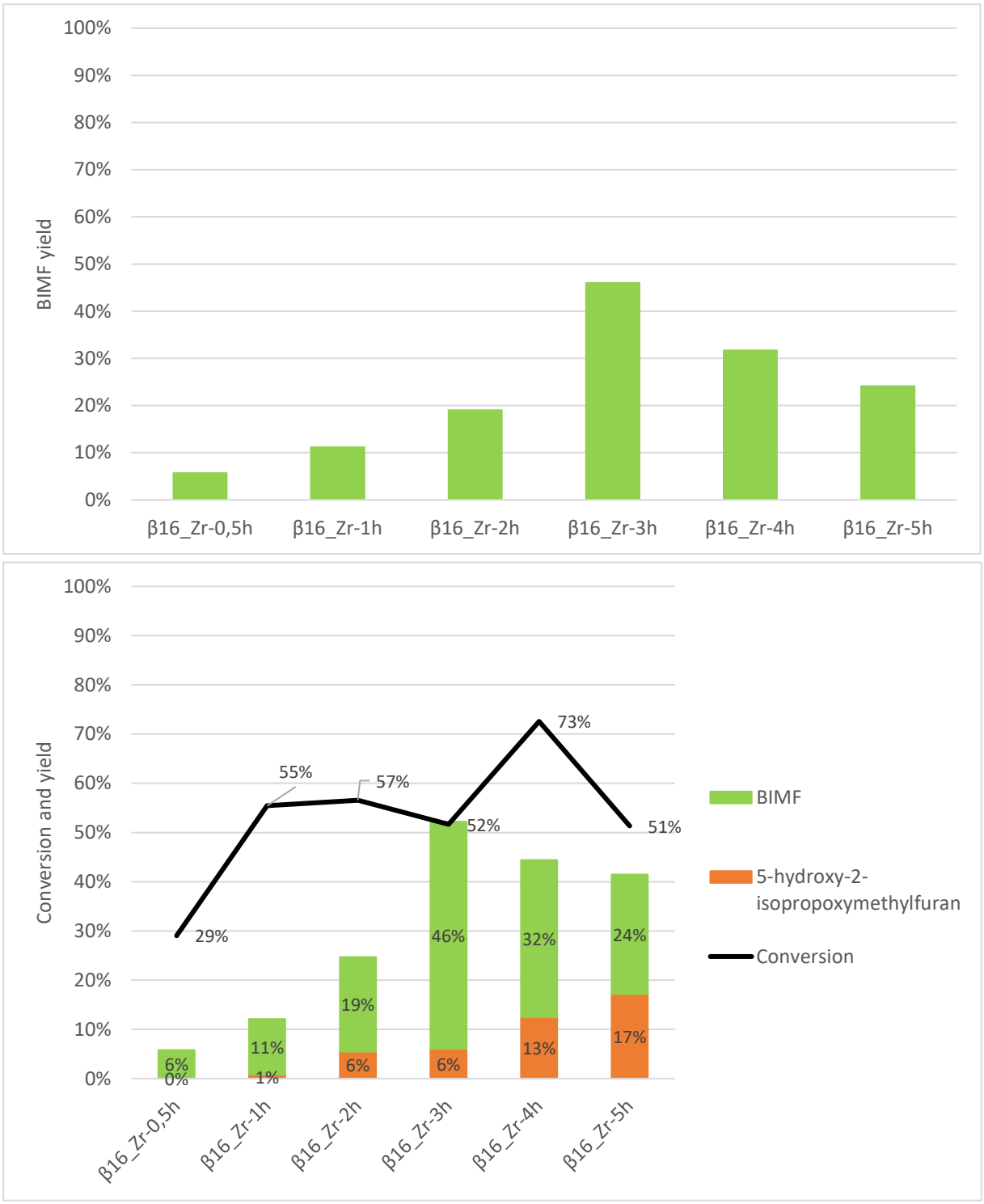

Figure 49. Results of HMF etherification with the use of β-16_Zr at different reaction time. Above are shown only BIMF yield. Below HMF conversion, 5-hydroxy-2-isopropoxymethylfuran and BIMF yield .

Figure 50. Results of HMF etherification with the use of β-96_Zr at different reaction time. Above are shown only BIMF yield. Below HMF conversion, 5-hydroxy-2-isopropoxymethylfuran and BIMF yield .

From Figure 48, Figure 49 and Figure 50 the carbon balance values can be obtained. It is evident that the carbon balance increases with the reaction time, reaching almost 100% in some cases. The reason behind these results when a lower carbon balance is reported, is the fact that the zeolites do not release all the compounds but some of them remain adsorbed in their pores. This is due to the fact that there are strong interactions between the zeolite beta structure and the HMF molecules. HMF has a kinetic diameter of 6.2 Å[121] while beta zeolite pores size are around 7-8 Å[115], the small difference between these two makes it easier for the molecules to remain entrapped in the pores, causing a low carbon balance[121]. Keeping the reaction mixture at temperature for longer times will let the substances to be released and the carbon balance to increase. After the reaction the catalysts gained dark coloration, that is caused by the polymerization and formation of carbon deposits[121]. The deposition of carbon in the catalyst was evaluated by CHN elemental analysis. The results obtained are shown in Table 9. It is possible to see that the amount of carbon present on the catalyst increases from the fresh catalyst (0.26%) to the used catalysts, where the percentages of carbon increase reaching around 9% for the two samples analyzed. It is interesting to see how the carbon percentage is not increasing linearly, but during time the carbon deposition decreases[122,123]. This is due to the presence of etherified groups that, acting as protecting groups, make the molecules more stable[121].

The comparison of these results with a work present in literature[90] where, instead of a acid-base catalyst, a basic catalyst is used shows how the presence of both the type of sites is extremely important to reach high BIMF yields. Indeed, the use of YCl_3 catalyst, kept constant reaction conditions, permits of only reaching a 35% BIMF yield. Compared to the 91% yield obtained with the use of β-10_Zr is clear how this new type of synthesis requires a deeper study and improvement.

Catalyst	%C	%H	%N
β-10_Zr	0.26	1.05	0.25
Recovered β-10_Zr 30 min	8.62	1.35	0.24
Recovered β-10_Zr 2h	9.97	1.36	0.22

Table 9. Elemental CHN analysis of the catalyst, fresh and used.

4.4.2. Comparison between Zr doped zeolites and non-doped zeolites

The dealuminated zeolites were also tested in the process as a blank test at 150 ºC for 5 h (Figure 51). Indeed, the zeolites were able to catalyze the process and obtain BIMF. But compared to the zeolites functionalized with Zr atoms, at the same reaction conditions (Figure 48, Figure 49, Figure 50), BIMF yield and total carbon balance were reduced. β-10 catalyst passes from a 95% BIMF yield for the zeolite functionalized with Zr to 9% without it. β-16 catalyst passes from a 24% BIMF yield for the zeolite functionalized with Zr to 14% without it. β-96 catalyst passes from a 71% BIMF yield for the zeolite functionalized with Zr to 8% without it. At the same time, it can be observed an increase in 5-hydroxy-2-isopropoxymethylfuran yield, an intermediate of the reaction, especially with the use of β-10 and β-96 catalysts that is respectively 15% and 22%. Thus, we can confirm the incorporation of zirconium employing Zr n-propoxide was successful in the production of catalysts with very high selectivity towards the desired products.

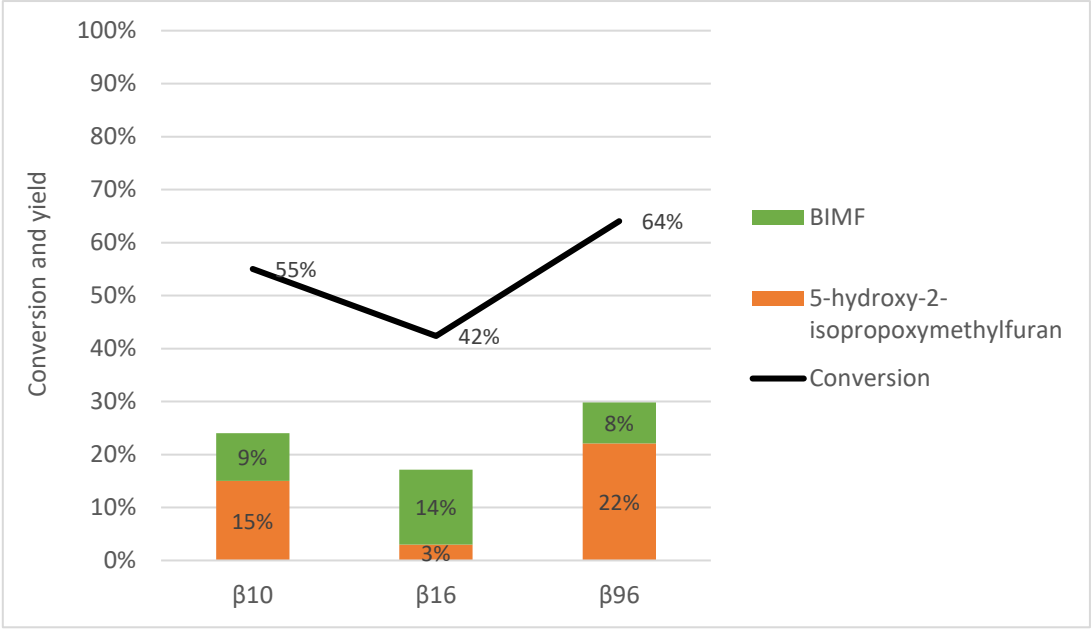

Figure 51. Catalytic tests of the β-zeolites without Zr.

4.4.3. Effect of reaction temperature

Taking into account that the best results were obtained after 5 hours, it was decided to evaluate the effect of reaction temperature on the catalytic performance. The other experimental conditions were kept constant. The tests were carried out at 120, 150 and 180 °C with the three Zr-doped zeolites, but, as an example, Figure 52 displays the results obtained with β-10_Zr.

It is evident that below 150 °C the catalyst is not active, reducing the formation of BIMF, with a HMF conversion lower than 50%. On the contrary, when the reaction temperature reaches 180°C, there is almost no change in conversion or yield.

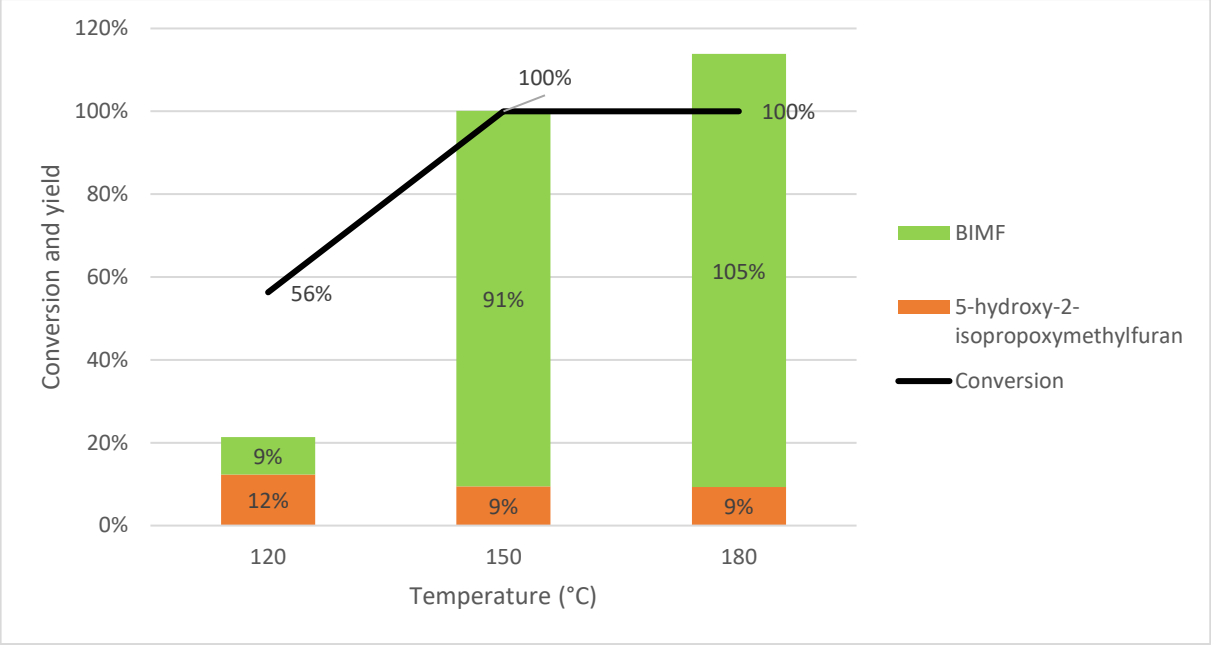

Figure 52. Tests of β-10_Zr at three different temperatures keeping constant the other conditions: HMF 150 mg, catalyst 50 mg, isopropanol 5 mL, time 5 hours.

Considering that the reaction at 180 °C gave the same results as the one performed at 150 °C using the β-10_Zr catalyst we can observe two points. First of all, the high stability of the compounds since the carbon balance is stable at both 150 °C and 180° C. Second of all, how these materials do not suffer from severe adsorption and the unaccounted carbon balance is due to HMF adsorption; this explains how the presence of aldehyde groups strongly influences the chemical adsorption of HMF on the zeolite.

Taked into consideration the results obtained at 180°C, the catalytic tests were done using β-16_Zr and β-96_Zr, keeping constant the experimental conditions. Figure 53 reveals that the increase in temperature improves the catalytic activity, reaching a 100% carbon balance and over 80% BIMF yield. In consequence, HMF conversion also increases and the intermediate yield is decreased. Especially for what concerns the carbon balance, it is possible, as explained before, that the increase in BIMF yield has reduced the amount of aldehyde groups and so reduce the chemical interactions with the zeolite. The here obtained results were compared to some present in literature[87] that used the same catalytic conditions and only changed the synthesis of Zr doped β-zeolite. It was seen that in the paper[87], even if the reaction time is of 6

h, the BIMF yield is around 80% and 5-hydroxy-2-isopropoxymethylfuran yield is around 20%, meaning that the different type of synthesis used in this work has increased the selectivity.

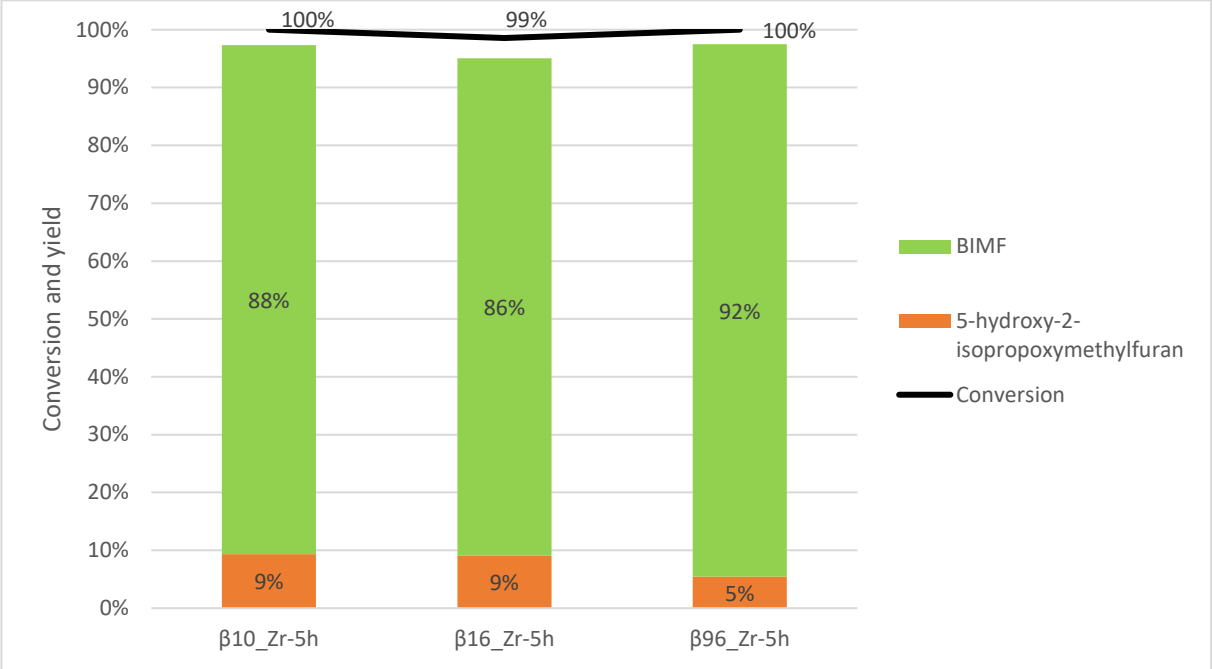

Figure 53. Catalytic data of tests carried out at 180°C for 5 h, with150 mg HMF and 50 mg catalyst.

4.4.4. Effect of reaction time at 180 °C

The next catalytic test was carried out to assess if the reaction can be performed at high temperature (180 °C), but decreasing the reaction time. The results of the reactions performed at 180°C for 3 h are shown in Figure 54. Clearly the carbon balance and the BIMF yield are reduced compared to the reaction performed for 5 h due to the formation of byproducts, but the carbon balance is almost 80% using β-16_Zr and β-96_Zr, while it is still over 90% for β-10_Zr. Regarding the BIMF yield, even though it is reduced compared to the reactions kept at temperature for 5 h, it is still higher than the ones performed at 150 °C. It was possible to obtain 87% BIMF yield in 3 h using β-10_Zr catalyst, while, at 150°C for 3 h, it was only 51%. The increase in the BIMF yield is impressive also for the reactions with the other two catalysts: using β-16_Zr, it goes from 46% at 150°C to 52%, and with β-96_Zr, from 43 to 70%. Compared to the reaction performed for 5 h, the catalytic results are worse, but remain interesting, especially using catalyst β-10_Zr from which is possible to obtain 87% BIMF yield.

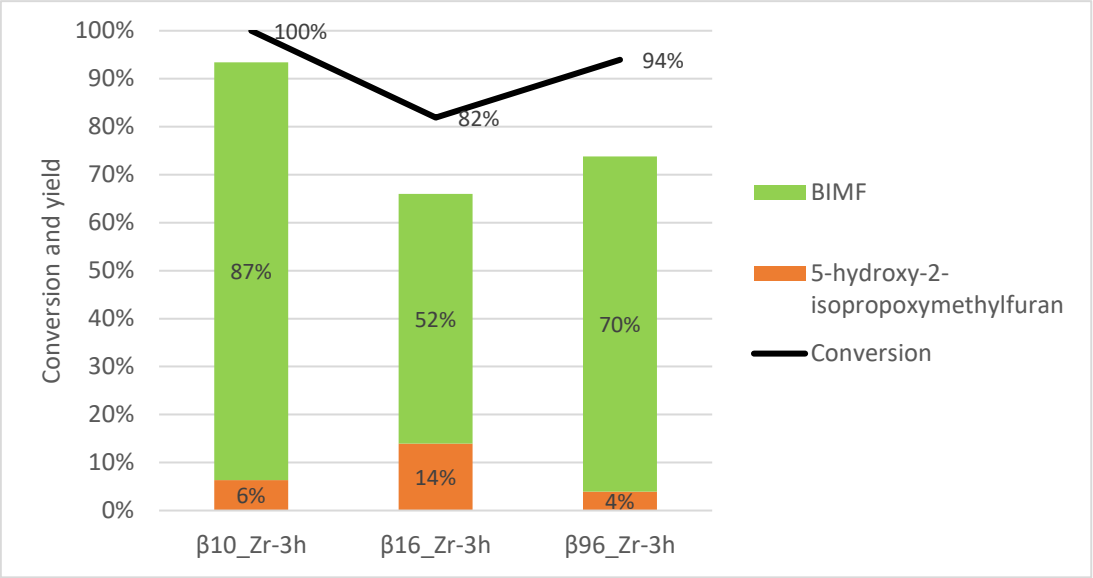

Figure 54. Catalytic data of tests performed at 180°C for 3 hours using 150 mg HMF, 50 mg catalyst, under constant stirring.

4.4.5. Effect of the catalyst amount

Finally, the influence of the amount of catalyst was studied, by using the following experimental conditions: 150 °C, 5 h, 150 mg HMF, and reducing the amount of catalyst. In this case only β-10_Zr catalyst was used. The reactions were carried out using 30, 40 and 50 mg of catalyst.

Figure 55 evidence how the reduction of the catalyst amount strongly influences the product yield and the conversion. Using only 30 mg of catalyst reduces the BIMF yield to only 22% and increases the intermediate yield to 25%, with a conversion around 50%. Taking into accountthe results obtained using 40 mg of catalyst, it is obvious that the BIMF yield has increased reaching 61%, still lower than when 50 mg are used, the intermediate yield is reduced to 17% and the conversion has gone up to 78%. Compared to the test with 50 mg of catalyst, there is an unexpected decrease in the carbon balance, that is only 60% when only 30 mg of β-10_Zr are used. This result is difficult to explain but among the hypothesis there is one that seems more convincing. It could be thought that the blocking of active sites caused by the adsorption of HMF, and other intermediates or reaction products, is easier when a low amount of catalyst is used, that leaving less available active sites to catalyze the etherification process.

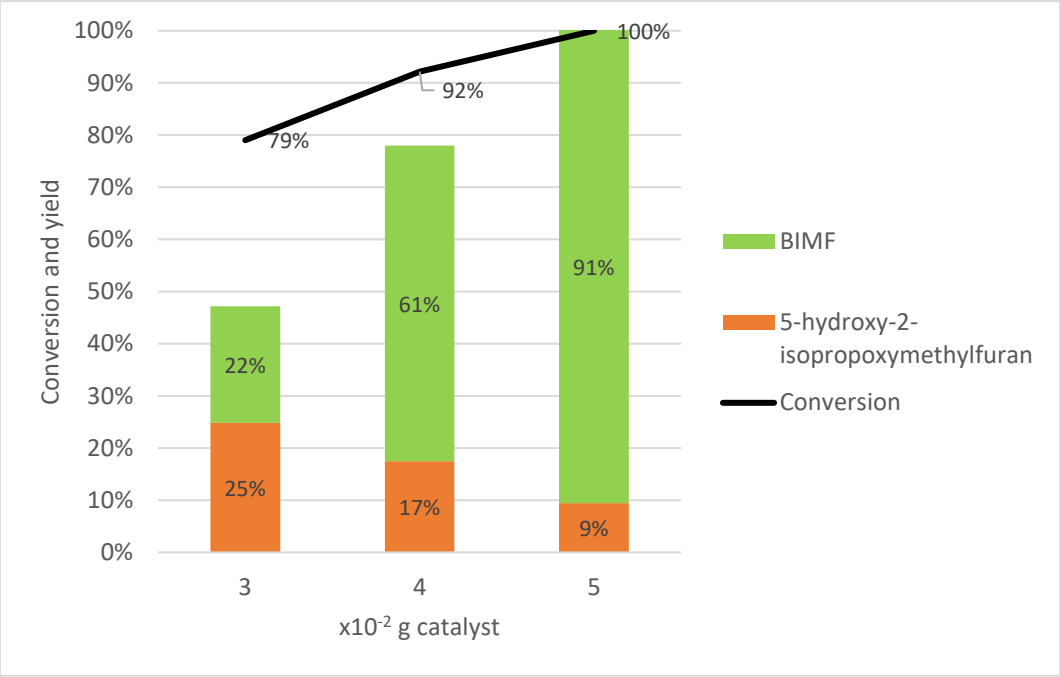

Figure 55. Catalytic results of tests performed by varying the amount of catalyst. (Experimental conditions: 150°C, 5 h, 150 mg HMF).

5. Conclusions

The presented work is part of studies toward a shift from the use of fossil resources to renewable and sustainable sources. The main objectives of this study were two: synthesize a catalyst active on the HMF etherification to BIMF and optimize the reaction conditions of glucose isomerization to fructose using a commercial zeolite.

The isomerization of glucose to fructose is an important process to be optimized because it is governed by the thermodynamic equilibrium between the two compounds and finding a process that permits to obtain a high fructose yield at low costs can be an important turning point because from fructose dehydration is possible to obtain HMF. Three different commercial zeolites were tested to evaluate which one possess the properties more suitable for the process. β-zeolite (CP814E) resulted in having the better results compared to the USY and ZMS5 zeolites. The study of the optimization parameters were so performed with the β-zeolite. Several parameters were investigated to improve the final fructose yield: temperature, reaction time, amount of water added, type of alcohol used. The best results were obtained at 120 °C, for 2 hours for each reaction step, using 2.5 mL of ethanol and 2.5 mL of water permitting to obtain around 28% fructose yield. A further study was conducted to evaluate if the elimination of the alcohol in between the first and the second step through evaporation could reduce the mannose production and increase fructose yield. This passage was discovered to be essential to reduce

the mannose as by-product going from 22% to 9% and increasing fructose yield from 27% to around 30% (Figure 56).

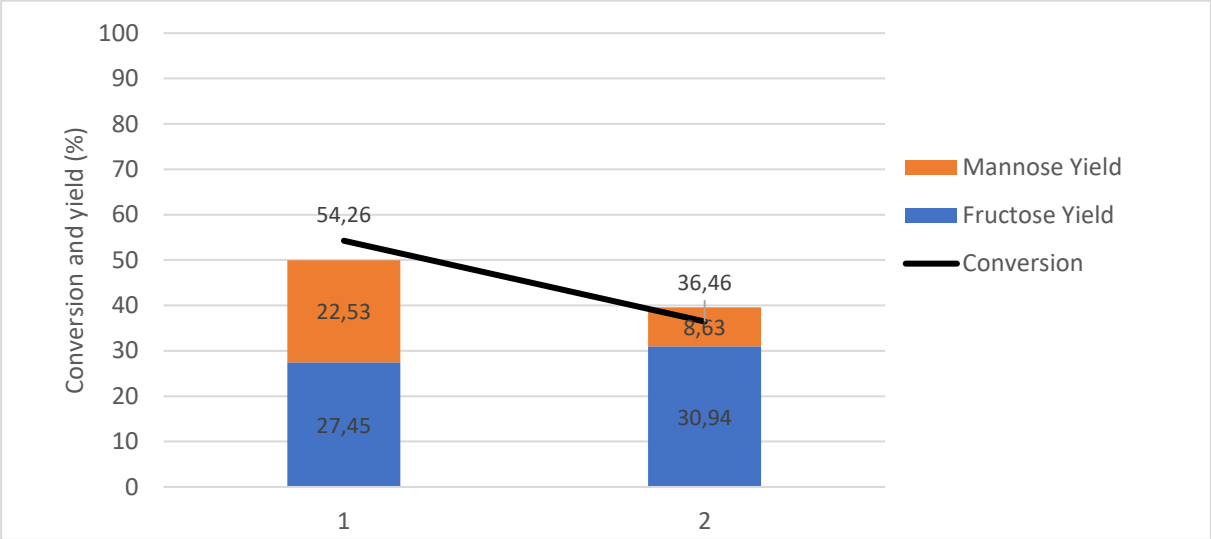

Figure 56. Results of the tests without (left, 1) and with (right, 2) evaporation step before the addition of water.

The catalyst synthesis was prompted toward the production of mixed metal oxides and doped zeolites because they possess strong acid-base properties, are easily customizable and they have both seen to be active on HMF etherification able to produce biochemicals useful in several fields.

The metal mixed oxides of $HNbMoO_6$ and $HNbWO_6$ were synthesized with a solid state synthesis to their precursors $LiNbMoO_6$ and $LiNbWO_6$ and were then acidified exchanging the Li cation with the proton of the acid. The synthesis was evaluated through XRD analysis to understand if the crystalline structure was correctly formed and if it changes after the acid exchange. It was seen that for what concerns $HNbMoO_6$ synthesis the Li-H exchange has not provoked a structural change. Meanwhile, $HNbWO_6$ and its precursor diffractograms showed a slight difference of peak angles and intensities; this behavior was explained by the different size of Li^+ and H^+ that modified that crystalline structure.

These catalysts were then tested on HMF etherification to evaluate their selectivity towards BIMF. The results showed that the mixed metal oxides were active on HMF etherification but on isoproxymethylfuran production due to the type of acidic sites.

Three different types of zeolites were synthesized through dealumination and consequent Zr grafting in the Al vacancies. Different Si/Zr ratios were used and it was seen that the higher the amount of Zr on the catalyst the lower was the activity. The catalysts were characterized using

different techniques. With the use of N_2 adsorption/desorption it was possible to compare the zeolites surface area and average pore dimensions before and after the Zr doping. The results showed that the presence of Zr slightly reduced the surface area and the pore volume due to the presence of Zr that has an bigger atom size. SEM images showed that the Zr doping increases the particle size and their agglomeration.

The zeolites, with and without the Zr, were then tested on HMF etherification. The presence of Zr was seen to be extremely important to obtain high BIMF yields. Reaction conditions of HMF etherification were optimized as well. The conditions that were studied were: time, temperature, catalyst amount. It was possible to see that the best results were obtained at 180°C, revealing a high stability of the catalyst even at high temperatures, for 5 h, using 0.05 g of catalyst and using β10_Zr catalyst, the one containing the least amount of Zr. The study of the reaction time led to the discovery of a non-linear behavior of the carbon deposit on the catalyst, showing that an increase of reaction time led to an increase of carbon balance.

Further work can be envisaged on improvement of zeolites synthesis and characterization. The before mentioned catalysts Zr doping synthesis should be improved to obtain a higher stability on the Zr % desired. Further characterization of the catalysts might be interesting to get more information about the reasons for their different activity. NH_3-TPD and pyridine-DRIFT to define the number, strength of the acid sites and the ratio between Brønsted and Lewis acid sites together with TEM analysis to calculate the mean particle size are two important techniques that can be used to improve the characterization of the materials. Another interesting development is the synthesis of new materials using a different metal instead of Zr, for example Sn. Another important advancement is the study of catalyst reusability, to understand the stability of the catalyst after more than one cycle. Moreover, the characterization of the used catalysts would be important using N_2-adsorption/desorption and SEM analysis.

Further study on mixed metal oxides can be interesting too, especially on the improvement of the synthesis. An example might be trying to reduce the high temperature treatment time or changing the precursor ratios. Other characterization techniques can be used to increase the understanding of the catalyst properties. TEM and SEM images can be used to understand the layered structure, while NH_3-TPD can be used to define the strength of the acid sites.

6. References

1. Tursi, A. A review on biomass: importance, chemistry, classification, and conversion. *Biofuel Res. J.* **6**, 962–979 (2019).
2. Menegazzo, F., Ghedini, E. & Signoretto, M. 5-Hydroxymethylfurfural (HMF) Production from Real Biomasses. *Molecules* **23**, 2201 (2018).
3. Jacobsson, S. & Johnson, A. The diffusion of renewable energy technology: an analytical framework and key issues for research. *Energy Policy* **28**, 625–640 (2000).
4. McKendry, P. Energy production from biomass (part 1): overview of biomass. *Bioresource Technology* **83**, 37–46 (2002).
5. Abbasi, T. & Abbasi, S. A. Biomass energy and the environmental impacts associated with its production and utilization. *Renewable and Sustainable Energy Reviews* **14**, 919–937 (2010).
6. Kosa, M. & Ragauskas, A. J. Bioconversion of lignin model compounds with oleaginous Rhodococci. *Appl Microbiol Biotechnol* **93**, 891–900 (2012).
7. Pandey, M. P. & Kim, C. S. Lignin Depolymerization and Conversion: A Review of Thermochemical Methods. *Chemical Engineering & Technology* **34**, 29–41 (2011).
8. BÃ©guin, P. & Aubert, J.-P. The biological degradation of cellulose. *FEMS Microbiology Reviews* **13**, 25–58 (1994).
9. Chen, J. *et al.* A review of biomass burning: Emissions and impacts on air quality, health and climate in China. *Science of The Total Environment* **579**, 1000–1034 (2017).
10. Carpenter, D., Westover, T. L., Czernik, S. & Jablonski, W. Biomass feedstocks for renewable fuel production: a review of the impacts of feedstock and pretreatment on the yield and product distribution of fast pyrolysis bio-oils and vapors. *Green Chem.* **16**, 384–406 (2014).
11. Jindal, M. K. & Jha, M. K. Hydrothermal liquefaction of wood: a critical review. *Reviews in Chemical Engineering* **32**, 459–488 (2016).

12. Xu, F., Zhong, X.-C., Sun, R.-C. & Gwynn, L. J. Lignin distribution and infrastructure of Salix psammophila. *Zhongguo Zaozhi Xuebao/Transactions of China Pulp and Paper* **20**, 6–9 (2005).

13. Fromm, J., Rockel, B., Lautner, S., Windeisen, E. & Wanner, G. Lignin distribution in wood cell walls determined by TEM and backscattered SEM techniques. *Journal of Structural Biology* **143**, 77–84 (2003).

14. Alper, K., Tekin, K., Karagöz, S. & Ragauskas, A. J. Sustainable energy and fuels from biomass: a review focusing on hydrothermal biomass processing. *Sustainable Energy Fuels* **4**, 4390–4414 (2020).

15. Kalita, D. Hydrocarbon plant—New source of energy for future. *Renewable and Sustainable Energy Reviews* **12**, 455–471 (2008).

16. *Anaerobic Digestion Processes*. (Springer, 2018). doi:10.1007/978-981-10-8129-3.

17. Tong, X., Ma, Y. & Li, Y. Biomass into chemicals: Conversion of sugars to furan derivatives by catalytic processes. *Applied Catalysis A: General* **385**, 1–13 (2010).

18. Rinaldi, R. & Schüth, F. Design of solid catalysts for the conversion of biomass. *Energy Environ. Sci.* **2**, 610–626 (2009).

19. Fayad, G., Boullay, P. & Clet, G. Simultaneous monitoring of acidity and intercalation for layered transition metal oxides in liquid media. *Journal of Colloid and Interface Science* **570**, 41–51 (2020).

20. Van Putten, R.-J. *et al.* Hydroxymethylfurfural, A Versatile Platform Chemical Made from Renewable Resources. *Chem. Rev.* **113**, 1499–1597 (2013).

21. Busca, G. Acid Catalysts in Industrial Hydrocarbon Chemistry. *Chem. Rev.* **107**, 5366–5410 (2007).

22. Tanabe, K. Industrial application of solid acid–base catalysts. *Applied Catalysis A: General* **181**, 399–434 (1999).

23. Yan, P., Wang, H., Liao, Y. & Wang, C. Zeolite catalysts for the valorization of biomass into platform compounds and biochemicals/biofuels: A review. *Renewable and Sustainable Energy Reviews* **178**, 113219 (2023).

24. Dusselier, M. & Davis, M. E. Small-Pore Zeolites: Synthesis and Catalysis. *Chem. Rev.* **118**, 5265–5329 (2018).

25. Schmidt, J. E., Deem, M. W., Lew, C. & Davis, T. M. Computationally-Guided Synthesis of the 8-Ring Zeolite AEI. *Top Catal* **58**, 410–415 (2015).

26. Y-type Zeolites. https://www.acsmaterial.com/blog-detail/y-type-zeolites.html.

27. Jeon, H.-Y., Shin, C.-H., Jung, H. J. & Hong, S. B. Catalytic evaluation of small-pore molecular sieves with different framework topologies for the synthesis of methylamines. *Applied Catalysis A: General* **305**, 70–78 (2006).

28. Mumtaz, F., Irfan, M. F. & Usman, M. R. Synthesis methods and recent advances in hierarchical zeolites: a brief review. *J IRAN CHEM SOC* **18**, 2215–2229 (2021).

29. Otomo, R., Yokoi, T., Kondo, J. N. & Tatsumi, T. Dealuminated Beta zeolite as effective bifunctional catalyst for direct transformation of glucose to 5-hydroxymethylfurfural. *Applied Catalysis A: General* **470**, 318–326 (2014).

30. Che, Q. *et al.* Preparation of mesoporous ZSM-5 catalysts using green templates and their performance in biomass catalytic pyrolysis. *Bioresource Technology* **289**, 121729 (2019).

31. Cui, Q. *et al.* Synthesis and characterization of Zr incorporated small crystal size Y zeolite supported NiW catalysts for hydrocracking of vacuum gas oil. *Fuel* **237**, 597–605 (2019).

32. Paniagua, M. *et al.* Understanding the role of Al/Zr ratio in Zr-Al-Beta zeolite: Towards the one-pot production of GVL from glucose. *Catalysis Today* **367**, 228–238 (2021).

33. Yu, Q. *et al.* Ketonization of Propionic Acid on Lewis Acidic Zr-Beta Zeolite with Improved Stability and Selectivity. *ACS Sustainable Chem. Eng.* **9**, 7982–7992 (2021).

34. Vannucci, J. A. *et al.* Al-free Zr-beta zeolite as a selective catalyst for the ketalization of glycerol. *Molecular Catalysis* **528**, 112497 (2022).

35. Wang, J., Okumura, K., Jaenicke, S. & Chuah, G.-K. Post-synthesized zirconium-containing Beta zeolite in Meerwein–Ponndorf–Verley reduction: Pros and cons. *Applied Catalysis A: General* **493**, 112–120 (2015).

36. B. Gawande, M., K. Pandey, R. & V. Jayaram, R. Role of mixed metal oxides in catalysis science—versatile applications in organic synthesis. *Catalysis Science & Technology* **2**, 1113–1125 (2012).

37. Lintz, H.-G. H. H. Kung: Transition Metal Oxides: Surface Chemistry and Catalysis, Vol. 45 aus der Reihe: Studies in Surface Science and Catalysis, Elsevier, Amsterdam, Oxford, New York, Tokyo 1989. 285 Seiten, Preis: DM 215,—. *Berichte der Bunsengesellschaft für physikalische Chemie* **94**, 895–895 (1990).

38. Reddy, B. M. *et al.* Structural Characterization of Nanosized CeO2−SiO2, CeO2−TiO2, and CeO2−ZrO2 Catalysts by XRD, Raman, and HREM Techniques. *J. Phys. Chem. B* **109**, 3355–3363 (2005).

39. Singh, S. J. & Jayaram, R. V. Chemoselective O-tert-butoxycarbonylation of hydroxy compounds using NaLaTiO4 as a heterogeneous and reusable catalyst. *Tetrahedron Letters* **49**, 4249–4251 (2008).

40. Yang, F. *et al.* Fully catalytic upgrading synthesis of 5-Ethoxymethylfurfural from biomass-derived 5-Hydroxymethylfurfural over recyclable layered-niobium-molybdate solid acid. *Applied Catalysis B: Environmental* **256**, 117786 (2019).

41. Dias, A. S. *et al.* Exfoliated titanate, niobate and titanoniobate nanosheets as solid acid catalysts for the liquid-phase dehydration of d-xylose into furfural. *Journal of Catalysis* **244**, 230–237 (2006).

42. Takagaki, A., Sasaki, R., Tagusagawa, C. & Domen, K. Intercalation-induced Esterification over a Layered Transition Metal Oxide. *Top Catal* **52**, 592–596 (2009).

43. Takagaki, A., Tagusagawa, C. & Domen, K. Glucose production from saccharides using layered transition metal oxide and exfoliated nanosheets as a water-tolerant solid acid catalyst. *Chem. Commun.* 5363–5365 (2008) doi:10.1039/B810346A.

44. Bhuvanesh, N. S. P. & Gopalakrishnan, J. Synthesis of Rutile-Related Oxides, LiMMoO6 (M = Nb, Ta), and Their Proton Derivatives. Intercalation Chemistry of Novel Broensted Acids, HMMoO6.cntdot.H2O. *Inorg. Chem.* **34**, 3760–3764 (1995).

45. Salehabadi, A., Dawi, E. A., Sabur, D. A., Al-Azzawi, W. K. & Salavati-Niasari, M. Progress on nano-scaled alloys and mixed metal oxides in solid-state hydrogen storage; an overview. *Journal of Energy Storage* **61**, 106722 (2023).

46. Majid, A. & Bibi, M. Wet Chemical Synthesis Methods. in *Cadmium based II-VI Semiconducting Nanomaterials: Synthesis Routes and Strategies* (eds. Majid, A. & Bibi, M.) 43–101 (Springer International Publishing, 2018). doi:10.1007/978-3-319-68753-7_3.

47. Delidovich, I. & Palkovits, R. Catalytic Isomerization of Biomass-Derived Aldoses: A Review. *ChemSusChem* **9**, 547–561 (2016).

48. Marianou, A. A. *et al.* Glucose to Fructose Isomerization in Aqueous Media over Homogeneous and Heterogeneous Catalysts. *ChemCatChem* **8**, 1100–1110 (2016).

49. Gallezot, P. Conversion of biomass to selected chemical products. *Chem. Soc. Rev.* **41**, 1538–1558 (2012).

50. Hanover, L. & White, J. Manufacturing, composition, and applications of fructose. *The American Journal of Clinical Nutrition* **58**, 724S-732S (1993).

51. Saravanamurugan, S., Paniagua, M., Melero, J. A. & Riisager, A. Efficient Isomerization of Glucose to Fructose over Zeolites in Consecutive Reactions in Alcohol and Aqueous Media. *J. Am. Chem. Soc.* **135**, 5246–5249 (2013).

52. Jensen, V. J. & Rugh, S. [33] Industrial-scale production and application of immobilized glucose isomerase. in *Methods in Enzymology* vol. 136 356–370 (Academic Press, 1987).

53. Moliner, M., Román-Leshkov, Y. & Davis, M. E. Tin-containing zeolites are highly active catalysts for the isomerization of glucose in water. *Proceedings of the National Academy of Sciences* **107**, 6164–6168 (2010).

54. Angyal, S. J. The Lobry de Bruyn-Alberda van Ekenstein Transformation and Related Reactions. in *Glycoscience: Epimerisation, Isomerisation and Rearrangement Reactions of Carbohydrates* (ed. Stütz, A. E.) 1–14 (Springer, 2001). doi:10.1007/3-540-44422-X_1.

55. De Wit, G., Kieboom, A. P. G. & van Bekkum, H. Enolisation and isomerisation of monosaccharides in aqueous, alkaline solution. *Carbohydrate Research* **74**, 157–175 (1979).

56. Román-Leshkov, Y., Moliner, M., Labinger, J. A. & Davis, M. E. Mechanism of Glucose Isomerization Using a Solid Lewis Acid Catalyst in Water. *Angewandte Chemie* **122**, 9138–9141 (2010).

57. Rendleman, J. A. & Hodge, J. E. Complexes of carbohydrates with aluminate ion. Aldose-ketose interconversion on anion-exchange resin (aluminate and hydroxide forms). *Carbohydrate Research* **75**, 83–99 (1979).

58. van den Berg, R., Peters, J. A. & van Bekkum, H. The structure and (local) stability constants of borate esters of mono- and di-saccharides as studied by 11B and 13C NMR spectroscopy. *Carbohydrate Research* **253**, 1–12 (1994).

59. Vuorinen, T. & Sjöström, E. Kinetics of alkali-catalyzed isomerization of D-glucose and D-fructose in ethanol-water solutions. *Carbohydrate Research* **108**, 23–29 (1982).

60. Delidovich, I. & Palkovits, R. Catalytic activity and stability of hydrophobic Mg–Al hydrotalcites in the continuous aqueous-phase isomerization of glucose into fructose. *Catal. Sci. Technol.* **4**, 4322–4329 (2014).

61. Román-Leshkov, Y. & Davis, M. E. Activation of Carbonyl-Containing Molecules with Solid Lewis Acids in Aqueous Media. *ACS Catal.* **1**, 1566–1580 (2011).

62. Cho, H. J., Dornath, P. & Fan, W. Synthesis of Hierarchical Sn-MFI as Lewis Acid Catalysts for Isomerization of Cellulosic Sugars. *ACS Catal.* **4**, 2029–2037 (2014).

63. Gounder, R. & Davis, M. E. Titanium-Beta Zeolites Catalyze the Stereospecific Isomerization of d-Glucose to l-Sorbose via Intramolecular C5–C1 Hydride Shift. *ACS Catal.* **3**, 1469–1476 (2013).

64. Paniagua, M., Saravanamurugan, S., Melian-Rodriguez, M., Melero, J. A. & Riisager, A. Xylose Isomerization with Zeolites in a Two-Step Alcohol–Water Process. *ChemSusChem* **8**, 1088–1094 (2015).

65. Newth, F. H. The Formation of Furan Compounds from Hexoses. in *Advances in Carbohydrate Chemistry* (eds. Hudso, C. S. & Canto, S. M.) vol. 6 83–106 (Academic Press, 1951).

66. Feather, M. S. & Harris, J. F. Dehydration Reactions of Carbohydrates°°Issued as Journal Paper No. 6502 of the Missouri Agricultural Experiment Station, Columbia, Mo. in *Advances in Carbohydrate Chemistry and Biochemistry* (eds. Tipson, R. S. & Horton, D.) vol. 28 161–224 (Academic Press, 1973).

67. Teong, S. P., Yi, G. & Zhang, Y. Hydroxymethylfurfural production from bioresources: past, present and future. *Green Chem.* **16**, 2015 (2014).

68. Wang, T., Nolte, M. W. & Shanks, B. H. Catalytic dehydration of C_6 carbohydrates for the production of hydroxymethylfurfural (HMF) as a versatile platform chemical. *Green Chem.* **16**, 548–572 (2014).

69. Bicker, M., Hirth, J. & Vogel, H. Dehydration of fructose to 5-hydroxymethylfurfural in sub- and supercritical acetone. *Green Chem.* **5**, 280–284 (2003).

70. Gomes, F. N. D. C., Pereira, L. R., Ribeiro, N. F. P. & Souza, M. M. V. M. PRODUCTION OF 5-HYDROXYMETHYLFURFURAL (HMF) VIA FRUCTOSE DEHYDRATION: EFFECT OF SOLVENT AND SALTING-OUT. *Braz. J. Chem. Eng.* **32**, 119–126 (2015).

71. Albonetti, S. *et al.* Selective oxidation of 5-hydroxymethyl-2-furfural over TiO2-supported gold–copper catalysts prepared from preformed nanoparticles: Effect of Au/Cu ratio. *Catalysis Today* **195**, 120–126 (2012).

72. De Vries, J. G. Green Syntheses of Heterocycles of Industrial Importance. 5-Hydroxymethylfurfural as a Platform Chemical. in *Advances in Heterocyclic Chemistry* vol. 121 247–293 (Elsevier, 2017).

73. He, R. *et al.* The Synthesis of 5-Hydroxymethylfurfural from Glucose in Biphasic System by Phosphotungstic Acidified Titanium–Zirconium Dioxide. *Waste Biomass Valor* **9**, 657–668 (2018).

74. Hu, L. *et al.* Catalytic conversion of biomass-derived carbohydrates into fuels and chemicals via furanic aldehydes. *RSC Adv.* **2**, 11184 (2012).

75. Carlini, C., Patrono, P., Galletti, A. M. R. & Sbrana, G. Heterogeneous catalysts based on vanadyl phosphate for fructose dehydration to 5-hydroxymethyl-2-furaldehyde. *Applied Catalysis A: General* **275**, 111–118 (2004).

76. Sidhpuria, K. B., Daniel-da-Silva, A. L., Trindade, T. & Coutinho, J. A. P. Supported ionic liquid silica nanoparticles (SILnPs) as an efficient and recyclable heterogeneous catalyst for the dehydration of fructose to 5-hydroxymethylfurfural. *Green Chem.* **13**, 340–349 (2011).

77. Seri, K., Inoue, Y. & Ishida, H. Highly Efficient Catalytic Activity of Lanthanide(III) Ions for Conversion of Saccharides to 5-Hydroxymethyl-2-furfural in Organic Solvents. *Chem. Lett.* **29**, 22–23 (2000).

78. Jeong, J. *et al.* Commercially attractive process for production of 5-hydroxymethyl-2-furfural from high fructose corn syrup. *Journal of Industrial and Engineering Chemistry* **19**, 1106–1111 (2013).

79. Chheda, J. N., Román-Leshkov, Y. & Dumesic, J. A. Production of 5-hydroxymethylfurfural and furfural by dehydration of biomass-derived mono- and poly-saccharides. *Green Chem.* **9**, 342–350 (2007).

80. Kröger, M., Prüße, U. & Vorlop, K.-D. A new approach for the production of 2,5-furandicarboxylic acid by in situ oxidation of 5-hydroxymethylfurfural starting from fructose. *Topics in Catalysis* **13**, 237–242 (2000).

81. Antal, M. J., Mok, W. S. L. & Richards, G. N. Mechanism of formation of S(hydroxymethyl)-2-furalde- hyde from D-fructose and sucrose.

82. Moreau, C. *et al.* Dehydration of fructose to 5-hydroxymethylfurfural over H-mordenites. *Applied Catalysis A: General* **145**, 211–224 (1996).

83. Artz, J. & Palkovits, R. Cellulose-based platform chemical: The path to application. *Current Opinion in Green and Sustainable Chemistry* **14**, 14–18 (2018).

84. Artz, J., Mallmann, S. & Palkovits, R. Selective Aerobic Oxidation of HMF to 2,5-Diformylfuran on Covalent Triazine Frameworks-Supported Ru Catalysts. *ChemSusChem* **8**, 672–679 (2015).

85. Hou, Q. *et al.* Biorefinery roadmap based on catalytic production and upgrading 5-hydroxymethylfurfural. *Green Chem.* **23**, 119–231 (2021).

86. Pasini, T. *et al.* Selective oxidation of 5-hydroxymethyl-2-furfural using supported gold–copper nanoparticles. *Green Chem.* **13**, 2091–2099 (2011).

87. Jae, J., Mahmoud, E., Lobo, R. F. & Vlachos, D. G. Cascade of Liquid-Phase Catalytic Transfer Hydrogenation and Etherification of 5-Hydroxymethylfurfural to Potential Biodiesel Components over Lewis Acid Zeolites. *ChemCatChem* **6**, 508–513 (2014).

88. Wu, L., Moteki, T., Gokhale, A. A., Flaherty, D. W. & Toste, F. D. Production of Fuels and Chemicals from Biomass: Condensation Reactions and Beyond. *Chem* **1**, 32–58 (2016).

89. Haan, R. J. & Lange, J.-P. Gasoline composition and process for the preparation of alkylfurfuryl ether. (2013).

90. Natsir, T. A. & Shimazu, S. Fuels and fuel additives from furfural derivatives via etherification and formation of methylfurans. *Fuel Processing Technology* **200**, 106308 (2020).

91. López-Asensio, R. *et al.* Selective production of furfuryl alcohol from furfural by catalytic transfer hydrogenation over commercial aluminas. *Applied Catalysis A: General* **556**, 1–9 (2018).

92. Natsir, T. A., Hara, T., Ichikuni, N. & Shimazu, S. Highly Selective Transfer Hydrogenation of Carbonyl Compounds Using La2O3. *BCSJ* **91**, 1561–1569 (2018).

93. Nguyen, H. *et al.* Role of Lewis and Brønsted Acidity in Metal Chloride Catalysis in Organic Media: Reductive Etherification of Furanics. *ACS Catal.* **7**, 7363–7370 (2017).

94. Luo, J. *et al.* The effect of oxide acidity on HMF etherification. *Catal. Sci. Technol.* **4**, 3074–3081 (2014).

95. Balakrishnan, M., Sacia, E. R. & Bell, A. T. Etherification and reductive etherification of 5-(hydroxymethyl)furfural: 5-(alkoxymethyl)furfurals and 2,5-bis(alkoxymethyl)furans as potential bio-diesel candidates. *Green Chem.* **14**, 1626–1634 (2012).

96. Neves, P. *et al.* Production of biomass-derived furanic ethers and levulinate esters using heterogeneous acid catalysts. *Green Chem.* **15**, 3367–3376 (2013).

97. Li, X.-L. *et al.* A cobalt catalyst for reductive etherification of 5-hydroxymethyl-furfural to 2,5-bis(methoxymethyl)furan under mild conditions. *Green Chem.* **20**, 1095–1105 (2018).

98. Patil, C. R. & Rode, C. V. Selective Production of Furanic Ethers from Lignocellulosic Biomass over Mesoporous Zr-Incorporated SBA-15 Catalyst. *ChemistrySelect* **3**, 12504–12511 (2018).

99. Zhang, Y. *et al.* Hydrogen Transfer Reaction as an Alternative Reductive Process for the Valorization of Biomass-Derived Building Blocks. in *Studies in Surface Science and Catalysis* vol. 178 195–214 (Elsevier, 2019).

100. Minteer, S. D. 11 - Biochemical production of other bioalcohols: biomethanol, biopropanol, bioglycerol, and bioethylene glycol. in *Handbook of Biofuels Production* (eds. Luque, R., Campelo, J. & Clark, J.) 258–265 (Woodhead Publishing, 2011). doi:10.1533/9780857090492.2.258.

101. Fang, W. & Riisager, A. Recent advances in heterogeneous catalytic transfer hydrogenation/hydrogenolysis for valorization of biomass-derived furanic compounds. *Green Chem.* **23**, 670–688 (2021).

102. The Golden Age of Transfer Hydrogenation. https://pubs.acs.org/doi/epdf/10.1021/acs.chemrev.5b00203 doi:10.1021/acs.chemrev.5b00203.

103. Graauw, C. F. de, Peters, J. A., Bekkum, H. van & Huskens, J. Meerwein-Ponndorf-Verley Reductions and Oppenauer Oxidations: An Integrated Approach. *Synthesis* **1994**, 1007–1017 (1994).

104. Qiu, M., Guo, T., Xi, R., Li, D. & Qi, X. Highly efficient catalytic transfer hydrogenation of biomass-derived furfural to furfuryl alcohol using UiO-66 without metal catalysts. *Applied Catalysis A: General* **602**, 117719 (2020).

105. Li, H. *et al.* Acid–Base Bifunctional Zirconium N-Alkyltriphosphate Nanohybrid for Hydrogen Transfer of Biomass-Derived Carboxides. *ACS Catal.* **6**, 7722–7727 (2016).

106. Gao, Z., Fan, G., Liu, M., Yang, L. & Li, F. Dandelion-like cobalt oxide microsphere-supported RuCo bimetallic catalyst for highly efficient hydrogenolysis of 5-hydroxymethylfurfural. *Applied Catalysis B: Environmental* **237**, 649–659 (2018).

107. Zhang, J., Li, D., Yuan, H., Wang, S. & Chen, Y. Advances on the catalytic hydrogenation of biomass-derived furfural and 5-hydroxymethylfurfural. *Journal of Fuel Chemistry and Technology* **49**, 1752–1766 (2021).

108. Gu, J. *et al.* Efficient transfer hydrogenation of biomass derived furfural and levulinic acid via magnetic zirconium nanoparticles: Experimental and kinetic study. *Industrial Crops and Products* **145**, 112133 (2020).

109. Grasemann, M. & Laurenczy, G. Formic acid as a hydrogen source – recent developments and future trends. *Energy Environ. Sci.* **5**, 8171–8181 (2012).

110. Basu, B., Das, P. & Das, S. Transfer hydrogenation using recyclable polymer-supported formate (PSF): Efficient and chemoselective reduction of nitroarenes. *Mol Divers* **9**, 259–262 (2005).

111. Chemoselective Reduction of the Carbonyl Functionality through Hydrosilylation: Integrating Click Catalysis with Hydrosilylation in One Pot | The Journal of Organic Chemistry. https://pubs.acs.org/doi/full/10.1021/jo501505j?casa_token=1uYSXURb3FEAAAAA%3AdW3GUvF7mMN-h_aFq-HbWX6KC12FiGivPoZnZ_3vBD39m00KLfc0QBSK9DP5W3miyRqTgNv2tEnoi6M.

112. da Silva Lisboa, F., Barbosa Ferreira, E., Josiane Liana Baumgardt da Silva, F. & Rosa da Silva, F. Catalytic activity in methyl esterification reactions and characterization of the superacid $HNbMoO_6$ treated with different inorganic acids: Catalytic activity in esterification reactions of the superacid $HNbMoO_6$. *Biofuels* 1–9 (2023) doi:10.1080/17597269.2023.2170035.

113. Sotomayor, F. J., Cychosz, K. A. & Thommes, M. Characterization of Micro/Mesoporous Materials by Physisorption: Concepts and Case Studies. (2018).

114. Combined Function of Brønsted and Lewis Acidity in the Zeolite-Catalyzed Isomerization of Glucose to Fructose in Alcohols - Saravanamurugan - 2016 - ChemCatChem - Wiley Online Library. https://chemistry-

europe.onlinelibrary.wiley.com/doi/full/10.1002/cctc.201600783?casa_token=47OriGeo48wAAAAA%3ArkOegzwsMh44LVQJIoLL4b5oKy2iprmKsQoD1jgB-w3qeYBl3DQ9IkbbDA8_rPc7KaRZSgIcNyjtsg.

115. Jae, J. *et al.* Investigation into the shape selectivity of zeolite catalysts for biomass conversion. *Journal of Catalysis* **279**, 257–268 (2011).

116. Tukur, N. M. & Al-Khattaf, S. Catalytic Transformation of 1,3,5-Trimethylbenzene over a USY Zeolite Catalyst. *Energy Fuels* **21**, 2499–2508 (2007).

117. Johnson, L. *et al.* Methyl α-D-fructofuranoside: Synthesis and conversion into carboxylates. *Tetrahedron: Asymmetry* **5**, 2475–2484 (1994).

118. Rasmussen, H., Sørensen, H. R. & Meyer, A. S. Formation of degradation compounds from lignocellulosic biomass in the biorefinery: sugar reaction mechanisms. *Carbohydrate Research* **385**, 45–57 (2014).

119. Andary, J. *et al.* Stability study of furans, glucose and xylose under overliming conditions: Effect of sugar degradation products. *Bioresource Technology Reports* **15**, 100722 (2021).

120. Zhu, P., Meier, S., Saravanamurugan, S. & Riisager, A. Modification of commercial Y zeolites by alkaline-treatment for improved performance in the isomerization of glucose to fructose. *Molecular Catalysis* **510**, 111686 (2021).

121. Wang, K., Zhang, J., H. Shanks, B. & Brown, R. C. Catalytic conversion of carbohydrate-derived oxygenates over HZSM-5 in a tandem micro-reactor system. *Green Chem.* **17**, 557–564 (2015).

122. Papanikolaou, G. *et al.* Use of zeolites in green chemicals and bio-fuel production via HMF valorisation. *Microporous and Mesoporous Materials* **358**, 112330 (2023).

123. Yan, P., Wang, H., Liao, Y. & Wang, C. Zeolite catalysts for the valorization of biomass into platform compounds and biochemicals/biofuels: A review. *Renewable and Sustainable Energy Reviews* **178**, 113219 (2023).